BAYESIAN NETWORK MODEL OF MERCURY EXPOSURE TO AQUATIC ECOSYSTEMS OF THE MACKENZIE WATERSHED

A Thesis Submitted to the Committee of Graduate Studies in Partial Fulfillment of the Requirements for the Degree of Master of Science in the Faculty of Arts and Science

TRENT UNIVERSITY – Peterborough, Ontario, Canada

Environmental & Life Sciences M. Sc. Graduate Program

September 2023

ABSTRACT:

BAYESIAN NETWORK MODEL OF MERCURY EXPOSURE TO AQUATIC ECOSYSTEMS OF THE MACKENZIE WATERSHED

By Una Jermilova

A significant portion (15-20%) of mercury (Hg) in the Arctic Ocean is believed to originate from Arctic rivers, such as the Mackenzie River watershed in the NWT. Recent (2005-2020) Hg monitoring data of freshwater and fish tissue and environmental model outputs were compiled and used to develop a Bayesian Network Relative Risk model (BN-RRM), a probabilistic model capable of analyzing causal relationships. The objectives of the model were to estimate the risk posed to fish health and the subsequent dietary Hg-exposure to humans; to compare the relative risks between regions of the watershed; and to identify the influential Hg sources. The output of the BN-RRMs differed significantly throughout the watershed, with atmospheric Hg deposition and soil erosion Hg release consistently flagged as important explanatory variables. Analysis of the endpoint uncertainties revealed gaps in knowledge and in Hg datasets, which should be the focus of study for future monitoring programs.

KEYWORDS:

Bayesian Network, Mercury, Aquatic Ecosystems, Arctic, Toxicology, Risk Assessment

DEDICATION

This thesis is dedicated to my family members who have loved and supported me throughout this journey.

Truthfully though, this thesis should be dedicated to the Canadian wilderness, my love with which was the true inspiration for undertaking this research. I would eagerly dedicate the rest of my life towards ensuring that the natural treasures of this nation are granted the value they so obviously hold.

ACKNOWLEDGEMENTS

I would like to thank my thesis advisor and the two other members of my graduate committee: Holger Hintelmann, Jane Kirk, and Wayne Landis. Thank you all for your encouragement and the many opportunities that have helped me to grow as a student and a scientist. Furthermore, I would like to thank the many colleagues whose advise and comradery was integral to the successful completion of this thesis: Emma Sharpe (Western Washington University), Maeve McGovern (NIVA), Sophie Mentzel (NIVA), Sam Welch (NIVA), Beatriz Bento (Trent University), and Geoff Andrews (Trent University). Finally, the work by Jannicke Moe, Cathrine Brecke Gundersen, and Hans Fredrik Vieteberg Braaten (NIVA) was essential for the initiation of the ARCRISK Project. Thank you all for your support.

This project would not have been possible without numerous mercury monitoring datasets and environmental model outputs. Environmental models were graciously shared by Camile Sothe (McMaster University and World Wildlife Fund Canada), Kevin Schaeffer (National Snow and Ice Data Center, University of Colorado Boulder) and Ashu Dastoor (Environment Climate Change Canada) through private correspondence. Publicly available mercury monitoring data was obtained from the Mackenzie DataStream (https://mackenziedatastream.ca/), and the following individuals: Mary Gamberg (Northern Contaminants Program funded projects), David Depew (Canadian Fish Mercury Database), Aimee Guile (Wek'èezhìı Renewable Resources Board), Lisa Loseto (University of Manitoba). Finally, the MaDGIC Unit at Trent University provided support with precuring and applying the GIS datasets.

TABLE OF CONTENTS

LIST OF FIGURES

APPENDIX A

LIST OF TABLES

APPENDEX B

LIST OF EQUATIONS

LIST OF ABBREVIATIONS

ACAP: Arctic Contaminants Action Program

AMAP: Arctic Monitoring and Assessment Program

AMDE: Atmospheric Mercury Deposition Event

ARCRISK: Mercury Risk Evaluation, Risk Management, and Risk Reduction Measures in the Arctic

BN(-RRM): Bayesian Network (– Relative Risk Model)

CCME: Canadian Council for Ministers of the Environment

CIRNAC: Crown Indigenous Relations and Northern Affairs Canada

CPT: Conditional Probability Table

DHg: Dissolved Mercury

DOC: Dissolved Organic Carbon

EMAB: Environmental Monitoring Advisory Board

ED (20/50): Effective Dose (20% effectivity/ 50% effectivity)

GBS: Great Bear Subbasin

GEM: Gaseous elemental mercury

GEM-MACH-Hg: Global Environmental Multiscale – Modelling Air quality and CHemistry – Mercury

GIS: Geographic Information System

GOC: Government of Canada

GOM: Gaseous oxidized mercury

GNWT: Government of the Northwest Territories

GSL: Great Slave Subbasin

HYDAT: Hydroclimatological Data Retrieval Program

INAC: Indigenous and Northern Affairs Canada

LC20/50: Lethal Concentration (20% fatality / 50% fatality)

MeHg: Methylmercury

MJ: Megajoules

MW: Megawatts

MRB(B): Mackenzie River Basin (Board)

NCCAH: National Collaborating Centre for Aboriginal Health

NDVI: the Normalized-Difference Vegetation Index

NGO: Non-governmental organization

NIVA: Norwegian Institute for Water Research

NWT: Northwest Territories

OCAP: Indigenous principle of "ownership, control, access, and possession"

PHg: Particulate mercury

pTDI: Provisional Tolerable Daily Intake

pTWI: Provisional Tolerable Weekly Intake

RUSLE: Revised Universal Soil Loss Equation

SiBCASA-Hg: Simple Biosphere/ Carnegie-Ames-Stanford Approach mercury model

STKI: Slope Thermokarst Features Impacted

THg: Total mercury

TSS: Total Suspended Solids

UNEP: United Nations Environment Programme

UNESCO: United Nations Educational, Scientific and Cultural Organization

US. EPA: United States Environmental Protection Agency

WHO: World Health Organization

Chapter 1: Introduction

1.1 Mercury in the Arctic

Mercury is a pollutant of global concern because once released into the atmosphere it is deposited onto landscapes and waterbodies both near and far from point sources, such as Arctic regions (Li *et al.* 2017; Dastoor *et al.* 2014; UNEP, 2002). A seafood diet of high-trophic level species is the primary route of mercury (Hg) exposure to humans living in remote areas (Sheehan *et al.* 2014; AMAP, 2011; UNEP, 2002). The traditional diet of Arctic Indigenous people is essential for food security, cultural identity, nutrition, and health (Ratelle *et al.* 2019; Laird *et al.* 2018; Halseth and the NCCAH 2015; Parlee and Maloney 2016). Fetal neurotoxicity is the most sensitive endpoint of Hg exposure and is the basis behind Hg regulatory thresholds (NRC, 2000; WHO, 1990; Coull, 2003). Concerned Indigenous groups in the Arctic have initiated numerous collaborative monitoring studies aimed at understanding the presence of Hg in their surrounding environment and wildlife (NCP, 2017; Houde *et al.* 2022). These studies have identified potential food safety issues and allowed communities greater control in making informed decisions regarding their diet (Houde *et al.* 2022). However, food consumption advisories are not an acceptable management strategy for communities struggling with food security (Laird *et al.* 2018; Hoover, 2013). There is a need for international policies aiming to reduce the release of Hg from the source (UNEP, 2002).

The Minamata Convention is a multilateral agreement to reduce the anthropogenic inputs of Hg into the environment; it was signed in 2013 by 128 countries that pledged to reduce Hg use across manufacturing, energy, and gold mining industries by 2030 (UNEP, 2021; UNEP, 2019). Nonetheless, global atmospheric Hg emissions increased by approximately 20% from 2010 to 2015, driven by industrial growth in South America and Asia (Dastoor *et al.* 2022). Additionally,

recent experiments show that thawing permafrost soils (Schuster *et al.* 2018; Schaeffer *et al.* 2020), biomass burning (Fraser *et al.* 2018; Dastoor *et al.* 2022), and Arctic rivers (Soerensen *et al.* 2016; Campeau *et al.* 2022), are important Hg sources to the Arctic Ocean, especially when considering climate change stressors (Chetelat *et al.* 2022; AMAP, 2011). Reducing the risk of exposure to vulnerable populations requires comprehensive and local management strategies that target these additional pathways. Ecological risk assessments which identify influential Hg accumulation pathways in freshwater and biota are essential to the development of a resilient risk reduction strategy.

1.2 The ARCRISK project

Rivers are the largest net sources of Hg to the Arctic Ocean, accounting for approximately 20% of the mass budget (Soerensen *et al.* 2016). This thesis supports the ARCRISK project, a circumpolar collaboration to develop Hg risk assessments for four Arctic River systems in Norway, Canada, and Russia (Gundersen *et al.* 2020). Together these assessments will present a comprehensive study of the pathways driving Hg accumulation in Arctic Rivers. The main objectives of the ARCRISK project are: (1) to identify Hg sources to land and water, (2) to evaluate the associated risk for the environment and human health, and (3) to develop an action plan to reduce environmental risk to the Arctic (Gundersen, 2020).The project employs the Bayesian Network - Relative Risk Model (BN-RRM) framework for the environmental risk assessments (Landis, 2020). The BN-RRM can be conceptualized as a causal web which can aid in deducing the strength of the interactions between pollutant sources and endpoints. They have been successfully developed to predict risk to endpoints (Harris *et al.* 2017; Ayre, and Landis 2012), to compare management strategies (Johns *et al.* 2016; Herring *et al.* 2015; Ayre *et al.* 2014), and to evaluate complex multi-stressor systems (Bruen *et al.* 2022;

Peeters *et al.* 2022). The Canadian contributions to the ARCRISK project are the BN-RRMs for the Great Bear and Great Slave subbasins of the Mackenzie River watershed.

A Bayesian risk framework was selected for four reasons. First, it can integrate observations from a variety of sources including environmental models, primary data, and expert opinion into a single framework (Kaikkonen *et al.* 2020; Uusitalo, 2007). This is essential for a project which is studying a sparsely sampled riverine system and is combining analytical data from multiple monitoring sources. Second, Bayesian Networks utilize conceptual diagrams, and this visual component facilitates straightforward communication with Indigenous rightsholders, stakeholders, and policy makers (Kaikkonen *et al.* 2020; Landis, 2020). Third, since Bayesian networks employ probability distributions to describe variables, this allows for the explicit determination of both intrinsic and model uncertainty (Kaikkonen *et al.* 2020). Finally, Bayesian Networks can aid with decisions on how to best manage the risk (Kaikkonen *et al.* 2020; McCann *et al.*2006). Once the influential variables affecting an endpoint are identified, management strategies can be inserted into the model. This is useful for directly comparing different management strategies, their predicted influence on the risk to endpoints, and the associated uncertainties of this benefit (Kaikkonen *et al.* 2020; McCann *et al.* 2006).

1.3 The Mackenzie River Basin – The Canadian study site

The Mackenzie River Basin (MRB) is the largest watershed in Canada and encompasses six smaller sub-basins: the Athabasca, Peace, Great Slave, Liard, Peel, and Great Bear (MRBB, 2003). It also contains three of Canada's Great Lakes (the Athabasca, Great Slave, and Great Bear Lakes) as well as three protected delta regions (the Slave River delta, Mackenzie River delta, and the Peace-Athabasca delta- a UNESCO World Heritage Site; MRBB, 2003). The official start of the Mackenzie River is at the outlet of Great Slave Lake, at the boundary of the

Great Bear and Great Slave subbasins. As warming temperatures expedite snow and glacial melt, freshwater flow to the Arctic Ocean by circumpolar rivers has increased by 7% (Emmerton *et al.* 2013), releasing nutrients and Hg contaminants previously trapped in the frozen soil and ice (Campeau *et al.* 2022; Schaefer *et al.* 2020). The Mackenzie River discharges approximately 325 km^3 of freshwater into the Arctic Ocean annually, making up 10% of the annual freshwater contribution and transporting up to 2 tons of Hg (Rood *et al.* 2016; Leitch *et al.* 2007). The Mackenzie River drains an immense area of 1.8 million km^2 (MRBB, 2003) and each subbasin is hydrologically connected to the Mackenzie River.

The Great Bear subbasin is the largest of the six MRB subbasins, covering an area of approximately 400,000 square kilometers (MRBB, 2003). There are 15 communities in the basin, with populations ranging from 100 to 3300 individuals (Statistics Canada, 2017). Indigenous people comprise between 60- 95% of the community populations, with slightly lower ratios in administrative centers. To assess the spatial variation in Hg concentrations, I further divided the Great Bear subbasin into four study regions: north, west, east, south (Figure 1; Table 1). Oil and natural gas extraction facilities in the Ikhil (north) and Norman Wells (west) regions are the major anthropogenic Hg sources in the Great Bear subbasin (Supplemental Figure 12). Soil erosion and mass wasting events were also more common in these subbasins, due to the steep geography of the western mountain ranges, and the expansion of permafrost thaw slumps (Kokelj *et al.* 2015; Lantz and Kokelj, 2008). However, it is the discontinuous permafrost underlaying the southern study region that is thawing at unprecedented rates (Schaefer *et al.* 2020). This may be exacerbated by the higher frequency of wildfires, which also contribute to elevated atmospheric Hg deposition (Gaboriau *et al.* 2022; Scholten *et al.* 2021; Fraser *et al.* 2018). The southern region is also where the Great Slave Lake drains into the Mackenzie River, which may

be introducing Hg from the mining industries present on the lake shores (Thienpont *et al.* 2016; Cott *et al.* 2016; Supplemental Figure 13). Mercury monitoring data was sparce for the east region, potentially due to the low human population and the lack of known Hg sources; as such, the uncertainty in the model output for this region is greater than the other three.

The second model was developed for a 50 km zone delineated around Great Slave Lake, rather than the entire Great Slave subbasin. Nearly half of the 46,000 individuals in the Northwest Territories reside in the capital city of Yellowknife, which is located on the Great Slave Lake shoreline (Statistics Canada, 2017). Great Slave Lake has supported the Northwest Territory's largest commercial fishing industry and a long-lived history of gold mining exploration (Fisheries Act; Silke, 2009). Underlain by the mineral-rich soils of the Canadian Shield ecozone, the North and East Arms of Great Slave Lake contain deposits of precious metals which have supplied 35 small historic gold mines and three large gold-producing mines (Silke, 2009; Thienpont *et al.* 2016). Arsenic and Hg concentrations are elevated in the vicinity of the Con and Giant gold-producing mines, which have potentially released contaminants into Great Slave Lake through mine effluent and ore roasting emissions (Thienpont *et al.* 2016). In contrast, the southwestern shores of Great Slave Lake have little history of mining (Silke, 2009). This is because the Interior Plains ecozone is characterized by carbon-rich soils; since dissolved metals bind to organic carbon, erosion of these soils may be a source of biologically available Hg that is not present in east. The Great Slave Lake study area was divided into four regions: North Arm, East Arm, Middle Basin, and Outlet (Figure 1). The choice of these four study regions will allow for the potential identification of mining as a Hg source to Great Slave Lake and in turn, Great Slave Lake to the Great Bear subbasin.

1.4 Introduction to the study area and the Bayesian Network Models

The model for the Great Bear subbasin was prioritized because it alone fully encompasses the Mackenzie River. A second model was prepared for Great Slave Lake as it is the largest riverine input (35% total flow; Environment Canada, 2013) into the Mackenzie River. Finally, the Great Bear and Great Slave subbasins were selected for the initial models because higher fish Hg concentrations have been observed in these regions compared to the other subbasins (Evans *et al.* 2005; Lockhart *et al.* 2005). Lockhart *et al.* (2005) found that more than 90% of marine mammals and piscivorous fish in the MRB had Hg concentrations above Canada's subsistence consumption limit (0.2 ppm), and between 20-50% had concentrations above the threshold for the commercial sale of fish (0.5 ppm) (Lockhart *et al*. 2005); bedrock type was the only abiotic explanatory variable considered. Advancements in environmental models and GIS technologies allow for the consideration of additional Hg sources which may explain the elevated Hg concentrations in aquatic biota.

There is a long history of Hg monitoring studies conducted in the Mackenzie River Basin (MRB) and the Beaufort Sea (Morris *et al.* 2022; Houde *et al.* 2022; Rigét *et al.* 2011; Lockhart *et al.* 2005; Evans *et al.* 2005). This project compiled the publicly available Hg monitoring data of freshwater and fish tissue collected since the Lockhart e*t al.* (2005) report. The Hg sources considered include model outputs of atmospheric deposition and permafrost thaw release; proximity to mines, oil and natural gas wells, wildfires, and permafrost-thaw slumps; and a proposed calculation of terrestrial Hg release by soil erosion. Soil erosion was calculated by combining 4 abiotic factors: soil texture, rainfall intensity, vegetation density, and terrestrial slope. Soil erosion has not been included in other Hg models that considered other habitat or geology variables (Moslemi-Aqdam *et al.* 2022; Lescord *et al.* 2015; Evans *et al.* 2005).

In summary, two BN-RRMs were prepared for a total of 8 study regions. The goal of these models was to provide a spatial assessment of how Hg data (2005 - 2020) in freshwater and fish varied along the Mackenzie River and to identify the influential sources driving Hg accumulation in each region. These models are the Canadian contribution to the ARCRISK project, which was initiated to resolve an important gap in our understanding of how major freshwater tributaries are contributing to Hg pollution in the Arctic (Gundersen *et al.* 2020). The impacts on fish health, human dietary Hg exposure, and the potential catch losses of commercial fisheries are the endpoint variables for which risk probabilities were estimated. Ultimately, these models can be used to develop and compare management strategies based on their predicted influence on the endpoints (Gundersen *et al.* 2020).

Chapter 2: Methods and Review of Data Sources

2.1 Bayesian Network Models

The Bayesian Network Relative Risk models have been successfully applied to ecological risk assessments, the process of studying and predicting the threat posed to humans or ecosystems by a stressor (Landis, 2020). Bayesian Networks are particularly useful when studying complex systems with numerous influence pathways, latent variables, and competing stakeholder interests (Marcot *et al.* 2006; Kaikkonen *et al.* 2020). The primary step to BN-RRM development is conceptualizing the causal pathways and explanatory nodes (variables) which relate to the research objectives (Landis, 2020). The purpose of this project was to identify the Hg sources impacting water and biota concentrations along sections of the Mackenzie River. Following a literature search, the causal diagram was constructed with a unidirectional flow of information between the categories of Source, Stressor, Habitat, Effect, and Impact (Landis, 2020). Purposeful causal diagrams are developed in collaboration with scientists (mercury, fish biology, climate change experts) and stakeholders (industry, NGOs, local communities). The endpoints and model structure presented in this thesis were selected by scientists only and did not include industry or community stakeholders. Stakeholder involvement must be the primary focus before there is an attempt to implement these model results into a risk management strategy.

Several variables of the initial model (Figure 2) will not meet the data requirements for inclusion in the final model (Figure 3). Variables which can be included must be observable, measurable, or predictable; all other variables are removed and become part of the uncertainty of the model output (Pollino and Hart, 2008). Figure 3 shows the final model structure for the Great Slave North Arm study region. Note that several water chemistry variables have been removed,

due to: i) lack of scientific understanding of key processes; ii) no clear correlation observed in data between variables; iii) lack of spatially variable primary data on key variables. The initial model (Figure 2) included proxy variables for Hg, such as dissolved organic carbon (DOC) and total suspended solids (TSS), as well as four forms of mercury: total (THg), particulate (PHg), dissolved (DHg), and methylmercury (MeHg). The simplified model considered only THg because the dominant water monitoring dataset (Communities of the Northwest Territories, 2023) lacked monitoring data for the PHg and MeHg forms, and much (99%) of the DHg monitoring data was below the detection limit (10 ng/L).

Two significant ($p < 0.05$) relationships (Supplemental Figure 22) were observed in the freshwater monitoring data from lakes and rivers in the study area (Communities of the Northwest Territories, 2023) between DOC and DHg ($r^2 = 0.079$, $p= 3.1e^{-9}$) and TSS and THg ($r^2= 0.522$, $p= 1.4e^{-7}$). These significant relationships have been observed in other datasets (Lavoie *et al.* 2019; Bravo *et al.* 2018) and DOC and TSS have been key predictors of Hg in riverine systems (Campeau *et al.* 2022). The bulk mercury flux from the Mackenzie River is as PHg associated with other particulate matter which can be measured as TSS or as turbidity; likewise, DHg is associated with dissolved matter, principally DOC (Carrie *et al.* 2012; Leitch *et al.* 2007; Emmerton *et al.* 2013). DOC is also believed to play an important regulatory role in the formation of methylmercury, both promoting and inhibiting mercury methylation (French *et al.* 2014). A causal model for mercury would therefore have the links: DOC -> DHg -> THg and TSS -> PHg -> THg; however, the simplified model without the DHg and PHg forms would need to have a direct link from DOC or TSS to THg, which does not accurately represent the causal relationships. The DOC and TSS proxy variables were ultimately removed in the simplified model to describe the causal relationships more accurately, as well as to limit the

number of assumptions made and their contribution to the model uncertainty. Deficient understanding of the variables controlling bacterial mercury-methylation processes and the lack of primary MeHg data resulted in the removal of a key causal link between freshwater THg and fish tissue Hg. A recent publication (Moslemi- Aqdam *et al.* 2022) suggests that Hg concentrations in fish can be reasonably predicted if there is available data on freshwater MeHg, invertebrate MeHg, and sediment THg.

BN models are probabilistic and require the variables to be discretized such that nodes are described by their probability distributions across several categorical states (ie. Low/ Medium/ High) that signify their quality and effects on an endpoint (Marcot *et al.* 2006). The boundary values for these states should represent meaningful information whenever possible, such as regulatory thresholds or toxicological values (Supplemental Table 4). To populate the nodes, publicly available data was compiled from Hg monitoring programs, environmental model outputs, and GIS datasets (Supplemental Tables 1 - 3). Populated nodes display the probability distribution for the variable, while nodes that lack data and remain unpopulated will appear to have equal probability of all states (Kaikkonen *et al.* 2020). The state of these "parent" nodes is used to predict the outcome of the "child" node, a variable that the parent nodes have a perceived effect on, through the formation of conditional probability tables (CPTs) (Marcot *et al.* 2006). Case file learning, equations, linear regression models, peg-the-corners methods, and expert elicitation are commonly employed to populate CPTs (Marcot *et al.* 2006). The number of parent nodes and categorical states should be limited even when large environmental monitoring datasets are available, as these complex models will rarely have sufficient combinations of states and parent variables necessary to identify interesting dependencies (Uusitalo, 2007). In developing this model, the number of parent nodes linked to the "Freshwater THg" (4 parent

nodes in GBS model) and "Fish tissue Hg" (5 parent nodes in GBS model) effect nodes were limited to considering only the most-likely Hg sources. However, this is still more complex than is recommended for a BN model; Marcot *et al.* (2006) recommends that no more than 3 parent nodes are applied to a given variable, particularly for variables that are dependent on expert elicitation in informing the CPTs. Reducing model complexity to improve accuracy is another reason why the TSS and DOC water quality variables were not included in the simplified BN model.

Case file learning, equations, linear regression models, expert elicitation, and peg-the-corner methods (where well-defined combination of parent node states are the first to be populated) are commonly employed to populate CPTs (Marcot *et al.* 2006). Case-file learning was the primary method used to develop the causal relationships between mercury sources and effects on freshwater and fish in this project. As is standard practice (Chen and Pollino, 2012), the mercury monitoring dataset was split in two, half to be used for setting the prior probability distributions, and the other half for elucidating the cause-and-effect relationships. To confirm that the order of data upload had no effect on the model output, a second model was prepared by switching the prior-probability and case-learning datasets.

Uncertainty in system processes is explicitly defined in the CPTs and visually communicated by the width of the node's probability distributions (Kaikkonnen *et al.* 2020). For example, the wide and flat distribution of the "Fish Tissue Hg" nodes can be attributed to the high spatial variation in the data and the reliance on machine learning algorithms such as Netica's Count-Learning model (Norsys, 2009). One method of reducing model uncertainty is to expand the dataset, ideally through strategic sample collection at locations with different combinations of stressors. Once the model is parameterized, the influential explanatory variables

can be identified with an entropy-based sensitivity analysis, where entropy represents the expected uncertainty of a variable (Pollino and Hart 2008; Norsys, 2009). The sensitivity analysis quantifies the mutual information, which is the information available about a variable based on a finding at another linked variable (Norsys, 2009). The product of the Netica sensitivity analysis is a list of nodes ranked on the strength of their correlation to the dependent variable. Management nodes are then inserted into the BN-RRM to target these influential variables, and the optimal management strategy can be selected with consideration to uncertainty (Pollino and Hart 2008; Kaikonnen *et al.* 2020).

The strength of Bayesian Network models over other statistical models is that they allow for counterfactual analysis- the exploration of realities which have not occurred. They thus allow for questions such as "If there were low levels of atmospheric deposition over this area, how would this impact the distribution of the downstream nodes? What would be the expected effect on fish tissue concentrations?". Since it is difficult to perform a controlled experiment on the effect of atmospheric Hg deposition on fish Hg concentrations, developing these relationships using Netica's Count Learning algorithms can help predict and compare the impact of various management strategies, such as the Minamata treaty (Norsys, 2009). The ability to perform counterfactual analysis makes BN uniquely qualified to examine various management scenarios and predict how further stress will impact the downstream variables (Pearl and Mackenzie, 2018).

2.2 BN-RRM Category- Sources

Variables that represent potential Hg sources were characterized as point or non-point sources. The Hg sources which were considered in this model are: i) proximity to oil and natural gas extraction and exploration facilities; ii) proximity to historic and recent mining; iii) proximity to permafrost thaw slumps; iv) terrestrial to aquatic Hg transfer by rainfall-induced soil erosion; v) atmospheric deposition (GEM-MACH-Hg model); vi) permafrost thaw release into aquatic ecosystems (SiBCASA-Hg model). The impact of forest fires on mercury was included as part of the atmospheric Hg deposition environmental models and in the estimation of rainfall-induced soil erosion. The next chapter will describe these sources, their discretization, and how their presence varies between the study areas.

2.2.1 Fossil fuel developments:

Fossil fuels (coal, oil, natural gas) contain trace amounts of metals, including mercury (Hollebone and Yang, 2007). There are several pathways for Hg release from fossil fuel exploration and processing. Mercury is volatilized during oil refinement, and this gaseous Hg can contaminate processing equipment, poison chemical catalysts, and even be a health hazard to maintenance workers (UNEP, 2022). Fossil fuel exploration and well-drilling can erode soils, resulting in mass nutrient and carbon runoff into freshwater following rainfall events. Organic carbon (OC) forms stable complexes with inorganic Hg, thereby increasing the freshwater THg input (Littlefair *et al.* 2017; St. Pierre *et al.* 2018). Natural gas exploration may use a combination of drilling and acid fracturing, which uses acid water to dissolve carbonate salts and produces Hg enriched wastewater (UNEP, 2022). Leaching from improperly stored waste may also contaminate soils and groundwater. In the NWT there are concerns about the industrial waste frozen in mud sumps, which are hollow pits in permafrost regions (Kokelj and GeoNorth

Ltd., 2002). The mobilization of this previously frozen waste is a major potential source of Hg in permafrost regions experiencing climate warming.

The location of the 257 fossil fuel exploration and production areas in the NWT were obtained from the GNWT servers (GNWT Centre for Geomatics: Oil and Gas Resources, 2022). These sites can be grouped into four regions: Ikhil, Norman Wells, Fort Liard, and Cameron Hills (INAC, 2009; GNWT, 2015; CIRNAC, 2022). Oil and gas production has steadily declined during the 2005-2021 period (Figure 12). Following the closure of the Cameron Hills production facilities in 2015, Norman Well's has been the sole location of oil production (CIRNAC, 2021). Many sites in the NWTs are under a Significant Discovery Licene. This grants the company exclusive rights over the well-drilling, petroleum exploration and testing, and allows for the development of the area for production (Harrison, 2016). There are few areas with an active Production Licence- two in the Ikhil region (owned by MG Energy and AltoGas Ltd.), six in Fort Liard (owned by Paramount Resources Ltd. And Canadian Natural Resources Ltd.), and fifteen in the Cameron Hills region (owned by Strategic Oil & Gas Ltd.).

A study by Kelly *et al.* (2010) collected freshwater and snow samples at numerous (> 30) sites along a 200km transect of the Athabasca River, both upstream and downstream of major oil sands developments in the Athabasca subbasins of the MRB. The results showed that surface waterbodies located near the Athabasca Oil sands had significantly higher Hg concentrations at distances <50 km from the bitumen upgrading facilities (THg concentrations of 1.5 – 5.4 ng/L at sites near disturbances, and 0.7 – 1.8 ng/L at distant sites). However, none of the measured concentrations exceeded the CCME guidelines for the protection of aquatic life (CCME, 2007). Additionally, Wasiuta et al. (2019) used an Inverse Distance Weighting model which predicted higher atmospheric deposition rates of THg and MeHg to watersheds in a 50-km radius from Oil

Sands smelters, but again this study did not measure any freshwater THg concentrations which exceeded regulatory guidelines (CCME, 2007). Kirk *et al.* (2014) sampled snowpack at 89 sites and a maximum of 200 km from major roaster stacks in the Athabasca Oil Sands and confirmed the findings from Kelly *et al.* (2010) that atmospheric mercury deposition from local source decreases at distances > 50km. However, the authors note that maximum deposition was observed at sites within 20 km from the roaster stacks. Finally, Cooke et al. (2017) measured sediment cores from lakes at varying distances of 10- 108 km from the Athabasca Oil Sands developments. While THg concentrations did not vary significantly with distance from the smelters, the Cooke et al. (2017) study did characterize lakes as being near-field (< 20 km), mid-field (20 km – 50 km) or far-field (> 50 km), further supporting the use of 50 km as an appropriate value with which to discretize the fossil fuel developments source node. Freshwater or fish sampling locations that were within 50 km of an active Oil and Gas licence were classified as being near this point source. Note that in the dataset there were only two fish sampling sites, both located in the GBS North study region, near an active oil or gas claim; lake trout were the only fish harvested at these locations. Comparison of the mercury concentrations (Figure 1) with the location of oil/ natural gas facilities (Supplemental Figure 12) showed that freshwater THg concentrations were not elevated above the regulatory guidelines for the protection of aquatic life (26 ng/L) in the vicinity of the fossil fuel developments.

2.2.2 Mining developments

There are four operational mines (3 diamond mines, 1 tungsten mine) in the NWT, as well as 81 decommissioned mines, 48 of which were gold mines (MRBB 2003; Silke, 2009). Historic gold mining practices utilized Hg to extract and concentrate gold ore (Yoshimura *et al.* 2021). Many of the historic mines in the study area were small-scale producers or exploratory

expeditions which were decommissioned or abandoned prior to the 1980s (Silke, 2009). However, four of these gold mines had processed over 1 million tons of ore each during their period of operation. These are the Colomac, Con, Discovery, and Giant mines; all are in the Great Slave North sub-subbasin (Figure 13). There is also the Eldorado uranium mine which was in production from 1931-1981 and was located on the east shores of Great Bear Lake (Silke, 2009).

Of the four mines that are currently in operation, none require Hg for the industrial process, and no Hg has been reported in the mining effluent (EMAB Diavik Project, 2020). A literature review shows that concentrations of total suspended solids, arsenic, mercury, and sulfide concentrations were elevated in lake sediments at Pocket Lake, located 1km from the Giant mine (Thienpont et al. 2016). Furthermore, Houben *et al.* (2016) showed that freshwater arsenic concentrations exhibited a significant negative relationship with distance from a mine roaster stack; concentrations drastically decreased from >100 µg/L to 2 µg/L at distances greater than 17 km from Giant Mine in Yellowknife NWT, one of the most heavily polluted mining areas in Canada. Freshwater THg concentrations did not show the same trend of decreasing concentrations with increased distance from mining activities. Additionally, with THg concentrations ranging from 0.5 – 2.4 ng/L, none of the freshwater samples exceeded CCME (2003) inorganic mercury guidelines for the protection of aquatic life. However, the study did find elevated MeHg:THg ratios, which can be an indication of inorganic mercury methylation rates, with an average of 22.4 % (Houben *et al.* 2016, Table S3) at lakes within 15 km (% MeHg:THg range from 9.4% - 67%) to the Giant Mine roasters, which is drastically higher than the natural background % MeHg:THg ratios of ~1% (Schaefer, 2020; Houben et al. 2016). Mean methylation ratios % MeHg:THg in lakes from 15 – 25km of the roaster stacks were ~ 8.5%,

ranging from 1.3 % - 31 %. While the Houben et al. (2016) study did not find significant trends between freshwater THg concentrations and distance to the mines, these trends were apparent for arsenic and MeHg formation.

Mining locations were grouped into two types: historic mining and active mining claims. Historic mines range from small exploratory and producing mines (many of which were closed prior to 1950) to the four advanced-production gold mines (Silke, 2009). Active mines are those for which active mining claims or mineral leases are present (GNWT Centre for Geomatics. Mineral Claims Mineral Tenure Data, 2022). There are also two states to each of the mine proximity source nodes: Below 15 km and above 15 km. Mercury concentrations from sample sites (<15 km) near mining sources were compared to the Hg measurements within the same study region which are not near mining sources (> 15 km). Netica Count-Learning algorithms (Norsys, 2009) was used to predict the effect of mine proximity on Hg concentrations in freshwater and fish of the Great Slave Lake region.

2.2.3 Permafrost thaw slumps

Permafrost is a layer of soil that remains frozen year-round. Permafrost extends through much of the study area, although the permafrost continuity varies significantly (Bouchard *et al.* 2016; Palmer *et al.* 2008; MRBB, 2003). In the southern portions of the basin, permafrost is either absent or is found in discontinuous and sporadic patches (Palmer *et al.* 2008). In the north, the permafrost is thicker and classified as continuous, although there are signs that permafrost thaw is occurring in these regions (Chételat *et al.* 2022; Lantz *et al.* 2008; St. Pierre *et al.* 2018). The loss of the ice-rich layer, which is stabilized against soil erosion, results in the subsistence of soil and the formation of thermokarst, a wetland landscape characterized by irregular hollows (St. Pierre *et al.* 2018). Retrogressive thaw slumps are a type of rapid erosion event caused by

slope failures around the edges of thermokarst lakes. Retrogressive thaw slumps can be initiated when permafrost is exposed, increasing its susceptibility to erosion (Lantz *et al.* 2008; Burn and Leqkowicz,1990). Additional stressors of thaw slumping include soil erosion, flooding, wildfires, construction, or mining (Burn and Leqkowicz, 1990). Retrogressive thaw slumps are common in Canada's northwest regions, particularly in deltas and at the confluence of rivers (Burn and Leqkowicz, 1990). The wasting of these thaw slumps creates an influx of sediment and carbon-rich soil into aquatic ecosystems, impairing the water quality (Kokelj *et al.* 2021).

A recent study has mapped the location of permafrost thaw slumps in the Great Bear subbasin study area, with a focus on the Peel Plateau and Mackenzie Delta in the northern study regions (Kokelj *et al.* 2021). This map does not include the "Great Bear South" study region, which is characterized by a lack of permafrost soil (Palmer *et al.* 2008). The Gwich'in Indigenous community located near the confluence of the Peel and Mackenzie Rivers have reported concerns over riverbank erosion and heavy sediment loads in freshwater (Parlee and Maloney 2016; Littlefair *et al.* 2017). Increased sediment loads correspond to increased inputs of ubiquitous metals which are associated with organic carbon, such as mercury (St. Pierre *et al.* 2018). A recent study in the Peel Plateau recorded some of the highest THg and MeHg concentrations (range of 1.9 – 1270 ng/L and 0.16 – 7.6 ng/L respectively) in unfiltered freshwater samples from a minimally impacted freshwater study sites. Freshwater THg concentrations were elevated downstream of retrogressive thaw slumps (mean THg of 448 ± 87 ng/L) compared to upstream concentrations of 5.56 ± 1.13 ng/L (St. Pierre *et al.* 2018). Thermokarst landscapes such as the Mackenzie Delta have been identified as hot spots for mercury methylation (Jonsson *et al.* 2022; St. Pierre *et al.* 2018) as it is hypothesized that the

continuous nutrient and carbon input from sediment influx and the subsequent anoxic conditions create an ideal environment for mercury-methylating bacteria (Jonsson *et al.* 2022).

The recent retrogressive thaw slump mapping project (Kokelj *et al.* 2021) also developed the slope thermokarst inventory (STKI) of waterbodies impacted directly or downstream of active slumps. This dataset was used to select the waterbodies for which Hg is a potential stressor (Figure 12). Sampled lakes within 10 km of a waterbody included in the STKI dataset (Kokelj *et al.* 2021) were classified as being "Near" this point source; however, this distance was arbitrarily selected and is likely overestimating the distance at which permafrost thaw slumps are expected to affect waterbodies. Note that for the fish monitoring dataset, only three of the sampling sites were near a permafrost thaw slump, and all were within the GBS North study region.

2.2.4 Proximity to Great Slave Lake (GSL) outlet

While mining developments are not included in the Great Bear BN-RRM, historic and active mining on Great Slave Lake may have elevated Hg concentrations relative to surrounding waters. Great Slave Lake is a major tributary of the Mackenzie River and may be a relatively large Hg source. To determine if freshwater and fish Hg concentrations near the GSL outlet are elevated relative to further downstream the Mackenzie River, a 50 km buffer was delineated around the outlet of Great Slave Lake (Supplemental Figure 13, coordinates: 61.362638, -117.832952). Sampling sites that fell within this buffer zone were categorized as "Near" the GSL Outlet. Fish mercury concentrations near the GSL outlet were elevated (> 0.5 ug/g ww, Figure 1), but this trend does not hold for the freshwater lake and river monitoring data (Figure 1).

2.2.5 Permafrost Thaw and Hg release

Mercury in the Arctic originates from lower latitudes, from industrial sources which release gaseous elemental mercury (GEM) (Fraser *et al.* 2018). GEM is relatively unreactive and can persist in the atmosphere for upwards of a year, allowing sufficient time for transport to the Arctic via atmospheric transport (Dastoor *et al.* 2015). The direct deposition of GEM, also known as dry-deposition, is the dominant source of Hg to terrestrial vegetation, soil organic matter, and snowpack (Obrist *et al.* 2017). Soil carbon dating suggests that these Hg deposition processes have been occurring over millennia, resulting in the accumulation of large Hg reserves in Arctic soils (Schuster *et al.* 2018). In permafrost-dominated zones the cold temperatures impede the microbial decay process and significantly slow the release of Hg, making permafrost a sink for terrestrial Hg (Campeau *et al.* 2022). However, as global temperatures increase and unprecedented rates of permafrost thaw are being observed, there is concern that permafrost soils could become a major source of Hg in the Arctic (Schaefer *et al.* 2020; Schuster *et al.* 2018). A global permafrost model predicted that permafrost soils store more Hg than the combined amount found in oceans, the atmosphere, and other soils (Schuster *et al.* 2018).

Permafrost thaw can result in the weathering of soil and subsequent ground-subsidence, which poses a major risk to Arctic infrastructure such as human communities and industrial developments. Global maps of geohazard risk for infrastructure development in permafrost-dominant regions are publicly available (Hjort *et al.* 2018). Additionally, permafrost thaw can increase stream flow and is believed to already have altered near-surface hydrological connections in key tributaries of the Mackenzie River (Connon *et al.* 2014). The increased hydrological connection has been linked to the conversion of forest ecosystems to wetlands (Connon *et al.* 2014). Because wetlands are hypothesized to be hot-spots of Hg methylation (Xu

et al. 2021), their expansion may result in higher seasonal concentrations of bioavailable mercury.

Schaefer *et al.* (2020) recently used the terrestrial biogeochemistry model SiBCASA to estimate the Hg released by thawing permafrost in the Yukon River Basin, which is adjacent to the Mackenzie River Basin. This study also produced global maps of two permafrost-thaw driven Hg evasion pathways: atmospheric evasion, and leaching into groundwater to be exported by rivers. For the second pathway, the model assumes that all Hg to be exported to rivers is immediately transported to the river mouth. The model makes several other key assumptions that should be highlighted. First, based on a large dataset of ~11,000 soil samples across North America, it assumes that Arctic soils have a mercury-to-carbon ratio of 1.6 +/- 0.9 g Hg/ kg C, thereby assuming a linear relationship between the organic carbon and the mercury found in Arctic soils. Second, the model assumes that 1.5% of the Hg mobilized during permafrost thaw is exported to the aquatic ecosystem as dissolved mercury (DHg), and that 1% of this DHg will be methylated to MeHg. However, observational field studies suggests that the percentage of total mercury that is MeHg (%MeHg : THg) can be elevated in lakes impacted by soil erosion, such as the lakes near permafrost thaw slumps or mining sites (St. Pierre *et al.* 2018; Houben *et al.* 2016). Finally, it does not consider how warming temperatures impact riverine discharge and local hydrology. The numerous model assumptions, high model uncertainty (58% - Schaefer *et al.* 2020), and low spatial resolution are some of the limitations of utilizing the SiBCASA mercury model output in this project. Nonetheless, environmental models represent our current best state of knowledge for complex systems, and their output is necessary to conduct a spatial risk assessment over a large, remote, and relatively under-sampled study area like the Mackenzie River Basin.

The SiBCASA model (Schaefer *et al.* 2020) was used to estimate monthly mercury (DHg) fluxes (ng/m^2) from soil to aquatic ecosystems over the 2004- 2020 study period, which were then summed to produce maps of annual Hg flux using ArcGIS (Supplemental Figure 14). The model predicted significant seasonal variation but not significant interannual variations. This is expected because the model was developed to predict permafrost-thaw Hg emission over a 300-year period under two climate change scenarios where differences in temperature and precipitation trends become significant only when comparing distant time points. While there was significant seasonal variation which would be interesting to explore further, this would require seasonal fish and water sampling data that was not available in our dataset. Annual flux values were used to populate the "Permafrost Hg Release" node of the BN-RRM (Supplemental Figure 14). Due to a lack of regulatory policy and thresholds, the discretization of this node was based on the range of permafrost thaw values over the study area. Therefore, the node states do not represent management goals or toxicological thresholds. The node was discretized into 6 categories: 0 ng/ m^2*yr ; 0- 2 ng/ m^2*yr ; 2- 4 ng/ m^2*yr ; 4- 6 ng/ m^2*yr ; 6- 10 ng/ m^2*yr ; and >= 10 ng/ m^2*yr. The first category of 0 ng/ m^2*yr represents the southern regions of the study area which are free of permafrost (Supplemental Figure 14). There is no direct link between the "Permafrost Hg Release" node and the "Freshwater THg" and "Freshwater Fish Tissue Hg" effect nodes; rather, the Hg release rate of the three non-point Hg sources (atmospheric Hg deposition, permafrost thaw Hg release, soil erosion Hg release) were summed to produce a "Total Annual Mercury Input" node, which was then connected to the nodes in the Effect BN-RRM category.

2.2.6 Atmospheric Hg deposition

The Minamata treaty was established in 2017 as a policy to reduce global Hg anthropogenic emissions. The highest emissions are believed to originate from industries in East and Southeast Asia (ECCC, 2020) with coal combustion and small-scale artisanal gold mining (AMAP/ UNEP, 2015) being the major sources. Atmospheric Hg is the sum of three forms: Gaseous elemental mercury (GEM), gaseous oxidized mercury (GOM) and particle bound mercury (PBM). Of the three, GEM is the least soluble form and persists in the atmosphere for 6-24 months (Dastoor *et al.* 2015), allowing for the pollutant to be dispersed throughout the globe prior to deposition. GOM and PBM are more prevalent near the industrial sources (Fraser *et al.* 2018). Modelling studies have revealed a spatial correlation between regions of high Hg deposition and elevated Hg in seawater (AMAP/UNEP, 2015). In Canada, over 95% of the deposited anthropogenic Hg originates from other countries (Fraser *et al.* 2018), and since the closure of the last chlor-alkali hg cell plant in 2008, Canada has no domestic industries that utilize mercury (Canada Gazette, 2019). Thus, in Canada, and especially in the Canadian North, global management initiatives such as the Minamata treaty are necessary to reduce Hg deposition levels since domestic industries are not the major input.

Mercury deposition to the study region was estimated using Environment and Climate Change Canada's primary Hg model, GEM-MACH-Hg (Global Environmental Multi-scale, Modelling Air quality and Chemistry model, mercury version) (Dastoor *et al*. 2015), which was then used to populate the "Atmospheric Hg Deposition" node. The key Hg cycling factors in the GEM-MACH Hg model include anthropogenic Hg emissions, Hg emissions from wildfire events, dry and wet (precipitation driven) deposition rates, the impact of gas phase oxidization on deposition rates, and post-Atmospheric Mercury Deposition Event (AMDE) re-emission of Hg

from the snowpack (Dastoor *et al.* 2015). The GEM-MACH model outputs included in the BN-RRM presented here were spatial predictions of the annual net total mercury (THg) deposition ($ng/m^2/yr$). Like the permafrost thaw Hg release node, an average annual flux was calculated in ArcGIS and used to generate the distributions for the BN-RRM (Supplemental Figure 14). Note that the uncertainty associated with the GEM-MACH-Hg and the SiBCASA model outputs were not integrated and propagated in this BN-RRM. Additionally, the discretization of the "Atmospheric Hg Deposition" node represents the distribution of atmospheric deposition values and not a management goals or experimentally obtained threshold. The Atmospheric Hg deposition node is linked to the freshwater and fish tissue effect nodes via the "Total Annual Mercury Input" node, which includes the model outputs for permafrost thaw and soil erosion mercury release.

2.2.7 Estimating Hg release due to rainfall-induced soil erosion

The soil erosion calculation required the K-factor (soil erodibility/ texture), R-factor (rainfall intensity), C-factor (vegetation density), and LS-factor (topographic/ slope) variables. For details about the calculation of these factors and the soil erosion potential, see the Stressors and Habitat sections.

The erosion potential and soil Hg variables were combined to estimate the release of Hg from soils into nearby surface waters. First, the carbon maps developed by Sothe *et al*. (2022) were combined with the methods described by Schuster *et al.* (2018) to estimate the concentration of Hg at soil depths of 0cm and 5cm (Supplemental Figure 16). Briefly, the carbon content of soils (measured as g Carbon/ kg soil) is multiplied by a Mercury-Carbon ratio (Schuster *et al.* 2018) to produce a soil mercury map. The Mercury-Carbon ratios are not expected to differ with soil type, depth, and age (Schuster *et al.* 2018) with studies conducted on

northern permafrost soils of Alaska and the Yukon River finding Mercury-Carbon ratios of 1.6 ± 0.9 g Hg/ kg C (Schuster *et al.* 2018, Schaefer *et al.* 2020).

At each of the sampling locations, the freshwater Hg was calculated as the product of the soil Hg concentration, the erosion potential (converted to standard units of g m^{-2} yr^{-1}), the resolution of the erosion potential GIS layer (Supplemental Table 3), and the time period over which erosion was calculated. A set time of 1 year was used to determine the annual load of Hg into surrounding waterbodies. The soil released during erosion processes travels to nearby waterbodies, including the waterbody sample sites for which water or fish Hg measurements are available. A polygon was created for each sample site waterbody and the erosion potential values within the shape were summed, and then divided by the waterbody area. These ratios were used to compare the annual erosion input between sampling sites. This method assumes that the Hg released from erosion processes are equally distributed to nearby surface waters. Based on modelling work by Schaefer *et al.* (2020), only about 1.5% (0.015) of Hg released from erosion enters surface waters, which is reflected in the equation below. The final units of this calculation are the annual mass (ug) of Hg released per square meter, which is identical to the units from the SiBCASA (permafrost thaw) and GEM-MACH-Hg (atmospheric deposition) models.

Concentrations of mercury in waterbodies impacted by soil erosion (g/L) were calculated using Hg concentrations in soil (ug Hg/kg soil), the soil erosion potential (kg*m^{-2}*yr^{-1}), and a temporal period (year):

Equation 1: $$[Hg]_{water} = [Hg]_{soil} * Erosion\ Potential * Time * 0.015$$

Similar to the other non-point sources, no regulatory policy or management thresholds were available to guide the node discretization of the "Soil Erosion Hg Release" node. Instead, the discretization represents the distribution of calculated values. The "Soil Erosion Hg Release" node was also linked to the effect nodes via the "Total Annual Mercury Input" node.

2.2.8 Mercury sources not included in the BN-RRM

Logging and the construction of dams for hydroelectricity production were also considered in the initial model (Figure 2) but were not included in the final iteration as detailed below.

The creation of reservoir areas for large dams has numerous undesirable social and environmental consequences, including involuntary resettlement of local communities, interrupted wildlife migrations, and altered hydrological regimes (Baird *et al.* 2021). Damming creates changes in river and sediment flow, causing decreased inputs of dissolved organic matter, oxygen, and nutrients (Maavara *et al.* 2017). The flooded soils and degradation of submerged organic matter results in anoxic environments favourable for mercury-methylating bacteria and will accelerate the formation of methylmercury. Methylmercury concentrations tend to spike 1-3 years following dam construction and return to background concentrations after ~10-20 years (Calder *et al.* 2016). Additionally, the construction of dams, or the act of dam peaking (where dams are only run during periods of high electricity demands) resulting in flooding and higher water levels and increasing the potential of soil erosion, which is one of the Hg input pathways considered in this project.

There are three hydroelectric facilities in the NWT, located at Yellowknife (Bluefish Hydro), Fort Smith (Taltson Hydro) and along the Snare River (Figure 14) which utilize

reservoirs. The Taltson Hydro dam constructed in 1966 and the rebuilding of the Duncan Lake dam (Bluefish Hydro facility) in 1974 were the most recent activities which would have required flooding. Further hydroelectric developments have been proposed for at La Marte River falls and at Lutsël K'e on the eastern side of Great Slave Lake, but there is no flooding required for the construction of these run-of-the-river facilities (GNWT, 2019; Mackenzie Valley Review Board, 2010). The proposed developments may have negligible impact on Hg release (Calder *et al.* 2016), but they are expected to adversely affect caribou populations and alter flow regimes at culturally significant sites for the Lutsël K'e Dene First Nation (Mackenzie Valley Review Board, 2010). The hydroelectric system at Fort Smith has the largest capacity at 18 megawatts (MW), although there is a recent proposal to expand the facilities to 80 MW (GNWT Industry, 2019). This will be accomplished by connecting to the North and South Slave electrical systems, but this proposal remains in the planning stages and requires more than 1 billion dollars in investments (GNWT Industry, 2018). There are currently no reports that indicate additional flooding will be necessary, as the Taltson hydroelectric plant has a maximum capacity of 200 MW. Because no additional flooding for hydroelectric power generation has been proposed in the NWT, this point source variable was not included in this model.

Like the wildfire node (Chapter 2.3.4), the effect of logging on soil erosion can also be used to approximate Hg release from terrestrial sources into surface waters. However, the literature search revealed that there are currently no commercial logging companies operating in the NWT (GOC, 2022). Any disturbance from logging should be attributed to subsistence wood harvesting for use as a heating and fuel source for remote Northern communities. The National Forestry Database estimates that annual logging harvested area for the entire NWT varies between 80-460 hectares, taking place on provincial land and using a seed tree harvesting

method (National Forestry Database, 2020), not a clearcut method. Clearcutting has not been practiced on NWT Provincial land since 2011; prior to this approximately 60 hectares were clearcut logged annually. Clearcut logging has more significant effects on the soil erosion potential because the disturbed bare soil has a higher C-factor. The NWT logging industry harvests less wood than all other provinces except for Nunavut and the Yukon. Most of this harvested wood (> 95 %) is classified as softwood; softwood tree species that grow in the NWT include White/ Black spruce, Jack pine, Subalpine fir, and Tamaracks (Bohning *et al.* 1997). Thus, logging activities in the NWT are sparce and not expected to have a significant impact on soil erosion or terrestrial Hg release and the logging variable was removed from the final model iteration.

2.3 BN-RRM Category: Stressors

The second category in the BN-RRM framework are the stressors which are the ecosystem variables which impact the probability distribution of a discretized continuous node. The stressors were grouped as abiotic (soil erosion, wildfire, and riverine flow variables) or biotic (fish length and dietary intake). The following section is a detailed discussion of the stressor variables.

Abiotic Stressors:

2.3.1 Soil Erosion Potential

The Mackenzie River is the largest source of sediment and organic matter to the Arctic Ocean (Rachold *et al.* 2000; Vonk *et al.* 2015). Erosion, sediment transport, and deposition are the three stages of the sedimentation cycle. In the Arctic the common forms of erosion are rainfall-induced erosion (Lamoreux, 2000), wind-erosion (Heindel *et al.* 2015), coastal erosion

(Nielsen *et al.* 2022), streambank erosion (Vonk *et al.* 2015), and rapid mass-movement events such as landslides or thaw slumps (Lumb *et al.* 2006; Lantz and Kokelj 2008). Communities throughout the Mackenzie River Basin have observed increased riverbank erosion, the presence of sandbars indicating greater sedimentation, decreased water levels, and altered hydrologic connectivity which have impacted water quality and riverine travel (MRBB, 2021; Parlee and Maloney, 2016; Parlee *et al.* 2019). Regions where sedimentation is of particular concern include the tributaries to Great Slave Lake (MRBB 2021), the enlargement of the artificial islands at Norman Wells constructed for oil-production (Carson, 1987; Lamberink, 2022), and in the Mackenzie Delta upstream of the Beaufort Sea (Parlee and Maloney 2016; Parlee *et al.* 2019). Mercury forms strong bonds with organic matter and elevated concentrations of Hg have been observed in thermokarst lakes impacted by sedimentation (Lavoie *et al.* 2019; St. Pierre *et al.* 2018). Therefore, the sedimentation cycle and soil erosion were included as a potential source of Hg to the Mackenzie River.

Many models have been developed for the estimation of soil erosion rates and remote GIS-driven methods have been an active area of research for decades (Hrabalíková and Janeček, 2015; Borelli *et al.* 2016). However, there is currently no Canadian model for soil erosion and no measurements of soil-loss over the project study area. Infrastructure and agricultural projects in Canada do account for soil erosion potential, which is primarily calculated using the Revised Universal Soil Loss Equation (RUSLE) method (Wall *et al.* 2002, GNWT Department of Transportation, 2013). The RUSLE model was developed to predict the rate of rainfall-induced soil erosion, and it considers several key habitat variables which were of interest to this project. The following paragraphs will include an in-depth discussion of how these stressor and habitat variables were quantified, the model assumptions, and sources of uncertainty.

Natural erosion resulting from rainfall can be modelled using the RUSLE Revised Universal Soil Loss Equation (GNWT Transportation, 2013) using rainfall intensity, soil erodibility (also known as soil texture), a topographic factor, and a vegetation density factor:

Equation 2: $$A = R * K * LS * C * P$$

A = erosion, measured as annual soil loss (tonnes ha^{-1} yr^{-1})

R = Rainfall factor (MJ mm ha^{-1} yr^{-1}) which represents rainfall intensity

K = The soil erodibility factor (tonnes hr MJ^{-1} mm^{-1}) determined by the soil texture

LS = The topographic factor (unitless), calculated from slope length and steepness

C = Vegetation and Management factor (unitless)

P = Support practice factor (unitless)

The best-practices P-factor was assumed to be equal to 1 throughout the study area because there is insufficient Canadian data available to predict P-factor values. This factor is primarily applied when estimating soil erosion for agricultural areas where erosion-control measures have been implemented (Wall *et al.* 2002). The erosion potentials are categorized into several risk categories ranging from Very Low to Very High (GNWT Transportation, 2013) and these category thresholds were used to discretize the node (Figure 3, Supplemental Figure 16, Supplemental Table 4). This calculation of soil erosion potential relied only on GIS datasets and represents a theoretical model of erosion. Some erosion factors, such as rainfall intensity, have been interpolated over the study area and are not an accurate representation of local conditions.

Monitoring studies of soil loss must be developed to quantify the accuracy of this model (Schmidt *et al.* 2019).

2.3.2 Rainfall Intensity (R-factor)

Rainfall intensity has been measured for select sites in the NWT, which are reported in the NWT Department of Transportation (2013) Appendix. The raw data for precipitation intensity was downloaded from the Open Canada Short-duration Rainfall intensity-duration-frequency dataset (Canada Open Government, 2015). Precipitation monitoring is scarce in the NWT; with only 8 climate stations, many of the sampling sites are in locations where rainfall intensity data is lacking. Modern precipitation data (temporal range of 2005-2017) from 46 climate stations across the Canadian North was compiled and the ArcGIS tool "Empirical Bayesian Kriging Interpolation" was applied to estimate the R-factor over the study area. A separate layer was produced for each year, which were then averaged to produce a map with generalized precipitation trends and intensities (Supplemental Figures 15 and 20). The result is a map with high precipitation intensity (> 300 MJ mm ha^{-1} yr^{-1}) in the west and south regions of the study area; the lowest intensities were observed in the Great Bear North and Great Bear East study regions (Supplemental Figure 15). The resolution of this raster layer was 250 m.

2.3.3 Vegetation Density (C-factor)

The C-factor represents the vegetation density and describes the stabilizing effect that vegetation has on soil integrity. The C-factor is estimated from the Normalized-Difference Vegetation Index (NDVI). The NDVI is calculated using satellite imagery data of visible and near-infrared light, by accounting for the fact that healthy vegetation and sparse vegetation have different reflection ratios for each wavelength class (NASA Earth Observatory, 2000). C-factor

values close to 0 correspond to dense and healthy vegetation, while values of 1 represent bare soil. Water features will also be assigned a high value close to, or above, 1. To calculate C factor from NDVI, the following equation was used (Oliveira, 2015):

Equation 3: $$C = e^{\frac{-2*NDVI}{(1-NDVI)}}$$

The expected C-factor value for undisturbed forests was ≤ 0.01 (Borelli *et al.* 2016), while regions recently affected by wildfire are typically assigned values as high as 0.4 (Depountis *et al.* 2020) and cities with paved roads are assigned values of 0.05 to account for the stabilizing effect of gravel (GNWT Transportation, 2013). The C-factor values calculated were higher than these expected ranges, with most of the samples in our study area having a C-factor values of 0.4 – 0.6 (Supplemental Figure 15). However, a study in the Himalayan Arctic reported similar C-factor values (Mu *et al.* 2020) calculated by the RUSLE method. The high calculated C values for the Arctic region may be due to the use of α and β values which were developed to simulate European climate conditions (Oliveira *et al.* 2015). The Arctic climate is unique, and the vegetation is dominated by smaller shrub-like vegetation rather than the dense forests of mainland Europe. The C-factor values are likely being overestimated across the study area; if a C-factor calculation for Arctic regions is developed in the future, this may provide a more accurate estimate of soil erosion.

2.3.4 Wildfire effect on Soil Erosion

Beyond being an essential component of the RUSLE soil erosion equation, the C-factor has also been applied in wildfire erosion research (Borelli *et al.* 2016; Depountis *et al.* 2020). Wildfires will reduce the vegetation density, increasing the C-factor and the susceptibility of the soil to rainfall-induced erosion. Wildfires are common across the study area, particularly in the

southern regions and around Great Slave Lake (Scholten *et al.* 2021). Wildfires and the burning of carbon-rich fuels release GEM that can travel long distances before deposition (Fraser *et al.* 2018). The GEM-MACH-Hg model (see previous Atmospheric non-point source discussion) includes wildfire-derived Hg in the model output for atmospheric Hg deposition. The model of soil erosion therefore also accounts for the effect of wildfires on the C-factor. The location of wildfires (from 2001 – 2018) in the Northwest territories was obtained from Scholten *et al.* (2021). This dataset is in the form of a point-layer with only the wildfire year data available. A detailed dataset by French *et al.* (2020) was also used to determine whether wildfire intensity influenced the C-factor value; this dataset was temporally and spatially limited to the 2014-2016 period and the Great Slave Lake region. Supplemental Figure 19 shows the locations of wildfires from both datasets. A spatial join was performed in ArcGIS between the C-factor layers and the wildfire locations from the former dataset (Scholten *et al.* 2021) to produce a point-layer dataset of wildfire locations which included C-factor values from the 2013- 2021 period. Statistical analysis showed that the C-factor does significantly increase [French *et al* 2020*:* $F(1, 128) = 67.86$, $p = 1.77e^{-13}$); Scholten *et al*. 2021: $(F(1, 4420)= 2290$, $p < 2e^{-16}$] following a wildfire year in both datasets. Following 3-years of recovery, the C-factor is still elevated but no longer drastically different from pre-fire values. Supplemental Figure 23 shows results for the French *et al*. (2020) dataset. For the Scholten *et al.* (2021) dataset, the mean C-factor value was highest on the year of the wildfire (0.65 ± 0.14), followed by three-years post fire (0.59 ± 0.11). The post-wildfire C-factors were greater than the values from the year prior to the fire (0.50 ± 0.11).

After confirming that wildfire occurrence will lead to an increase in the C-factor values, the Scholten *et al*. (2018) wildfire point locations (3296) were used to generate count data distributions of the C-factor ratio (C-factor post-fire: C-factor pre-fire) for Year 0 (year of

wildfire) and Year +3 (3 years post-wildfire). These ratios were input into the Bayesian Network model to calculate an "Adjusted C-factor" that predicts how the C-factor would change in an area affected by fires. When using the model in the Netica software, the effect of wildfires on erosion can be removed by selecting "No" in the "Wildfire Event?" node.

Using the detailed French *et al.* (2020) dataset, wildfire intensity was also found to influence the C-factor value post-fire (Supplemental Figure 23). Regions of high-intensity fires did have significantly higher C-factor values than regions of very low intensity; however, there were low-intensity and medium-intensity fires which saw similar C-factor shifts as the high-intensity locations. Since no clear statistically significant relationship could be derived from the one detailed dataset presented in French *et al.* (2020), the "Wildfire Intensity" node was not included in the Bayesian Network model. Any relationships that were found from the French *et al.* (2020) dataset would likely not be applicable to the far north regions of the study area due to differences in vegetation type and growth rates.

2.3.5 Permafrost effect on Soil Erosion

An adjustment to soil erosion for the stabilizing effect of permafrost was considered. Conversely, permafrost thaw can reduce soil stability and is accentuated by the heat-inductive effects of infrastructure like roads and buildings (Hjort *et al.* 2018). The effect of permafrost and permafrost thaw on soil erosion is not well characterized, and no soil erosion equation has been developed for Arctic permafrost regions. The NWT government recommends that the soil erodibility factor be adjusted by a factor of 0.8 in regions without permafrost (GNWT, 2013). This adjustment was not utilized in this project because it does not account for rate of permafrost thaw, the permafrost continuity, or the active layer depth; these factors vary throughout the study area and are expected to influence soil erosion rates. Further fundamental soil erosion modelling

studies are needed in Arctic tundra and permafrost-dominant ecosystems to improve soil loss estimates.

2.3.6 Riverine Discharge

The Mackenzie River is the 4th largest source of freshwater into the Arctic Ocean, preceded by the Yenisey, Lena and Ob rivers in Russia. The Mackenzie River is the Arctic Ocean's largest riverine source of organic carbon (Vonk *et al.* 2015; Emmerton *et al.* 2013; Rachold *et al.* 2000). Additionally, with an annual Hg flux of approximately 2 tons THg, it is also the largest mercury source to the Beaufort Sea (Leitch *et al.* 2007). Freshwater THg concentrations are the sum of the dissolved and particulate phases; dissolved mercury (DHg) is bound to dissolved organic carbon (Schuster, 2018), while particulate mercury (PHg) is strongly bound to suspended sediment (Dittman *et al.* 2010). Particulate bound Hg is the dominant phase of Hg in the Mackenzie River, corresponding to 78- 87% of the total Hg flux in the basin (Leitch *et al.* 2007; Emmerton *et al.* 2013). The particulate-bound Hg is mobilized by terrestrial erosion, with the majority (88%) originating from the erosion of natural coal deposits (10%) and weathering of the sulfide-enriched bedrock (78%) of the Cordillera ecozone mountain ranges (Carrie *et al.* 2012). The ARCRISK project is a circumpolar project that aims to understand how rivers contribute to Hg in the Arctic Ocean. The purpose of the riverine discharge nodes was two-fold: to support the inclusion of a "Mercury input into the Beaufort Sea" endpoint, and to identify another pathway by which climate change may impact Hg release.

Riverine flow rates were obtained from Canada's National HYDAT archive for water quantity and flow data, and were accessed through the R-studio *tidyhydat()* and *fasstr()* packages. The daily flow values (m^3/day) from the Arctic Red River Station (HYDAT, ID: 10LA002) during 2005- 2019 were divided into the freshet and non-freshet periods. The freshet

season began when the discharge rate was 1.5-fold greater than the average 30-day discharge, until 10-days after the peak flow (Leitch *et al.* 2007). Riverine discharge data was summed for the freshet and rest-of-year periods to obtain the annual total flow values. The Netica CPTs were populated with count data from the number of years where a flow value within a certain range was calculated. The discretization of the Total Flow variables was dependent on the observed flow data and not on regulatory or threshold values. Overall, the total riverine flow values calculated via this method were lower than the 5.1 km^3/year value reported by Leitch *et al*. (2007). In this project the average annual total flow through the Arctic Red River station was 3.4 km^3, with the freshet season lasting between 9 (in 2017) and 39 (in 2012) days, averaging at 18 days. The riverine discharge variables are based on data collected from the Great Bear North study region, prior to the Mackenzie River outlet to the Beaufort Sea; therefore, riverine discharge values are only relevant to the northern-most study region.

For the Great Slave Lake model, the "Mercury input into the Beaufort Sea" node was replaced by a "Mercury input into the Mackenzie River" endpoint. This endpoint is only relevant to the GSL Outlet study region, as this is the location where Great Slave Lake drains into the Mackenzie River. The Fort Simpson climate station at Strong Point (HYDAT, ID: 10FB006) was the nearest station to the GSL outlet but is located approximately 180 km downstream. Riverine discharge values from this station were used to populate and discretize the Total Flow variables for the freshet and non-freshet season.

Biotic Stressors

2.3.7 Fish Length

Methylmercury forms strong bonds to the sulfur-containing amino acids in tissue proteins and is slow to be eliminated by organisms, which leads to higher Hg body burdens in older individuals. Fish exhibit indeterminate growth, with growth rates varying significantly between habitats (Kozak *et al.* 2022). Rapid growth can result in growth dilution effects, where large individuals have lower than predicted Hg concentrations due to their young age. Fish age, or age-at-length, are the preferred explanatory variables across ecosystems but age measurements can be costly due to the specialized training and equipment required. In the NWT, fish consumption advisories typically include a size restriction, with most predatory fish over 600 mm being considered higher-risk food sources (GNWT, 2016). The discretization of the fish length node is based on the recommended sizes in fish consumption advisories (GNWT, 2016). For lake trout, northern pike and burbot, this was set to 600 mm; for walleye it was 450 mm. Because there are no advisories for lake whitefish, fish greater than 500mm in length were classified as large.

2.3.8 Fish Consumption Rates

Mercury exposure through diet depends on both the food Hg concentrations and the rate at which the food is consumed. A consumption rate variable was created for the five freshwater fish in the model (see Effects category for fish species information). The discretization of the fish consumption variable is based on the average weight of a fish portion, which is approximately 150g for an adult (of body weight at 60 kg) and 75g for a young child (Health Canada, 2007; GNWT, 2016). The fish consumption rate nodes are interactive when the models are accessed in

the Netica software, allowing the BN-RRM user to visualize how the cumulative consumption of a varied freshwater fish diet affects the weekly Hg exposure.

2.4 BN-RRM Category- Habitat

The Habitat variables are the third category in the BN-RRM. The purpose of this category is to identify where there is a spatial overlap between the sources and the endpoints. For example, habitat could be various forms of terrestrial and aquatic ecosystem classifications, such as freshwater bodies, seawater, or tundra vs. forested terrain. The models presented in this thesis did not have traditional habitat variables. Instead, the "Proximity to" point-source nodes and the study region scenario nodes were used to describe the intensity of stressor presence. Additionally, the topography (LS-factor) and soil texture (K-factor) variables from the soil erosion calculations are included in this category because these are descriptions of the habitat which are less likely to be impacted by climate change or the presence of Hg sources.

2.4.1 Soil Erodibility/ Texture Factor (K-factor)

The soil erodibility factor (tonnes hr MJ^{-1} mm^{-1}) or K-factor depends on several soil properties such as the organic matter content, the proportion of clay and sand content, and the porosity of the soil. The combination of these properties comprises the soil texture characteristics. The standard method of calculating the K-factor requires a spatial dataset on the clay, sand, and organic matter soil composition (GNWT Transportation, 2013). For the NWT, there is currently no detailed dataset for the clay and sand soil content, so a less accurate method was used. A polygon of soil texture classes was obtained from a Canada-wide GIS dataset "Soil Texture by Eco-district" (Supplemental Figure 15, Canada Open Government, 2013). The average K-factor value for the various soil texture classes was obtained from Table B-3 of the

GNWT Transportation (2013) Erosion manual. There were 6 major texture classes in the study area, listed in order of increasing K-factor: Water (0.000), Sand (0.002), Organic (0.015), Sandy Loam (0.017), Clay (0.030), Clay Loam (0.032), and Loam (0.042) (Supplemental Figure 15). In the study area, the "Organic" soil texture was the most common classification; unfortunately, there isn't a standard range of K-factor values for this soil classification. The K-factor calculation was developed for soils with OC content < 4% (Wall *et al.* 2002), therefore no literature values were available for organic soils. A K-factor value of 0.015 was utilized but it is possible that this value is much lower. This is because the organic matter will bind the soil particles, making the soil less susceptible to erosion (Wall *et al.* 2002). The lack of a spatial dataset of soil clay and sand content has resulted in several assumptions about the K-factor values. Detailed knowledge of local soil characteristics is necessary to improve the estimation of soil erosion potential in this study area. When this layer was converted to a raster, the resolution was set to 250 m.

2.4.2 Topographic Factor (LS-factor)

The calculation of the topographic LS-factor is a major limitation of the GIS-derived soil erosion method and is an active area of research (Hrabalíková and Janeĉek, 2017). The LS-factor is composed of the slope length (L), which is length between the higher-elevation origin and where the slope (S) decreases such that flow accumulation begins (Hrabalíková and Janeĉek, 2017). Accurate slope length values are best obtained from field measurements (Hickey, 2000), and GIS methods have replaced the slope length variable with a Unit Contributing Area (UCA) variable (Brychta and Brychtová, 2020). The UCA can be rapidly calculated in ArcGIS Pro using the Hydrology toolkit. First, the Digital Elevation Model (DEM) input layer must be pre-processed to fill in any sinks or depressions that are caused by errors in data collection (Zhang *et*

al. 2013). In this project, the 16m resolution Natural Resources Canada (2013) DEM Version 1.1 map was used (NRC, 2013). The flow direction was then calculated using either D8 or Multi-flow direction (MFD) methods (Zhang *et al.* 2013). The D8 method assumes that the flow will be in the direction of the lowest elevation, while the MFD method allows for the flow into several downslope neighbors (Zhang *et al.* 2013). The D8 method was used in this project, as this is the method that required the least computational power. The Flow Direction layer is then used to calculate Flow Accumulation; no weight raster was used during the calculation but an Accumulation threshold of 300 was applied (Brychta and Brychtová, 2020).

Finally, the slope length can be approximated as the flow accumulation multiplied by the cell size, also known as the raster resolution. Although there are several options for calculating the LS-factor (Hrabalíková and Janeĉek, 2017), the McCool equation (Equation 3) was ultimately used (Moore and Wilson, 1992) (Supplemental Figure 14).

The LS-factor (unitless) was calculated using values of slope length (meters) and slope angle (β, radians) following the recommended equation for the RUSLE Calculation (Moore and Wilson, 1992):

Equation 4: $$LS = (\frac{1}{22.13} * Length)^m * S$$

Factor S is calculated as:

$\beta < 0.09$	$S = 10.8 * \sin\beta + 0.03$
$\beta \geq 0.09$	$S = 16.8 * \sin\beta - 0.5$
Length< 4.5 m	$S = 3*(\sin\beta)^{0.8} + 0.56$

And m is:

$$m = F / (1+ F)$$

F is calculated as:

Length < 4.5 m F = 0

Length ≥ 4.5 m $F = \frac{(\frac{sin\beta}{0.0896})}{3*(sin\beta)^{0.8}+0.56}$

2.5 BN-RRM Category- Effects

In the BN-RRM, the effect category represents the nodes which are expected to respond to the influence of pollutant sources and stressors. Effect variables are often essential for maintaining ecosystem services or other systems of social, environmental, or economic importance, and are therefore coupled to the project endpoints. In these BN-RRMs there are three groups of effect variables: freshwater Hg concentrations, freshwater fish tissue concentrations, and human daily Hg ingestion via a fish-diet.

2.5.1 Freshwater Mercury Concentrations

Mercury exists in several forms in freshwater including dissolved (DHg), particulate (PHg), sediment-bound (sHg) and organometallic methylated mercury (MeHg). Analysis of dissolved and total Hg was standard in freshwater Hg monitoring programs in the NWT. There were 9 freshwater Hg monitoring datasets included in this project, with the majority of datapoints (79%) obtained from the "NWT-wide Community-based Monitoring" study (Supplemental Table 1). Most monitoring datasets were community-scale, with data being collected for local experimental studies or by Indigenous community-led projects. A limitation of the NWT-wide Monitoring study was the high detection limit value of 10 ng/L for DHg and THg. This is especially problematic for the DHg form, since freshwater DHg concentrations are

typically much lower than this limit (Leitch *et al.* 2007; Campeau *et al.* 2022). Thus the DHg concentration node was removed because the majority of datapoints were below this detection limit (99%) and drastically below any regulatory Hg thresholds; comparatively, 83% of THg values were below a threshold value. Figure 1 shows the Hg monitoring results included in the BN-RRM.

Only two studies (Supplemental Table 1) analyzed MeHg, so this variable was also removed from the model due to a lack of data across all study regions. The removal of the MeHg node is a major limitation of the BN-RRM structure presented in this thesis, because it is the variable that links freshwater and fish Hg concentrations (Moslemi-Aqdam *et al.* 2022). Freshwater MeHg is rapidly metabolized by aquatic biota and accumulated into the food chain. Mercury monitoring of species at various trophic levels in the food chain, including invertebrates and small non-food fish, may be necessary to derive accurate causal relationships between abiotic and biotic effects. Integration of the abiotic Hg models with food web models is beyond the scope of this project, but it is being pursued in other Bayesian Network models (Uusitalo *et al.* 2018).

The discretization of the Freshwater THg node was based on the highest detection limit value (10 ng/L) and the CCME-2003 regulatory threshold value (26 ng/L); there is an additional threshold for safe drinking water at 1000 ng/L but this limit was exceeded only once over the 15-year study period. The CCME-2003 inorganic Hg regulatory threshold of 26 ng/L was based on the most sensitive LOAEL for juvenile fathead minnows.

2.5.2 Fish Tissue Mercury Concentrations

High Hg concentrations in humans have been linked to the consumption of fish and marine mammals. Indigenous communities in the NWT rely on a subsistence diet of fish, caribou, moose, offal, eggs, poultry, and small mammals, with some individuals in the far North of the study area also consuming seal and beluga whale. However, the consumption of freshwater fish is the major dietary Hg input for communities across all study areas. Data from caribou tissue is available for future model iterations (Gamberg *et al.* 2020) if there is interest by stakeholders and land rightsholders. Consultation with Indigenous rightsholders should be conducted to select other culturally significant dietary Hg sources.

There are approximately 42 species of freshwater fish in the lower Mackenzie River Basin (Bodaly *et al.* 1989), although many of these are not a significant component of the subsistence diet. There are five freshwater fish species that have been extensively monitored in the Mackenzie River basin and were included in the Bayesian model. The species are lake whitefish, burbot, walleye, lake trout, and northern pike, and they differ in their trophic levels and popularity among the various Indigenous groups in the subbasins. Fish Hg concentrations (reported as wet weight) were pooled from 11 sources (Supplemental Table 2) and were limited to samples obtained from muscle tissue only.

Lake whitefish occupies the lowest trophic level of the five and is consumed by Indigenous communities throughout the basin. It is generally considered a safe food source and there are no consumption advisories for the study area currently. Walleye (pickerel) occupies a higher trophic level position (Cott *et al.* 2011; Zanden *et al.* 1997) than lake whitefish. Walleye are preferred by the Tłı̨chǫ, Chipewyan, and Dehcho Dene communities settled around Great Slave Lake (Halseth and the NCCAH 2015). Walleye monitoring data was only available for the

Great Bear South and West study regions and for Great Slave Lake. Next in trophic level position is burbot (*Lota lota*) (Cott *et al.* 2011). Burbot is not widely consumed in Indigenous communities but is preferred by elders who particularly enjoy burbot liver as a delicacy (Ratelle *et al.* 2019), which has lower Hg concentrations than muscle tissue (Cott *et al.* 2016). Finally, lake trout and northern pike (jackfish) occupy the highest trophic level of the five species (Zanden and Rasmussen, 1996; Cott *et al.* 2011). Northern pike is a piscivorous fish often consumed by individuals in the southern regions of the study area (Ratelle *et al.* 2019), however in the north it is considered an undesirable food fish and is commonly used as dog food (MRBB, 2021). Lake trout is an important food fish for the Sahtu Dene and Tłı̨chǫ communities, and Great Bear Lake is well-known amongst sports fishermen for its trophy lake trout. Additionally, lake trout comprise approximately a third of the annual harvest for the Great Slave Lake commercial fishery (Fisheries Act). The Gwich'in and Inuvik communities in the Great Bear North region do not harvest much lake trout due to preferences for other salmanoid species such as arctic char (Schuster *et al.* 2011; Stephenson, 2004). However, arctic char was not included in this project due to a lack of publicly available Hg monitoring data.

There are two Health Canada guidelines for acceptable Hg levels in fish, and a recommended guideline for subsistence consumers. The lowest guideline of 0.2 ppm (200 ng/g ww) is set for subsistence fishing practices, applying to individuals that harvest their own fish or have a higher fish intake (Lockhart *et al.* 2005). The two federal guidelines are 0.5 ug/g and 1.0 ug/g, the latter applying for certain species of fish such as tuna and shark, which are not considered in this model (Health Canada, 2007). The consumption advisories for predatory species are 150 g per week, equivalent to a single serving (Health Canada, 2019).

2.5.3 Human Daily Mercury Ingestion

The Canadian pTDI (Provisional tolerable daily intake) for total Hg in adults is 0.71 ug/kg bw/day, where no more than two-thirds is methylmercury (0.47 ug/kg bw/day) (Health Canada, 2007). A second Canadian federal guideline was established 30 years later for children and women of child-bearing age (0.20 ug/kg bw/day – Legrand e*t al.* 2010). Additionally, the USA and the Netherlands have adopted a lower guideline of 0.7 ug Hg/ kg bw/week for children and women of child-bearing age (U.S. EPA, 2000). The Canadian pTDI values were based on 10 ppm maternal hair methylmercury and an adult body weight of 60 kg (Health Canada, 2007). The probable daily Hg intake (ug/kg bw/day) can be calculated as the product of the fish muscle intake (FMI, g/day), the methylmercury concentration ([MeHg], ug/g ww) divided by the average body weight (BW, kg):

Equation 5: $$PDI = \frac{(FMI * [MeHg])}{BW}$$

The pTDI value was calculated from toxicological studies conducted by the Swedish Expert Group which found that a 200 ug/L concentration is the lowest blood concentration to cause adverse effects (Legrand *et al.* 2010). The recommended guideline adopted was 20 ug/L blood, which corresponds to 0.47 ug MeHg/kg bw/day as the daily intake limit (Legrand *et al.* 2010)

2.6 BN-RRM Category- Endpoints

The endpoints are the variables of social, environmental, cultural, or economic value for which we are quantifying the probability of a risk caused by mercury exposure. There are four endpoint variables in this model. Three of these variables are estimating risk probabilities: the probability that commercial fish catch will exceed national guidelines for sale, the probability of a subsistence consumer exceeding regulatory guidelines for Hg ingestion, and the probability

that fish tissue Hg concentrations are harmful to fish. The fourth endpoint is "Mercury input into the Arctic Ocean" which is a prediction of riverine Hg export and not a quantification of a risk probability, as there are no regulations on acceptable levels of riverine Hg flux.

2.6.1 % Fish not Eligible for Commercial Sale

There are approximately 110 lakes in the NWT which can be fished commercially, with lake whitefish and lake trout being the dominant commercial species (Fisheries Act). Great Slave Lake (GSL) has the largest fish quotas in the territory and has sustained a commercial fishing industry for over 50 years (Supplemental Figure 18). The GNWT has released a strategy to expand the Great Slave Lake commercial fishery by building a new local fish processing plant in Hay River, increasing fishing efforts, and negotiating with the Freshwater Fish Marketing Corporation (FFMC) to access larger markets in southern jurisdictions (GNWT, 2017). In Canada, the regulatory threshold for the retail sale of fish is 0.5 ppm (Health Canada, 2007). Mercury concentrations in lake whitefish harvested in Great Slave Lake are below this threshold; however, this regulatory guideline is commonly exceeded in higher-trophic level species like lake trout and northern pike. The endpoint "% Fish not eligible for sale" is a risk probability endpoint which was calculated by assigning any fish with concentrations above the threshold as being "Not eligible" for commercial sale. Thompson (1981) proposes that a 10% sales margin is acceptable for fishing skiffs, although this value has likely changed significantly in the past 40 years since the document was published. Engaging the commercial fisheries as stakeholders in this project can provide guidelines that represent present-day profit margins of fisheries in the NWT, to determine what economic loss can be sustained by the modern fishing operations at Great Slave Lake (GNWT, 2017). This will be a key step if the model is expanded to estimate

the risk to commercial fisheries; other steps include the integration of nodes that consider the frequency of Hg testing and any control or mitigation strategies employed by the fisheries.

2.6.2 Exceedance of Hg Consumption Thresholds

This endpoint was calculated as the ratio between the modelled "Weekly Hg ingestion from freshwater fish" to one of three pTWI regulatory threshold values. The probability of exceeding Hg exposure thresholds is quantified by a risk-quotient value, where a value of 1 indicates that the predicted Hg ingestion is equal to the selected threshold value. The calculation of the risk-quotient requires the BN-RRM user to select a diet by specifying the number of portions consumed of each of the five freshwater fish species. The user also selects a regulatory pTWI value (see "Human Daily Mercury Ingestion" node in the Effects Section). Risk-quotient values below 1 suggest that the selected rate of fish consumption is below the regulatory threshold, while values above 1 indicate that the threshold value is exceeded.

This endpoint is relevant for any individuals who consume harvested fish from the Mackenzie River and was not developed for a particular Indigenous community in the study area. With community-based framework projects, such as the NWT Cumulative Impact Monitoring Program (NWT CIMP) projects, the data generated will be subject to OCAP; a First Nations principle of "ownership, control, access, and possession" over the information that belongs to the First Nations people. OCAP ensures that First Nations peoples are involved and in leadership roles in these projects (FNIGC, 2014). For the purposes of the ARCRISK project, obtaining access to the data gathered on Hg concentrations in subsistence foods will be a time-consuming process, and could not be completed within the timeframe of the funding. Multiple site-visits and meetings with the communities are necessary if the project wishes to include

Indigenous rightsholders as stakeholders and gain access to data necessary for their inclusion in the BN-RRM model.

The Inuvaluit/, Gwich'in, Dehcho Dene, Sahtu Dene, Métis, Tłı̨chǫ, and Chipewyan peoples represent the seven Indigenous groups that occupy a large territorial range near the Mackenzie River (Halseth and the NCCAH, 2015) The populations of each of the communities is listed in descending order: Dehcho (4531), Chipewyan (4450), Tłı̨chǫ (3848), Métis (3385), Sahtu (2785), Gwich'in (2569), and Inuit (1690) (Statistics Canada, 2017). Much of the sample collection for Hg monitoring in the MRB is completed by Indigenous-lead groups concerned about pollution in the water and subsistence foods. Subsistence harvesting is the procurement of food or other resources for the direct use by the individual or community. Subsistence fishing is a cheap source of nutrients and is essential for meeting the food demands of many communities (Laird *et al.* 2018). There are several collaborative projects between university researchers and Indigenous communities that have recently published results for Hg concentrations in subsistence foods and in human hair or blood samples (Ratelle *et al.* 2020a; Ratelle *et al.* 2020b; Ratelle *et al.* 2019; Curren *et al.* 2015). While fewer than 5% of the participants had blood or hair Hg concentrations exceeding a regulatory threshold, many more community members have adjusted their dietary intake of traditional foods due to concerns over fish quality and pollutants (Ratelle *et al.* 2019; Parlee and Maloney, 2016).

2.6.3 % Injury to Fish

Tissue-residue toxicology studies are needed to predict at what tissue concentrations adverse health effects on freshwater fish become apparent. Dillon *et al.* (2010) compiled published toxicology studies and prepared composite dose-response curves, where the adverse effect endpoint was "% injury" and represents the combined impact of mortality, developmental

abnormalities, and spawning success endpoints. Dose-response relationships were developed in R using the *drc* package (Ritz *et al.* 2015) and the Dillon *et al.* (2010) supplemental data. This dataset combines experiments on fish of various life stages and trophic levels, from small medaka to predatory fish such as walleye and rainbow trout. Three dose-response models were initially prepared using a subset of data. The first model used all data, while the subsequent two models use data from the Fathead Minnow Juvenile or Juvenile/Adult life-stages respectively (Supplemental Table 6). The *drc* model LL.3( ) was used to develop the dose-response relationships.

The predicted effective dose (ED) values for the three models are presented in Supplemental Table 6. Environmental risk assessments often use ED20 and ED50 values for quantifying the impact of an adverse event (Fuschman, 2016). The ED20 value from the Juvenile/Adult model were the highest of the three models. However, the dose response equation generated with the Juvenile/Adult data converges to a maximum %injury value of 50% because the %injury at the highest tissue Hg concentration (7.6 ug/g ww) was relatively low (22%). When input into the BN Netica software, this resulted in a dose-response curve with a maximum %injury value of 50% even at extreme concentrations (>3 ug/g ww). For this reason, the Juvenile/Adult dose-response model was not used to predict the probability of injury in our BN-RRM. Data from only the Juvenile life stage was instead used to generate the dose-response curve and predict the probability of tissue-induced injury in three freshwater species: lake whitefish, lake trout, and northern pike.

A shortcoming of the Juvenile model was that it predicted a low ED20 value (of 0.33 ug/g ww) that are below modelled natural background fish tissue concentrations (Fuchsman *et al.* 2016). Additionally, field-collected fish with low Hg body burdens (below 0.5 ppm in tissue) did

not show adverse health effects, further supporting the application of a higher toxicological reference value (Fuschman *et al.* 2016). Field case studies suggest that even the Dillon *et al*. (2010) ED20 value of 0.77 overpredicts the degree of adverse effects on wild fish populations (Fuschman *et al.* 2016). Finally, the "All Fish Data" model was excluded because it compiles highly variable data and does not account for the effect of exposure route, species-specific sensitivities, trophic levels, or bioaccumulation with age class.

Only the data from the "Juvenile" life stage experiments was used in the model. The LL.3( ) model utilizes a log-logistic equation to describe the dose response curve, using the lower limit (c), the upper limit (d), the regression slope (b) and the ED50 (e) values as inputs:

Equation 6: $$f(x) = c + \frac{d-0}{1+\exp\left(b(\log(x)-\log(e))\right)}$$

The "Juvenile" dataset is solely comprised of data from fathead minnow fish, so this dose response curve is not a reliable estimate of the health impacts on the five freshwater species of interest in the BN-RRM. Fathead minnows are a small, low-trophic level fish species and their toxicity response does not accurately represent the five freshwater fish species included in this model (Supplemental Table 4). The risk of injury to the fish species in the BN-RRMs are likely being underestimated, as fathead minnows are believed to be less sensitive to metal toxicity than salmonid species like lake trout and whitefish (Teather and Parrott, 2006; Dillon *et al*. 2010). There is a need for future toxicological studies on salmonid species or adult fish of a higher trophic level position (such as walleye and northern pike) to predict the probability of injury more accurately for the study organisms.

The average residue concentration that corresponds to an ED20 value across all the appropriate models for the "Juvenile" life stage was 0.33 ug Hg/kg tissue, and the ED50 value

was 2.43 ug Hg/kg tissue.. The predicted ED50 value was slightly lower than the value of 3.013 calculated with the Dillon model. Note that the LL.3( ) model equation is different than the Dillon *et al.* (2010) dose-response equation, and uses the Juvenile life stage data rather than the "Juvenile/Adult" data. Supplemental Table 6 shows a comparison of the predicted ED50 values across the three tested models and the Dillon *et al.* (2010) results. From these three models, the "Juvenile" dataset produced the closest replicate to the Dillon *et al.* (2010) dose-response curve and was the only one to converge to a 100% probability of injury.

2.6.4 Mercury Input into the Beaufort Sea

In the lower Mackenzie River, the highest riverine Hg concentrations are observed during the spring freshet. Freshet Hg concentrations were 7-fold greater than the comparative mid-summer samples (Leitch *et al.* 2007), corresponding to the increased riverine flow. Mercury flux is the product of discharge rate and Hg concentrations, and the total annual Hg flux is the sum of the freshet and rest-of-year Hg flux values (Leitch *et al.* 2007). This flux estimate was further improved by Emmerton *et al.* (2013), who concluded that the downstream Mackenzie Delta acts as a Hg sink and retains ~19% of the bulk Hg transported. Therefore, the Leitch *et al.* 2007 equation was multiplied by 0.81 to account for the Hg sedimentation in the Mackenzie Delta. As this project is using Hg monitoring data primarily collected during the summer season (84% Summer compared to Winter 1.7%, Spring 5.8%, and Fall 8.5%), the probability distributions were also multiplied by 7 to estimate the expected increase in bulk Hg release during the spring freshet (Leitch e*t al.* 2007). The following equation was used to populate the CPT for the "Mercury input into the Beaufort Sea" endpoint:

Equation 7:

*Annual Hg Input = 0.81 * [(7* Freshwater THg* Freshet flow) + (Freshwater THg* Rest of Year flow)]*

Management strategies looking to reduce the riverine flux of Hg into the Arctic Ocean would benefit from considering the impact of climate change stressors. Climate change stressors, such as increased temperatures or snowfall, will impact the annual riverine Hg flux through the riverine flow and water Hg variables. Riverine flow rates and Hg concentrations have a strong positive correlation (Leitch *et al.* 2007; Emmerton *et al.* 2013), indicating that most Hg is originating from natural flooding and riverbank erosion processes. The Mackenzie and Yukon rivers of North America have exhibited a 9% increase in riverine discharge over the past 3 decades (1975- 2015), and the six largest European rivers have a composite increase of 12% over the same period (Chetelat *et al.* 2022). In North America, riverine discharge is estimated to be accelerating at a rate of 3.4 km^3/yr/yr (Feng *et al.* 2021), a significant increase when considering that the flux of the Mackenzie River from the 2005- 2007 period was ~5.1 km^3/yr (Leitch *et al.* 2007). Applying the linear regression developed by Zolkos *et al.* (2020) which proposes that THg concentrations can be adequately predicted from data on riverine discharge (m^3/s), TSS, and DOC; assuming that the biogeochemistry of Arctic rivers is not significantly altered, this change in discharge would result in ~ 1.025-fold increase in riverine THg concentrations in 10-year period. However, it is expected that climate change and altered hydrological regimes will also impact nutrient flux and the biogeochemical processes governing mercury methylation and bioaccumulation. There are currently no estimates of what THg export levels warrant concern, and seawater THg concentrations in the Arctic Ocean (0.31 ± 0.11 ng/L) are similar to samples

collected from other oceans (north Atlantic 0.48 ± 0.32 ng/L; north Pacific 0.2 3± 0.17 ng/L; Southern Ocean 0.27 ± 0.09 ng/L – Kirk *et al.* 2012).

2.7 Methods Summary

In summary, I first developed a conceptual model that considers six potential Hg sources and their spatial relationship to Hg concentrations in freshwater and five fish species of the MRB. The variables included in the model were discretized according to regulatory thresholds or toxicological data (Supplemental Table 4) whenever possible, and were parameterized with data obtained from monitoring studies, GIS datasets, or environmental models (Supplemental Tables 1 – 3). The causal relationships between Hg sources and endpoints were quantified using the Netica software's Count Learning algorithms, and a sensitivity analysis was performed to identify the sources driving Hg accumulation in the study region. Ultimately, two models were prepared for the Great Bear subbasin and Great Slave Lake, respectively. Each of these study areas was further divided into four study regions to visualize both how the state of Hg and the predicted influential sources vary along the basin.

Chapter 3: Manuscript draft

Title: BAYESIAN NETWORK MODEL OF MERCURY EXPOSURE TO AQUATIC ECOSYSTEMS OF THE MACKENZIE WATERSHED

Abstract

A Bayesian Network Relative Risk Model (BN-RRM) was developed to assess the recent (2005-2020) state of mercury (Hg) in the freshwater ecosystems of Great Slave Lake and the Mackenzie River, in the Canadian Northwest Territories. Data from environmental models, Hg monitoring projects, and community reports were organized into a single causal model which considered six Hg input pathways. Sensitivity analysis was used to predict the sources influencing Hg concentrations in freshwater and fish tissue across eight study regions. The output of the BN-RRMs differed significantly throughout the study area (800,000 m^2), with atmospheric Hg deposition and soil erosion Hg release consistently flagged as important explanatory variables. However, the low sensitivity values imply that only a fraction of the observed Hg concentrations can be attributed to the input pathways. Analysis of the endpoint uncertainties revealed gaps in knowledge and in Hg datasets, which should be the focus of study for future monitoring programs.

Introduction

Effective ecosystem management projects adopt a holistic approach that enables natural resilience and preserves valuable ecosystem services while considering the socioeconomic and cultural needs of communities (DeFries and Nagendra, 2017). The management of natural resources is complicated by the competing interests of rightsholder and stakeholder groups, the absence of shared national databases, the temporal and spatial variation in ecosystem

components, and a lack of long-term monitoring and understanding of the causal relationships within (Cooke *et al*. 2016; DeFries and Nagendra, 2017). In the past 12 years, the Canadian provincial, territorial, and federal governments have cumulatively invested over 330 billion dollars on environmental protection projects (Statistics Canada, 2022). However, government ecosystem management projects would benefit from the implementation of a framework that can integrate many stakeholder endpoints, combine various knowledge types, and encourage communication between multidisciplinary departments (Cooke *et al*. 2016).

Bayesian Networks (BNs) are probabilistic tools that have been applied in ecological management to predict risk to ecosystems (Harris *et al.* 2017; Ayre and Landis, 2012), to develop and compare policy decisions (Johns *et al.* 2016; Herring *et al.* 2015; Ayre *et al.* 2014), and to perform retrospective environmental risk assessments (ERAs) of multi-stressor systems (Bruen *et al.* 2022; Peeters *et al.* 2022). An ERA is the process of studying and predicting the probability and consequences of an adverse effect posed to humans or ecosystems (Kaikkonen *et al*. 2020). Bayesian Network Relative Risk Models (BN-RRMs) are the integration of BNs and ERAs (Landis, 2020; Harris et al. 2017). The BN-RRM integrates all aspects of an ERA including exposure assessments and risk quantification (Kaikkonen *et al.* 2020; Landis, 2020). An additional strength of these models is that they can integrate a variety of knowledge including primary data, environmental models, and expert opinion. The capability to integrate expert opinion is uniquely relevant for ERAs conducted in Canada. In 2019 Canada passed Bill C-69 which requires that ERAs involve land-rights-holders throughout the assessment process, promoting the application of Traditional Ecological Knowledge (TEK) in parallel with Western Science approaches (Bill C-69; Houde *et al.* 2022). Expert knowledge like TEK can be integrated throughout the model, including the conceptualization of the causal models, the

selection of study regions and endpoints, and later when parameterizing the variables (Pollino *et al*. 2007).

The BN-RRM is visualized as a causal diagram linking variables (called nodes) along an exposure pathway from sources to endpoints (Landis, 2020). The relationships between downstream "parent" nodes and the variables on which they have a perceived effect ("child" nodes) are defined in the conditional probability tables (CPTs). Uncertainty is propagated throughout the model because variable states and their dependencies are described by probability distributions (Uusitalo, 2007; Kaikkonen *et al*. 2020). Quantifying uncertainty is imperative to the selection of a successful management strategy but is also useful for identifying knowledge gaps when developing future monitoring programs (Marcot *et al*. 2006). BN models can also be used to perform counterfactual analysis and predict the outcome of events under a novel situation, such as an unrealized management decision or climate scenario (Carriger *et al.* 2021). Uncertainty of the causal relationships, where parent variables are necessary and/ or sufficient to achieve an impact on the child nodes, will limit the accuracy of this prediction. Finally, the graphical nature of BN models facilitates communication with stakeholders and policy makers. Purposeful causal diagrams are developed in collaboration between scientists and stakeholders such as industry partners, NGOs, politicians, and local communities (Kaikkonen *et al*. 2020; Houde *et al.* 2022).

In this research, the BN-RRM framework was used as an assessment of risk probabilities and as an organizational tool to integrate mercury (Hg) monitoring data, environmental model outputs, and community reports (Parlee and Maloney, 2016; MRBB, 2021), using the lower Mackenzie River Basin as a case study. The five objectives of this research were:

1) To confirm that the BN-RRM is an appropriate framework for organizing data from multiple studies and for identifying knowledge gaps.
2) To develop a general framework for a Hg risk assessment in a circumpolar watershed.
3) To identify influential pollutant Hg sources and their spatial variation.
4) To evaluate the associated risk probabilities for the environment and human health.
5) To perform a counterfactual analysis predicting the impact of two management strategies: The Minamata treaty and fish consumption advisories

This research is the Canadian contribution to the ARCRISK project, a circumpolar collaboration to develop Hg risk assessments for Arctic Rivers in Norway, Canada, and Russia (Gundersen *et al.* 2020). Together these assessments will present a comprehensive study of the pathways driving Hg accumulation in Arctic Rivers. Arctic Rivers, like Canada's Mackenzie River (MR), are major sources (15-20%) of Hg for the Arctic Ocean (Soerensen *et al*. 2016). Lockhart *et al*. (2005) summarized Hg data collected from 1965-2004 in the MR and reported elevated (> 0.5 ug/g ww) Hg concentrations in upper-trophic level aquatic species. In this study, Hg monitoring data of freshwater and fish tissue collected during the 2005- 2020 period is compiled from publicly available databases (Supplemental Tables 1- 3). Monitoring data and Geographic Information Systems (GIS) were used to construct the cause-and-effect relationships, in the form of CPTs, between Hg sources and the effect on freshwater and five culturally valuable food fish species. Fish health and human dietary Hg exposure were the endpoint variables for which risk probabilities was estimated. Two counterfactual queries were considered; 1) to predict how a reduction in global atmospheric Hg concentrations (assuming successful implementation of Minamata Convention treaty (UNEP, 2021)) will impact water and fish Hg, and 2) to assess whether advisories restricting consumption of large fish can reduce

human Hg exposure. This model framework can be used to identify local Hg sources, estimate the probability of exposure, identify gaps in knowledge to improve monitoring programs, and act as support tool for planning risk-reduction initiatives (Gundersen et al. 2020).

Methods

The study area

Draining an area of 1.8 million km^2, the Mackenzie River Basin (MRB) is the largest watershed in Canada and is collectively managed by the federal government and the five provinces which it intersects (GOC, 1997). The MRB encompasses six smaller subbasins: Peace, Athabasca, Great Slave, Great Bear, Liard, and Peel (MRBB, 2021). Great Slave Lake is the major riverine input into the Mackenzie River (35%), followed by the Liard River (26%), Peel River (8%) and Great Bear River (6.5%) (Environment Canada, 2013; Palmer *et al*. 2008). The Mackenzie River begins at the outlet of Great Slave Lake, at the boundary of the Great Bear and Great Slave subbasins. There are approximately 40,000 individuals residing in the study area (Figure 1); 60- 95% of the communities identify as Indigenous, with slightly lower ratios in administrative centers (Statistics Canada, 2017).

Figure 1. The study area and Hg monitoring data for the Great Bear Subbasin (GBS) and Great Slave Lake (GSL) models. The GBS study area was divided into four study regions, labelled SR1 – SR4, spanning from the Alberta-Northwest Territory border to the Mackenzie River (blue line) outlet at the Beaufort Sea. The GSL study area was also divided into four regions (North Arm, East Arm, Middle and Outlet), spanning a 50 km buffer zone around Great Slave Lake. Mercury monitoring data (ng/L for water and ug/g wet weight for fish) was collected during the 2005- 2020 period. Fish monitoring datapoints include data from 5 fish species: lake trout, lake whitefish, northern pike, walleye, and burbot.

Warming temperatures are accelerating riverine discharge and the transport of nutrients and debris into the Arctic Ocean (Peterson *et al.* 2002; Campeau *et al.* 2022; Schuster *et al.* 2018; Pierre e*t al.* 2018). Globally, the Mackenzie River is the largest source of sediment and organic matter to the Arctic Ocean, in addition to contributing ~10 % of the freshwater flow and an average of two tons of Hg, annually (Vonk e*t al.* 2015; Rood *et al.* 2016; Leitch *et al.* 2007; Rachold *et al.* 2000). Particulate-bound Hg corresponds to 78-87 % of the total flux in the basin, originating mainly from the weathering of natural coal deposits (10%) or sulfide-enriched bedrock (78%) of the Liard and Mackenzie mountains (Carrie *et al.* 2012). Mercury is a ubiquitous element and is released by both anthropogenic and natural processes.

Table 1. Summary of the habitat and source proximity characteristics for the eight study regions across the Great Bear Subbasin (GBS) and the Great Slave Lake (GSL) models.

Category	Parameter	GBS Model				GSL Model			
		SR1	**SR2**	**SR3**	**SR4**	**East Arm**	**North Arm**	**Middle**	**Outlet**
Habitat variable	Ecozone	Taiga Plains	Taiga Cordillera	Taiga Plains/ Taiga Shield	Taiga Plains	Taiga Shield	Taiga Plains/ Taiga Shield	Taiga Plains	Taiga Plains
	Precipitation	Low/ Moderate	Moderate	Low	High	High	High	High	High
	Soil Organic Carbon	High, mixture	Lowest	Highest	Moderate, mixture	Low	Low	High	High
	Permafrost	Continuous	Continuous/ Extensive discontinuous	Continuous/ Extensive discontinuous	Sporadic discontinuous	Extensive discontinuous	Extensive discontinuous	Sporadic discontinuous	Sporadic discontinuous
	Total Area (km^2)	131879.7	133753.6	160522.0	101865.9	41303.2	25469.7	25131.7	21623.3
Potential Hg sources	Oil/Gas exploration	Yes	Yes	None	Not operational	None	None	None	None
	Mining	None	None	No active mining. Some historic mines	None, but near the GSL outlet	No active mining. Some historic mines	Dense mining region	No active mining. Some historic mines	None
	Wildfire frequency	Low frequency	Moderate frequency	Moderate Frequency	High frequency	High frequency	High frequency	High frequency	High frequency
	Soil Erosion	High, based on reports from Indigenous locals	High, based on presence of Mackenzie Mountain Range	Unknown. Little variation in slope suggests low erosion rates	Unknown. Little variation in slope suggests low erosion rates	Unknown. Little variation in slope suggests low erosion rates	Unknown. Urban center and mining developments may impact erosion.	Unknown. Little variation in slope suggests low erosion rates	Unknown. Little variation in slope suggests low erosion rates
	Permafrost thaw slumps	Present	Present	Present	None	None	None	None	None
	Atmospheric Hg deposition	Moderate	Low	Low	High	Low	Moderate	Moderate/ High	High
	Permafrost thaw Hg release	Moderate	Low/ Moderate	Moderate	None/ Moderate/ High	Moderate	Moderate/ High	None	None

The primary route of Hg exposure to humans is through the consumption of foods containing methylmercury (MeHg), the organometallic form of Hg which bioaccumulates and biomagnifies in the food chain (U.S. EPA, 2000; Health Canada, 2007). The highest concentrations of MeHg are found in freshwater fish, marine mammals, and the organs of some terrestrial animals, which are staples of the local diet (Ratelle *et al*. 2019; Ratelle *et al*. 2020a; Ratelle *et al.* 2020b). Recent human Hg monitoring studies of the Dehcho and Sahtu Dene communities, who occupy the southern study area, found that approximately 2% of individuals exceeded the strictest regulatory blood Hg guidelines (Ratelle *et al.* 2019). Consumption advisories are pursued as a Hg risk-reduction measure, but can diminish the community's diet, trust, relationship with the land, and overall sense of cultural connection (Laird *et al*. 2018; Hoover, 2013; Halseth and NCCAH, 2015). Because consumption advisories infringe on Indigenous rights to utilize their land and water, management strategies should instead prioritize reducing Hg release and implementing remediation strategies.

Six Hg sources were considered over two models for the MRB. Mercury sources include atmospheric Hg deposition (Dastoor *et al.* 2015); permafrost thaw Hg release (Schaeffer *et al*. 2020); proximity to point-sources like mines (radius r= 15 km; GNWT Centre for Geomatics), oil and natural gas wells (r= 50 km; GNWT Centre for Geomatics), and retrogressive permafrost-thaw slumps (r = 10 km; Kokelj *et al*. 2021); and a proposed calculation of Hg release to lakes due to rainfall-induced erosion (Wall *et al*. 2002). Logging, flooding for hydroelectric development, and agriculture were also considered as potential Hg sources (Figure 2 for initial conceptual model) but were removed following an extensive literature search that indicated these are minor sources in the study area. Note that the model structure and endpoints were selected without the consultation of industry or community rightsholders. As such, the model results are

based solely on physiochemical considerations. Inclusion of socio-economic factors is highly advised before employing any model outcomes for risk management strategies.

The conceptual model

The first step of constructing a BN model is preparing the conceptual framework by identifying the pathways of influence between contaminant sources and the species or outcomes of interest. (Marcot *et al.* 2006; Pollino and Hart, 2008). Variables which can be included in the conceptual model must be observable, measurable, or predictable; all other variables are removed and become part of the uncertainty of the model output (Pollino and Hart, 2008). The BN-RRM framework utilizes a unidirectional flow of information between the categories of Source, Stressor, Habitat, Effect, and Impact (Landis, 2020).

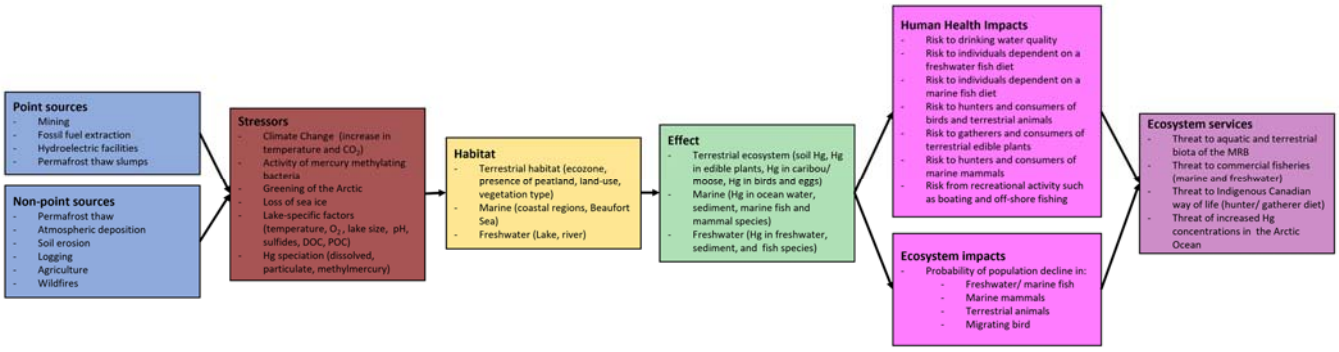

Figure 2. The initial conceptual model for estimating Hg exposure in the lower Mackenzie River basin. The initial model included terrestrial and marine exposure pathways and freshwater Hg speciation with lake-specific factors.

The conceptual model for Hg in the MRB (Figure 2) was simplified as the project focus was narrowed to freshwater aquatic habitats, thereby eliminating the terrestrial and marine processes. As such, the "Habitat" category is replaced by a "Scenario" category in this BN-RRM, where the Scenario represents a specific study region. The first BN-RRM was developed for the Great Bear subbasin (GBS), as this area fully envelops the Mackenzie River (Figure 1). A second model was developed for a 50 km buffer around Great Slave Lake (GSL) since some Hg contamination associated with gold mining (Thienpont *et al.* 2016; Houben *et al.* 2016; Cott *et al.* 2018) has been observed near the lake, making GSL a potential Hg source for the Mackenzie River (Cott *et al.* 2018; Campeau *et al.* 2018). To assess the spatial variations in Hg-associated risk probabilities, each model area was divided into four study regions (Figure 1). An overview of the study regions is offered in Table 1, but the probability distributions of the stressor variables in the parameterized models (Figure 3, Supplemental Figures 1 - 8) provide the comprehensive habitat descriptions.

Data sources

A literature search was conducted to identify publicly available Hg monitoring datasets that reported non-aggregated data which was collected during the 2005- 2020 period (Supplemental Tables 1-3). The initial MRB model (Figure 2) includes three types of freshwater Hg (dissolved, particulate, and methylmercury), as well as various lake factors. In the final iteration the Hg variables were simplified to include only "Total Hg", the sum of dissolved (DHg) and particulate Hg (PHg), due to a lack of DHg measurements above the analysis detection limit. Additionally, the organic matter variables were removed when exploratory analysis showed a weak correlation to THg concentrations (Supplemental Figure 22). Similarly, the MeHg node was removed due to a lack of monitoring data (Supplemental Table S1) and is a

limitation of this model since this is a key variable in establishing a link between freshwater and fish Hg concentrations. Mercury monitoring of species at various trophic levels in the food chain, including invertebrates and small non-food fish, may be necessary to derive accurate causal relationships between abiotic and biotic effects (Moslemi-Aqdam e*t al.* 2022; Rohonczy *et al.* 2020). The biotic effect variables are five freshwater fish species which are regularly sampled in the MRB due to their value as a subsistence food (Lockhart *et al.* 2005). These are the lake whitefish, lake trout, northern pike (jackfish), walleye (pickerel), and burbot (Lota lota). Lake whitefish are a particularly prized food species and are the major catch for the large commercial fishing industry at Great Slave Lake (Fisheries Act, 2020; GNWT 2017). Additionally, lake whitefish occupy a relatively low trophic position and there are no consumption advisories for this fish in the study area, unlike the remaining species (GNWT Health and Social Services, 2016).

GIS datasets were used to populate variables that describe habitat characteristics, proximity to point sources, and non-point Hg release (Supplemental Table 3). Point sources/ stressors include historic mining, active mine claims, active oil or natural gas claims, wildfires, lakes impacted by retrogressive permafrost thaw slumps, and the outlet of GSL. Non-point sources were the outputs of environmental models. Annual Hg deposition was populated from the results of a Canadian atmospheric Hg model, GEM-MACH-Hg, provided upon request by the Dastoor research group (Dastoor *et al.* 2015). A global model of Hg release via permafrost thaw was developed by the Schaeffer research group (Schaeffer *et al.* 2020), who shared monthly estimates of Hg release to aquatic ecosystems and advised on the model conditional probability table (CPT) construction. Mercury concentrations and deposition rates vary significantly with season, but this temporal layer was removed due to the lack of water monitoring data in the fall

and winter seasons. Monthly estimates of permafrost thaw Hg release were summed to approximate the annual trends.

Unlike the other two non-point sources, there is currently no Canadian model for soil erosion and no measurements of soil-loss over the project study area. The Revised Universal Soil Loss Equation (RUSLE) was used to model rainfall-induced soil erosion using the rainfall intensity, soil texture, vegetation density, and slope habitat variables (Wall *et al*. 2002). Supplemental Table 4 describes the steps behind the preparation of these layers. However, the RUSLE equation was developed for European agricultural areas, and likely needs to be adjusted for studies in Arctic and permafrost regions (Schmidt *et al*. 2019). Frozen soil is less prone to erosion, but no studies have modelled how permafrost depth and continuity will impact the RUSLE calculation (GNWT Transportation, 2013).

Discretization of nodes

Variables in the BN model can be categorical, discrete, or continuous, but continuous nodes must be discretized into states (Pollino and Hart 2008; Marcot *et al.* 2006). The boundary values for these states should signify their quality or effects on an endpoint, and regulatory thresholds or toxicological values should be applied where possible (Marcot *et al.* 2006; Landis and Wiegers, 2005). Generally, parsimonious models with fewer states are more accurate; however, some continuous variables, such as "Atmospheric Hg deposition", may benefit from a higher number of states to avoid reducing the model's precision (Marcot *et al.* 2006). Literature review was the primary method of discretization and a detailed description of the decisions can be found in Supplemental Table 4.

Parameterization of nodes

The alpha models were developed in Netica, a free Bayesian Network software. Parameterization is the process of populating the variable states and the CPTs with probabilities. Populated nodes display the probability distribution for the variable, while nodes that lack data appear as a uniform distribution across all states. Case file learning, equations, linear regression models, and expert elicitation can be used to populate CPTs (Marcot *et al.* 2006). Case-file learning was the primary method used to develop the causal relationships between Hg sources and effects on freshwater and fish in this project. Equations were used in the calculation of soil erosion potential and in the estimation of the risk probabilities to the endpoints, as described in Supplemental Table 4.

Sensitivity analysis

Following the model parameterization, the influential explanatory variables can be identified with an entropy-based sensitivity analysis (Pollino and Hart, 2008; Norsys, 2009). The sensitivity analysis quantifies the strength of dependencies, also known as mutual information, between two linked variables (Norsys, 2009). The product of a sensitivity analysis is a list of nodes ranked on the strength of their correlation to the dependent variable. Management nodes can later be inserted into the BN-RRM to target these influential variables, and the optimal management strategy can be selected with consideration to uncertainties (Pollino and Hart 2008; Kaikonnen *et al*. 2020; Landis, 2020).

Uncertainty analysis

Uncertainty comes in two forms: epistemic uncertainty arising from lack of knowledge, and linguistic uncertainty associated with ambiguous and context-dependent language (Regan e*t*

al. 2002). Missing data, temporal and spatial variations in the data, sampling methodologies, and the environmental model outputs are sources of epistemic uncertainty in these BN models. To reduce spatial uncertainty, the study area was divided into study regions (Table 1). Temporal uncertainty was not addressed in this study due to the lack of seasonal variation in the monitoring datasets. Because BN models are probabilistic, any uncertainty is explicitly communicated, propagated to downstream nodes, and integrated into the risk assessment (Kaikkonen e*t al.* 2020). Nodes with high uncertainty can be identified as those that have a high probability of a physically unobserved state in the dataset (see Figure 5 for dataset completeness). Missing data appears as a uniform distribution, with the probability of the "high risk" state being higher than would be observed in a natural system (Supplemental Table 5). Special attention should be given to child node probability distributions when comparing risk probabilities between regions or endpoints.

Linguistic uncertainty arises from miscommunication. This can occur when endpoint variable definitions do not reflect standard practices, when the discretization reasoning is not explicitly described, and when interpreting and communicating risk probabilities. For example, the endpoint of "% Fish not eligible for sale", which is the probability that fish tissue Hg will exceed the guideline for commercial sale (0.5 ppm- Health Canada, 2007), is not appropriate if fish catch is not regularly tested for Hg prior to commercial sale. Linguistic uncertainty and endpoint definition is best addressed during stakeholder consultations, which were not conducted in this study. Uncertainties caused by assumptions made during the discretization and calculation of variables are addressed in Supplemental Table 4. Finally, miscommunication can occur when end-users do not recognize that uniform probability distributions indicate high epistemic

uncertainty and not necessarily a high probability of risk. Failure to consider the probability distribution of child nodes can result in incorrect conclusions about risk of Hg exposure.

Risk analysis

This BN-RRM incorporates three groups of endpoints for which risk was estimated:

1. The risk-probability of fish catch exceeding the guidelines for commercial sale
2. The risk of Hg-induced injury to fish
3. The risk-probability to subsistence fish consumers of exceeding dietary Hg thresholds

The equations that define the CPTs for the endpoint nodes are described in Supplemental Table 4. Probabilities are explicitly communicated by the probability distributions (black bars) of the endpoint variables (Figure 3). Risk to an endpoint is overestimated if the child node has a uniform probability distribution; therefore, the uncertainty in both the child and parent nodes should be considered when analyzing the distribution of the endpoints. The endpoint "Annual Hg flux" does not estimate a risk probability because regulatory guidelines for riverine Hg export do not exist. In the GSL model this endpoint predicts the annual Hg flux from GSL to the MR; in the GBS model it predicts the flux from the MR into the Arctic Ocean. The calculation of Hg flux required several assumptions (Supplemental Table 4), and the results are only appropriate for the GSL Outlet and GBS North study regions, respectively.

It is important to note that the endpoints "% Fish not eligible for sale" and "Exceedance of pTWI" represent the probability that an adverse event will occur and are not an appropriate estimate of risk for a risk-assessment because they do not consider additional factors such as the consequence of the event, or potential control and mitigation measures (Fenton and Neil, 2011). The purpose of this model was to develop a BN-RRM framework to identify the Hg sources

driving Hg concentrations in freshwater and fish in an Arctic River system. This model can be improved if future goals are to produce sensible risk estimates. Some examples of factors that should be considered include the economic impacts to commercial fisheries from fish catch loss, the frequency of Hg testing by commercial fisheries, potential mitigation strategies to prevent the catch of fish with elevated Hg (such as fishing in select locations), and the impact that knowledge of fish Hg concentrations will have on people's dietary choices.

Analysis of counterfactuals

The Bayes theorem is the mathematical formula for conditional probabilities and is the basis of Bayesian Networks. The Bayes theorem states that:

$$(P(A= a) \mid P(B= b)) = (P_A = a)^* (P (B = b) \mid P(A = a)) / (P (B= b))$$

The theorem relates an event probability (ie. P (A = a)) to the probabilities of other causally linked events via conditional probabilities (P(A = a)| P(B= b) and vice versa), which are established by a dataset with observations of the two variables. An intervention can be performed by inserting a value for one of the variables. Counterfactual analysis is the process of elucidating the impact of an intervention on other variables in the model (Lu *et al.* 2022; Pearl and Mackenzie, 2018). An example of a counterfactual would be the quarry of how the anticipated reduction in atmospheric Hg deposition (variable B) following the Minamata treaty may influence Hg concentrations in freshwater (variable A). By selecting a value for B (ie. b = 3 ug Hg/m2/ yr), the P(B = b) factor becomes 1, and is effectively removed from the equation. Since the prior and conditional probabilities have been established with the training dataset, the calculation of P (A= a) | P (B = b) is a matter of calculus performed by the BN software. The ability to perform counterfactual analysis makes BN uniquely qualified to examine various

management scenarios and predict how further stress will impact the downstream variables (Pearl and Mackenzie, 2018).

Results and Discussion

Sensitivity analysis

The primary objective of the BN-RRMs (Figure 3, Supplemental Figures 1-8) was to perform a sensitivity analysis to identify the pollutant sources that are influencing Hg concentrations in freshwater and fish. Influential sources varied amongst study regions, particularly in the GBS model which covers an area 5 times larger than the GSL (Table 1). The sensitivity analysis results (Figure 4) display the mutual information (y-axis) shared between the dependent effect variables, listed in the sub-headings, and the explanatory source variables, defined by the coloured columns across all model study regions (x-axis). The Hg source with the largest relative mutual information value is the influential Hg source for a particular effect variable and region. There is no absolute mutual information value that defines when a source is influential. Higher mutual information values may be observed between variables that are causally linked. For the purposes of these models, this would mean that the non-point sources are likely to have lower mutual information, because they are connected to the Effect variables through the intermediate "Total Hg deposition" node. Effect variables with no data will have a blank result for the sensitivity analysis, while variables with low sample numbers tend to have low mutual information values. If the dataset has high variability with inconsistency in the conditional probabilities, this will also result in lower mutual information values because the causal relationships are unclear. Another reason for a lack of correlation would be that a Hg

source has been overlooked. This can be rectified by the integration of rightsholders and stakeholders in the conceptual model formation.

The CPTs were developed using a combination of GIS and monitoring data, but gaps in the monitoring dataset can bias the model predictions. Combinations of monitoring locations of effect variables (columns) and Hg source node states (rows) are summarized in Figure 5, where red squares indicate a lack of monitoring data. Sampling bias is evident when observations of effect variables are centered around a single Hg source node state. For example, in the GSL East Arm region (Figure 5, column 1 of GSL Model), all lake whitefish and northern pike monitoring locations are in proximity to a historic mine, while water monitoring locations are not. Consequently, exploratory analysis for a relationship between fish and water Hg was not possible because of temporal discrepancies between sample collection dates. Targeted monitoring programs are the primary method of correcting sampling biases. This occurs when monitoring data is available for all node states which are present in the natural system. These states can be identified by considering the probability distributions of the Hg source nodes (Supplemental Figures 1-8). The missing Hg source states which are contributing most to model bias were also identified by white text (Figure 5), and Supplemental Figures 13- 16 can be used to locate regions where a particular node state is present. Sampling of locations with those Hg source node states should be prioritized in future monitoring programs.

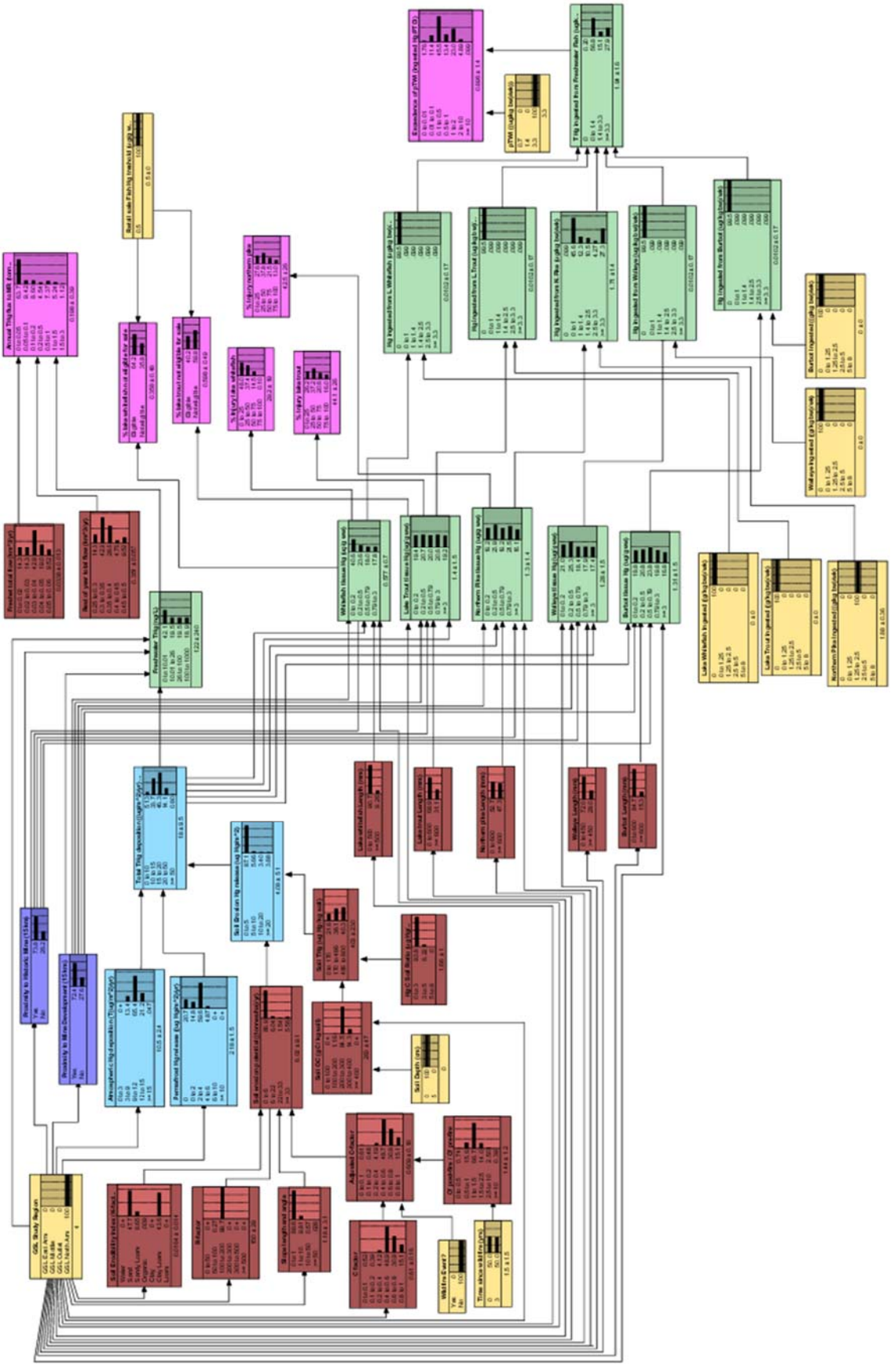

Figure 3. The parameterized GSL model for the GSL North Arm study region. Nodes in the BN-RRM are organized into categories, with a unidirectional flow of information between Scenario (yellow), Source (blue), Stressor (brown), Effect (green), and Endpoint (pink). The nodes are described by probability distributions (black bars) across several states. Scenario nodes are interactive; in this model configuration, the endpoint risk probabilities represent an adult male (pTWI = 3.3) consuming a single serving (2.5 g/kg bw/wk) of Northern pike per week, in a region of the GSL North Arm which has not experienced recent wildfires (Wildfire Event? = No).

A discussion of the sensitivity analysis results is provided only for the variables with non-negligible mutual information values to indicate reasonable predictive ability. For the GBS model this includes the lake trout, lake whitefish, and water THg variables. For the GSL model, it is only the lake whitefish, northern pike, and water THg variables that display significant trends. Neither model was able to reasonably predict walleye Hg or burbot Hg.

Soil erosion was identified as an influential variable in freshwater from the GBS study region (Figure 4), which supports the observations of Indigenous communities (Parlee and Maloney 2016; MRBB 2021) and results of Hg speciation experiments (Carrie *et al.* 2012; Leitch *et al.* 2007). This is the first Canadian study that has attempted to estimate soil erosion for a large region using the RUSLE method. Other studies have considered the effect of slope and habitat characteristics on freshwater and fish Hg but did not estimate soil erosion (Moslemi-Aqdam *et al.* 2022; Evans *et al.* 2013; Lockhart *et al.* 2005). In the GSL regions, atmospheric Hg deposition was the major influential Hg source, a pattern which correlates to the model output of the GEM-MACH-Hg atmospheric deposition model (Supplemental Figure 14; Dastoor *et al.* 2015). Permafrost Hg release had a lower impact on freshwater Hg, appearing to be a major source only in the GBS South (Figure 4), and to a lesser extent the GSL North Arm.

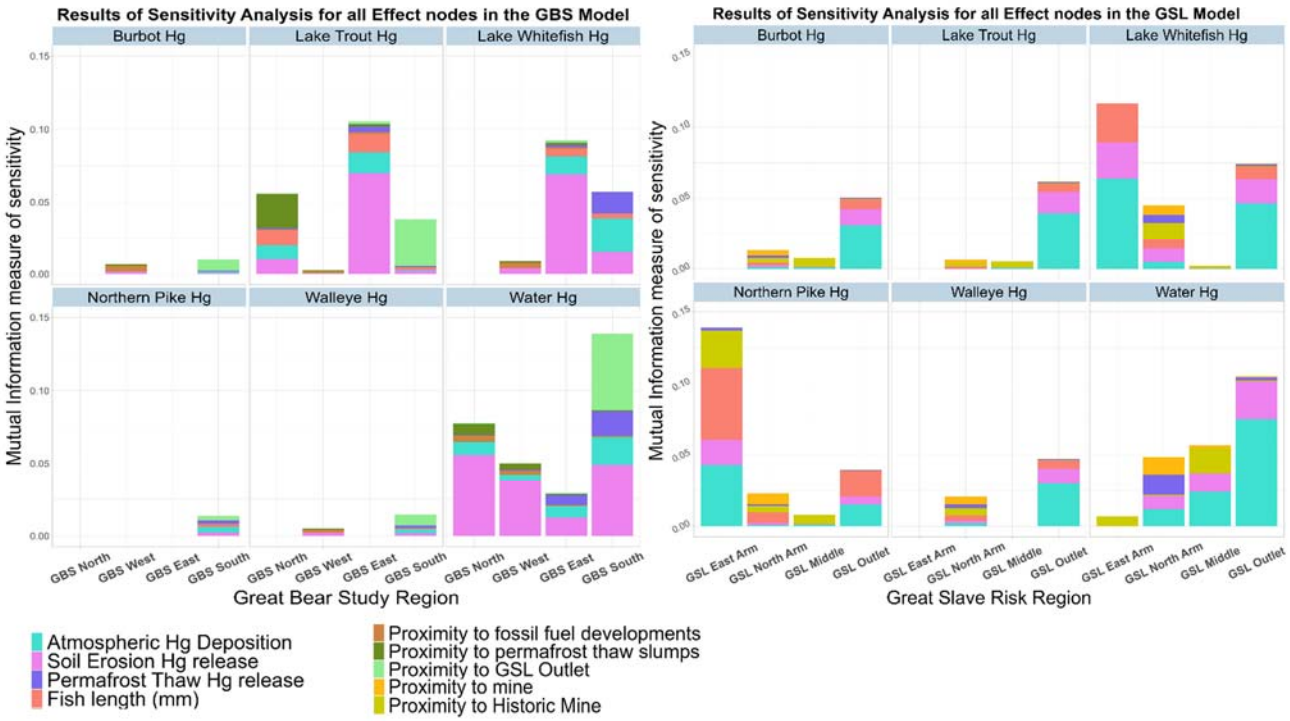

Figure 4. A bar-graph of the mutual information values produced by a sensitivity analysis on six variables in the Effect category: Freshwater THg and tissue Hg in five fish species. The Hg Source variables and their relative influence are represented by the coloured columns. Variables with negligible mutual information values are not adequately described by any of the Hg pathways considered in the BN-RRM framework. The left graph is for the four study regions (SR1 – SR4) of the GBS model, while the right is for the study regions of the GSL model: East Arm, North Arm, Middle and Outlet.

In the GBS model, the fossil fuel and natural gas extraction facilities in the North and West regions were the primary anthropogenic Hg sources considered. Sensitivity analysis results for fish species in this region were unreliable due to the lack of monitoring in proximity to these facilities (Figure 5). Lake trout collected from Yaya Lake in the GBS North region (Roux, 2014) were the only fish samples within 50 km of a fossil fuel development, which ultimately was not

identified as an influential source (Figure 4). The largest fossil fuel developments in the MRB are at Norman Wells; fossil fuel extraction is relatively low but seeing expansion (GNWT Centre of Geomatics, Supplemental Figure 12). There is currently a lack of fish data near facilities in Norman Wells, representing a knowledge gap that must be rectified. However, the Norman Wells Aquatic Monitoring Program (Imperial, 2019) has not yet proposed a plan to conduct Hg monitoring of food fish species.

Sensitivity results for lake trout in the GBS model were inconsistent between study regions. Lake trout were the only fish to be sampled in the GBS North study region, where Hg concentrations were primarily correlated to permafrost thaw slump proximity. However, all sampling sites were in proximity to thaw slumps (Figure 5) which produces a clear sampling bias in the model. Similarly, in the GBS South study region all lake trout monitoring locations are in proximity to the GSL Outlet. This is not the case for the lake whitefish sampling in GBS South region, where the variety of data ultimately resulted in the GSL Outlet not being an influential point source. Sensitivity results for the lake trout Hg variable in three GBS regions (SR1, SR2, SR4) are inaccurate due to the limited spatial variation in sampling sites.

In the GSL model, the sensitivity results for northern pike (Figure 4) are in line with expectations. This model uses fish length as a proxy variable for fish age, since length is a simple measurement that does not require specialty equipment or training. Northern pike are a keystone species in NWT lakes and are the largest and hyper-carnivorous of the five species considered in the model (Rohonczy *et al.* 2020). Therefore, it is logical that bioaccumulation and biomagnification pathways are of greater importance in this species. In comparison, lake trout and lake whitefish consume a varied diet of invertebrates, crustaceans, and small fish, and their tissue concentrations are lower than those observed in northern pike. A diet of low-trophic level

organisms may explain the higher correlation between lake whitefish tissue Hg and non-point sources such as soil erosion and atmospheric deposition.

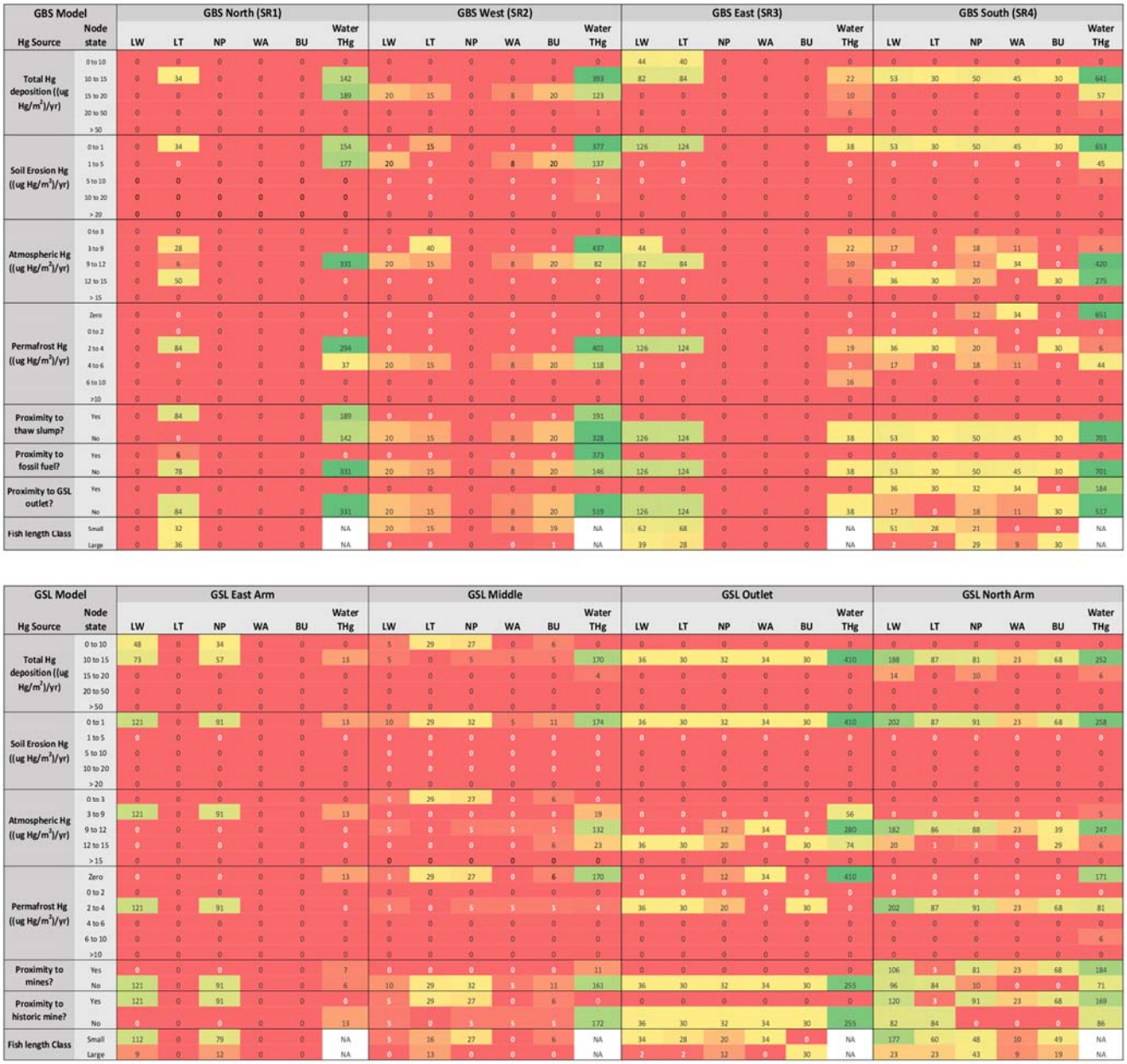

GBS Model		GBS North (SR1)						GBS West (SR2)						GBS East (SR3)						GBS South (SR4)					
Hg Source	Node state	LW	LT	NP	WA	BU	Water THg	LW	LT	NP	WA	BU	Water THg	LW	LT	NP	WA	BU	Water THg	LW	LT	NP	WA	BU	Water THg
Total Hg deposition ((ug Hg/m^2)/yr)	0 to 10	0	0	0	0	0	0	0	0	0	0	0	0	44	40	0	0	0	0	0	0	0	0	0	0
	10 to 15	0	34	0	0	0	142	0	0	0	0	0	393	82	84	0	0	0	22	53	30	50	45	30	641
	15 to 20	0	0	0	0	0	189	20	15	0	8	20	123	0	0	0	0	0	10	0	0	0	0	0	57
	20 to 50	0	0	0	0	0	0	0	0	0	0	0	1	0	0	0	0	0	6	0	0	0	0	0	1
	>50	0	0	0	0	0	0	0	0	0	0	0	0	0	0	0	0	0	0	0	0	0	0	0	0
Soil Erosion Hg ((ug Hg/m^2)/yr)	0 to 1	0	34	0	0	0	154	0	15	0	0	0	377	126	124	0	0	0	38	53	30	50	45	30	653
	1 to 5	0	0	0	0	0	177	20	0	0	8	20	137	0	0	0	0	0	0	0	0	0	0	0	45
	5 to 10	0	0	0	0	0	0	0	0	0	0	0	2	0	0	0	0	0	0	0	0	0	0	0	3
	10 to 20	0	0	0	0	0	0	0	0	0	0	0	3	0	0	0	0	0	0	0	0	0	0	0	0
	> 20	0	0	0	0	0	0	0	0	0	0	0	0	0	0	0	0	0	0	0	0	0	0	0	0
Atmospheric Hg ((ug Hg/m^2)/yr)	0 to 3	0	0	0	0	0	0	0	0	0	0	0	0	0	0	0	0	0	0	0	0	0	0	0	0
	3 to 9	0	28	0	0	0	0	0	40	0	0	0	437	44	0	0	0	0	22	17	0	18	11	0	6
	9 to 12	0	6	0	0	0	331	20	15	0	8	20	82	82	84	0	0	0	10	0	0	12	34	0	420
	12 to 15	0	50	0	0	0	0	0	0	0	0	0	0	0	0	0	0	0	6	36	30	20	0	30	275
	> 15	0	0	0	0	0	0	0	0	0	0	0	0	0	0	0	0	0	0	0	0	0	0	0	0
Permafrost Hg ((ug Hg/m^2)/yr)	Zero	0	0	0	0	0	0	0	0	0	0	0	0	0	0	0	0	0	0	0	0	12	34	0	651
	0 to 2	0	0	0	0	0	0	0	0	0	0	0	0	0	0	0	0	0	0	0	0	0	0	0	0
	2 to 4	0	84	0	0	0	294	0	0	0	0	0	401	126	124	0	0	0	19	36	30	20	0	30	6
	4 to 6	0	0	0	0	0	37	20	15	0	8	20	118	0	0	0	0	0	3	17	0	18	11	0	44
	6 to 10	0	0	0	0	0	0	0	0	0	0	0	0	0	0	0	0	0	16	0	0	0	0	0	0
	>10	0	0	0	0	0	0	0	0	0	0	0	0	0	0	0	0	0	0	0	0	0	0	0	0
Proximity to thaw slump?	Yes	0	84	0	0	0	189	0	0	0	0	0	191	0	0	0	0	0	0	0	0	0	0	0	0
	No	0	0	0	0	0	142	20	15	0	8	20	328	126	124	0	0	0	38	53	30	50	45	30	701
Proximity to fossil fuel?	Yes	0	6	0	0	0	0	0	0	0	0	0	373	0	0	0	0	0	0	0	0	0	0	0	0
	No	0	78	0	0	0	331	20	15	0	8	20	146	126	124	0	0	0	38	53	30	50	45	30	701
Proximity to GSL outlet?	Yes	0	0	0	0	0	0	0	0	0	0	0	0	0	0	0	0	0	0	36	30	32	34	0	184
	No	0	84	0	0	0	331	20	15	0	8	20	519	126	124	0	0	0	38	17	0	18	11	30	517
Fish length Class	Small	0	32	0	0	0	NA	20	15	0	8	19	NA	62	68	0	0	0	NA	51	28	21	0	0	NA
	Large	0	36	0	0	0	NA	0	0	0	0	1	NA	39	28	0	0	0	NA	2	2	29	9	30	NA

GSL Model		GSL East Arm						GSL Middle						GSL Outlet						GSL North Arm					
Hg Source	Node state	LW	LT	NP	WA	BU	Water THg	LW	LT	NP	WA	BU	Water THg	LW	LT	NP	WA	BU	Water THg	LW	LT	NP	WA	BU	Water THg
Total Hg deposition ((ug Hg/m^2)/yr)	0 to 10	48	0	34	0	0	0	5	29	27	0	6	0	0	0	0	0	0	0	0	0	0	0	0	0
	10 to 15	73	0	57	0	0	13	5	0	5	5	5	170	36	30	32	34	30	410	188	87	81	23	68	252
	15 to 20	0	0	0	0	0	0	0	0	0	0	0	4	0	0	0	0	0	0	14	0	10	0	0	6
	20 to 50	0	0	0	0	0	0	0	0	0	0	0	0	0	0	0	0	0	0	0	0	0	0	0	0
	>50	0	0	0	0	0	0	0	0	0	0	0	0	0	0	0	0	0	0	0	0	0	0	0	0
Soil Erosion Hg ((ug Hg/m^2)/yr)	0 to 1	121	0	91	0	0	13	10	29	32	5	11	174	36	30	32	34	30	410	202	87	91	23	68	258
	1 to 5	0	0	0	0	0	0	0	0	0	0	0	0	0	0	0	0	0	0	0	0	0	0	0	0
	5 to 10	0	0	0	0	0	0	0	0	0	0	0	0	0	0	0	0	0	0	0	0	0	0	0	0
	10 to 20	0	0	0	0	0	0	0	0	0	0	0	0	0	0	0	0	0	0	0	0	0	0	0	0
	> 20	0	0	0	0	0	0	0	0	0	0	0	0	0	0	0	0	0	0	0	0	0	0	0	0
Atmospheric Hg ((ug Hg/m^2)/yr)	0 to 3	0	0	0	0	0	0	5	29	27	0	6	0	0	0	0	0	0	0	0	0	0	0	0	0
	3 to 9	121	0	91	0	0	13	0	0	0	0	0	19	0	0	0	0	0	56	0	0	0	0	0	5
	9 to 12	0	0	0	0	0	0	5	0	5	5	5	132	0	0	12	34	0	280	182	86	88	23	39	247
	12 to 15	0	0	0	0	0	0	0	0	0	0	6	23	36	30	20	0	30	74	20	1	3	0	29	6
	>15	0	0	0	0	0	0	0	0	0	0	0	0	0	0	0	0	0	0	0	0	0	0	0	0
Permafrost Hg ((ug Hg/m^2)/yr)	Zero	0	0	0	0	0	13	5	29	27	0	6	170	0	0	12	34	0	410	0	0	0	0	0	171
	0 to 2	0	0	0	0	0	0	0	0	0	0	0	0	0	0	0	0	0	0	0	0	0	0	0	0
	2 to 4	121	0	91	0	0	0	5	0	5	5	5	4	36	30	20	0	30	0	202	87	91	23	68	81
	4 to 6	0	0	0	0	0	0	0	0	0	0	0	0	0	0	0	0	0	0	0	0	0	0	0	0
	6 to 10	0	0	0	0	0	0	0	0	0	0	0	0	0	0	0	0	0	0	0	0	0	0	0	6
	>10	0	0	0	0	0	0	0	0	0	0	0	0	0	0	0	0	0	0	0	0	0	0	0	0
Proximity to mines?	Yes	0	0	0	0	0	7	0	0	0	0	0	11	0	0	0	0	0	0	106	3	81	23	68	184
	No	121	0	91	0	0	6	10	29	32	5	11	161	36	30	32	34	30	255	96	84	10	0	0	71
Proximity to historic mine?	Yes	121	0	91	0	0	0	5	29	27	0	6	0	0	0	0	0	0	0	120	3	91	23	68	169
	No	0	0	0	0	0	13	5	0	5	5	5	172	36	30	32	34	30	255	82	84	0	0	0	86
Fish length Class	Small	112	0	79	0	0	NA	5	16	27	0	6	NA	34	28	20	34	0	NA	177	60	48	10	49	NA
	Large	9	0	12	0	0	NA	0	13	0	0	0	NA	2	2	12	0	30	NA	23	23	43	9	19	NA

Figure 5. Summary of the Hg monitoring data (2005 – 2020) used to construct the BN-RRM conditional probability tables (CPTs). Columns represent the study regions and the dependent (Effect) variables (LW= lake whitefish, LT= lake trout, NP= northern pike, WA= walleye, BU= burbot), while rows represent the Hg sources and their respective node states. The colours indicate sampling effort for a

unique combination of dependent variable and source state, from no sampling (red) and few samples (yellow) to a high (≥ 300) number of samples (green). The missing data which is driving bias in the model is identified by white text and sampling at these Hg node states should be prioritized in future monitoring programs.

A surprising result from the GSL model was the identification of historic and active mining as important Hg sources in the GSL East Arm. The historic mine in the GSL East arm is Beaulieu Gold mine, a minor producer from 1942- 1948 (Silke, 2009). A closer inspection of the dataset (Figure 5) revealed that all fish sampling locations in the GSL East Arm were in proximity to Beaulieu Gold mine, but not to an active mining claim (Figure 5, Supplemental Figure 8). The model is unable to determine whether mining proximity influences tissue Hg in the GSL East Arm without a targeted monitoring program to sample areas distant from Beaulieu mine. On the other hand, the GSL North Arm is a location with many historic mines and a greater number of active mining claims (GNWT Centre of Geomatics; Supplemental Figure 13). This region also had the highest concentrations of Hg in both lake whitefish and northern pike in the GSL model, but the spread of data was greater than in other GSL regions (Supplemental Table 5). Datapoints from lake whitefish and northern pike monitoring were available for all combinations of active mining (Figure 5). Despite the large number of samples, the mutual information values for the GSL North Arm were low (Figure 4), potentially due to variability in the dataset (Table 2). The sensitivity results indicate that historic and active mines in Great Slave Lake are impacting Hg levels in fish, but the low mutual information values (< 0.05) imply an insignificant effect, in part because of the incomplete dataset.

Using the model to predict risk probabilities to endpoints:

In the parameterized alpha models, the variables are grouped into the BN-RRM categories of Scenario, Source, Stressor, Effect, and Impact and are differentiated by colour (Figure 3, Supplemental Figures 1-8). Nodes in the Scenario category (yellow) are interactive and user determined; for example, the "Study region" variable specifies the spatial extent. The probability of observing a particular node state is listed left of the black bars (Figure 3). For example, a "Freshwater THg" measurement sampled in the GSL North Arm (Figure 3) has a 42.1% chance of falling into the 0 – 10.1 ng/L category. When nodes are discretized using regulatory thresholds as the boundary values, the probability of observing a particular state is equivalent to the probability of exceeding a regulatory guideline. In the same GSL North Arm region (Figure 3) there was a 38.4% probability that a "Freshwater THg" measurement will surpass the Canadian guideline for protection of aquatic life (26 ng Hg/L- CCME, 2003). However, this latter probability is being overestimated by the model due to uncertainties in downstream nodes being propagated to child nodes when the BN model is compiled; according to the observed data, only 3% of THg measurements in this region surpassed the CCME guideline (Table 2).

Table 2. A comparison of the probability distributions from the observed data and the modelled distributions for the GSL North Arm study region. Four effect variables had non-negligible distributions in the BN-RRMs. The most probable node states were underestimated in the model predictions, with negative discrepancy values over 40% across the four variables. Similarly, the least probable and coincidently the highest risk states, were overestimated and had the largest positive discrepancy values.

Effect variable	Total observations (n)	Node state	Observed data: Counts	Observed data: probability	Model probability prediction	Discrepancy
Freshwater THg (ng THg/L)	258	0 to 10	243	94.2	42.1	-52.1
		10 to 26	7	2.7	19.5	16.8
		26 to 100	7	2.7	19.5	16.8
		>100	1	0.4	18.9	18.5
Lake whitefish Hg (ug Hg/g tissue)	202	0 to 0.2	169	83.7	40.6	-43.1
		0.2 to 0.5	32	15.8	23.6	7.8
		0.5 to 0.79	1	0.5	18	17.5
		0.79 to 3	0	0.0	17.8	17.8
Northern pike Hg (ug Hg/g tissue)	91	0 to 0.2	14	15.4	19.2	3.8
		0.2 to 0.5	30	33.0	23.9	-9.1
		0.5 to 0.79	18	19.8	19.2	-0.6
		0.79 to 3	28	30.8	21.5	-9.3
		> 3	1	1.1	16.1	15.0
Lake trout Hg (ug Hg/g tissue)	87	0 to 0.2	10	11.5	19.4	7.9
		0.2 to 0.5	68	78.2	20.7	-57.5
		0.5 to 0.79	7	8.0	20	12.0
		0.79 to 3	2	2.3	20.6	18.3
		> 3	0	0.0	19.2	19.2

If the propagation of uncertainty is causing this discrepancy, the unobserved node state probabilities would be overestimated and the most populous state will be underestimated. Table 2 shows that this is the case for all Effect variables in the GSL North Arm- the node states with the fewest observations have the largest positive discrepancies, and vice versa for the most probable states. For the fish effect nodes, the model predicts that 59.4% of lake whitefish will

exceed the guideline for subsistence consumption (0.2 ppm- Health Canada, 2007), compared to 16.3% observed in the dataset (n= 202). For lake trout and northern pike, the model prediction is 80.5% of fish will surpass this guideline (88.5% observed in dataset, n= 87) and 80.7% (compared to 84.6% in dataset, n= 91), respectively (Table 2). Both lake trout and northern pike concentrations are being overestimated compared to the observed data because the lowest state (0 to 0.2 ug Hg/g tissue) is not the most probable, as was the case in the "Lake whitefish Hg" and "Freshwater THg" nodes. Supplemental Table 5 compares observed data and model outputs across all study regions. The discrepancy is highest when the number of samples is low (< 100) and when all observations of a variable are of the lowest state (Supplemental Table 5). Because these are relative risk models which are incorporating uncertainty, it is not surprising that the risk predictions are incongruous with the observed data. Instead, these models should be used to compare which of the study regions are experiencing the highest risk probabilities to endpoints and focus on identifying the influential variables driving this exposure.

Great Slave Lake supports the largest fisheries in the study region (Supplemental Figure 18), where nearly all commercial catch is attributed to lake trout and lake whitefish (Fisheries Act). In the GSL model, the observed Hg values (Supplemental Table 5) suggest that lake whitefish caught in the GSL Middle region will have the lowest probability (0%) of surpassing the Canadian guideline for subsistence consumers (0.2 ppm- Lockhart *et al.* 2005) and the GSL North Arm will have the highest (16.3%). To the contrary, the model "% Lake Whitefish not eligible for sale" endpoint suggests that lake whitefish from the GSL Middle region has the highest probability of exceeding the 0.2 ppm threshold (49.4%, Supplemental Figures 5-8). The low sample number in the GSL Middle region (n= 10) and high uncertainty mean that the resulting risk probabilities of exposure are unsubstantiated. Similarly, the model predicts that

lake trout from the GSL Outlet are least likely (45.7% compared to 20% in observations, n= 30) to exceed the commercial sale threshold (0.5 ppm- Health Canada, 2007), while trout from the GSL North Arm are most probable (59.9% compared to 10% in observations, n= 87; Supplemental Table 5).

Like the previous endpoint, the "% Injury to Fish" endpoint is also only dependent on fish tissue Hg concentrations and does not consider other pollutants or lake factors, such as temperature. Injury refers to the impact of tissue Hg on mortality, developmental abnormalities, and spawning success endpoints (Dillon *et al*. 2010). Mercury toxicity experiments on juvenile fathead minnows (Dillon *et al.* 2010) were used to develop a dose-response curve (Supplemental Figure 21) using the R-studio *drc* package (Ritz, 2015). According to the model outputs, lake trout caught in the GSL North Arm (n= 87) had the highest Hg concentrations, while lake whitefish (n= 10) and northern pike (n= 32) caught in the GSL Middle region were most likely to have elevated Hg concentrations (Supplemental Figures 5- 8). However, the monitoring data (Supplemental Table 5) shows that northern pike from the GSL North Arm exceeded the Dillon *et al*. (2010) ED20 threshold (0.79 ppm Hg) more times (14.3%, n= 91) than in other regions (East Arm- 1%; Middle- 6%; Outlet- 6%). There were no instances where lake whitefish exceeded the Dillon *et al.* 2010 ED20 threshold.

In the GBS model, lake trout and lake whitefish caught in the West (SR2) region had the highest likelihood of injury (Supplemental Figures 1-4). The predictions for the GBS model correspond to the observed data (Supplemental Table 5), although the sample numbers are small ($n \leq 20$). Note that fathead minnows are a small, low-trophic level fish species and their toxicity response does not accurately represent the five freshwater fish species included in this model (Supplemental Table 4). The risk of injury to the model species is likely being underestimated, as

fathead minnows are believed to be less sensitive to metal toxicity than salmonid species like lake trout and whitefish (Teather and Parrott, 2006; Dillon *et al*. 2010).

The "Exceedance of pTWI" endpoint is dependent on a user defined diet and a probable tolerable weekly intake (pTWI) guideline which represents the user (Supplemental Table 4). Values above 1 indicate the exceedance of the dietary Hg guidelines. For example, an adult male (pTWI threshold of 3.3 ug Hg $kgbw^{-1}$ wk^{-1}) in the GSL North Arm region consuming one portion (2.5 g $kgbw^{-1}$ wk^{-1}) of northern pike over a week will have ~28% chance of exceeding his appropriate guideline (Figure 3). As described previously, the predicted risk probability is likely being overestimated due to the high uncertainty in the "Northern Pike tissue Hg" node. The results of this Impact variable are not valid if no diet or pTWI threshold are selected; this is indicated by a flat distribution in the respective "Fish ingested" child nodes. The high uncertainty in the parent effect nodes will result in an overestimation of the risk probability to the endpoint child nodes. It is crucial to consider the uncertainty in the child nodes when reviewing the endpoint probabilities.

Counterfactual analysis 1: Impact of Minamata treaty

The Minamata Convention is a multilateral agreement to reduce the anthropogenic inputs of Hg into the environment; it was signed in 2013 by 128 countries that pledged to reduce Hg use across manufacturing, energy, and gold mining industries by 2030 (UNEP, 2021; UNEP, 2019). The BN-RRM for GSL was used for the counterfactual analysis of how a significant reduction in atmospheric Hg deposition concentrations will impact Hg concentrations in the lake. Sensitivity analysis of the freshwater Hg and lake whitefish tissue Hg nodes identified atmospheric deposition to be an influential source in the GSL Outlet study region (Figure 4). In the natural system, approximately 83% of the atmospheric deposition values in this region were above 9 ug

Hg m^{-2} yr^{-1}, with 16% falling between 3 and 9 ug Hg m^{-2} yr^{-1} (Supplemental Figure 5). An observation of an atmospheric deposition value between 3 – 9 ug Hg m^{-2} yr^{-1} was input into the model, impacting the distribution of downstream nodes (Supplemental Figure 12), including the two effect variables of interest. The results of this counterfactual analysis suggested that Hg concentrations in freshwater and fish tissue would increase with a decrease in atmospheric deposition (Supplemental Figures 5 and 9). This prediction is contrary to the expected results and is an example of a limitation in the current model. Since the causal relationships between effect and source variables were built with data only, the model uncertainties are high when probing low probability physical states. Increased sampling of locations experiencing lower atmospheric deposition will reduce the uncertainty associated with this node state and improve the model predictions. The sampling efforts over the study period (2005 – 2020) were summarized to aid the reader when interpreting the validity of the model outputs (Figure 5).

Counterfactual analysis 2: Impact of consumption advisories

In the NWT, fish consumption advisories include a size restriction, with most piscivorous fish over 600 mm being considered higher-risk food sources (GNWT Health and Social Services, 2016). While consumption advisories can reduce Hg exposure to at-risk communities, they also have undesirable nutritional, cultural, and food-security impacts (Houde *et al.* 2022; Hoover, 2013). The GSL BN-RRM was used to probe whether consuming predatory fish below the size restriction significantly reduces Hg exposure. The counterfactual analysis was performed on the northern pike variable in the GSL East Arm and GSL Outlet study regions, where fish size was an influential variable (Figure 4).

In the GSL East Arm region, 86% of northern pike samples were below 600 mm in length (Supplemental Figure 8). After selecting for the smaller size (< 600 mm), the model

suggests a 55.9% probability of tissue concentrations below 0.5 ppm, the Canadian threshold for the commercial sale of fish (Supplemental Figure 10a). If an adult male consumes 1 serving (2.5g tissue/kg bw/ wk) a week, this corresponds to ~23% probability of exceeding the weekly Hg threshold (Supplemental Figure 10a). When the larger size was selected, the model did perform as expected, with a ~43% probability of tissue concentrations below 0.5 ppm, corresponding to a 27% probability of exceeding the weekly dietary threshold (Supplemental Figure 10b).

In the GSL Outlet study region only 61% of the datapoints (Supplemental Figure 5) were northern pike below 600 mm, meaning that uncertainty for large fish is lower in this region. Adult males consuming 1 serving of a small northern pike will have a ~ 19% probability of exceeding their weekly Hg dietary threshold, while those consuming 1 serving of a large fish will have ~23% probability of exceedance (Supplemental Figure 11). The model performs as expected and confirms that consuming smaller fish will reduce the probability of Hg exposure. Additionally, it indicates that there is lower risk when consuming fish from the GSL Outlet region. The risk probabilities and uncertainties associated with consumption advisories can be presented to communities to aid their decisions on whether the benefits outweigh the cultural impacts.

Conclusions and Future Work

The aim of the project was to develop a causal framework to identify the Hg pathways that have the greatest influence on Hg concentrations in freshwater and fish of the lower Mackenzie River Basin (MRB). Models were prepared for the Great Bear subbasin (GBS) and Great Slave Lake (GSL) in Netica, a free Bayesian Network (BN) modelling software. These models are the Canadian contribution to the ARCRISK project, which was initiated to resolve an

important gap in our understanding of how major freshwater tributaries are contributing to Hg pollution in the Arctic (Gundersen, 2020).

A sensitivity analysis was used to identify the influential Hg sources. Risk probabilities were found to vary between regions and dependent variables, with no single pattern to the sensitivity analysis results (Figure 4). In the GSL model, "Atmospheric Hg deposition" was the influential source for freshwater and lake whitefish, while northern pike were most sensitive to the "Fish length" biological stressor. The GSL North Arm had the highest concentrations of freshwater and fish tissue Hg (Supplemental Table 5). This is the location of many historic and active mine claims which were flagged as an influential variable across all effect nodes, although the low mutual information values suggest that this result is inconclusive. In the GBS model, both freshwater Hg and lake whitefish Hg were correlated to Hg release via rainfall-induced soil erosion. Only lake trout were sampled across all study regions, with the highest Hg concentrations measured in the GBS West (SR2) region (Supplemental Figure 5). However, due to low sample numbers (n= 30) and resulting low mutual information values (Figure 4), the sensitivity analysis results were inconclusive. Missing data is biasing the sensitivity analysis since all fish sampled in the GBS West were classified as "small" size (<600 mm), and distant from both permafrost thaw slumps and fossil fuel explorations (Figure 5). Overall, the mutual information values across both models were low and only a fraction of the variation in the data was explained by the potential Hg sources. Epistemic uncertainty resulting from missing and skewed data was the largest source of uncertainty in the model output. Uncertainty can be reduced by expanding the monitoring dataset through collaborations with other research groups or by the initiation of additional Hg monitoring projects. Finally, the BN-RRMs were used to probe counterfactuals and to predict the effect and uncertainty associated with two management

strategies: the Minamata Convention and consumption advisories for northern pike. The model performed as expected for the consumption advisory counterfactual, but predicted counterintuitive trends for the Minamata Convention counterfactual which were driven by the low sample numbers from locations with low annual atmospheric Hg deposition rates.

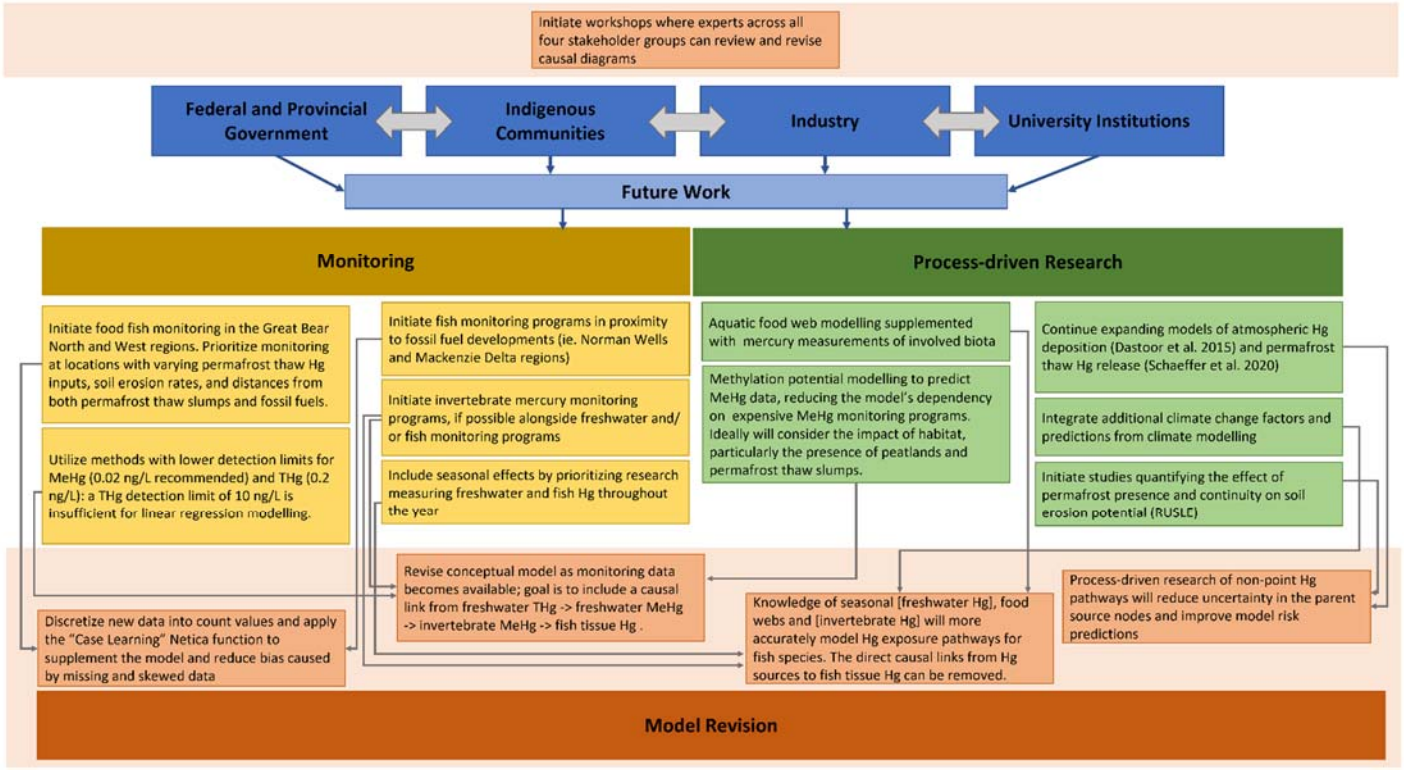

Figure 6. Future research recommendations developed from data gaps identified by a Bayesian network model of Hg exposure in the Mackenzie watershed. The chart is organized into long-term monitoring and shorter-term process-based research. The additional data will allow for revisions to the model and reduce the uncertainty from sampling bias and lack of knowledge of causal pathways.

Major gaps in monitoring data (Figure 5) which will need to be addressed include increasing freshwater MeHg monitoring, initiating invertebrate Hg programs, and prioritizing of fish Hg monitoring near fossil fuel developments in the GBS North and West study regions. To

address these gaps, collaborations with industry partners, Indigenous communities, academic institutions, and local government officials will be necessary (Figure 6). The primary step to validating the BN-RRMs is a workshop with experts from rightsholder and stakeholder groups to facilitate the review and revision of the causal models. Specific research recommendations for monitoring and shorter-term process-driven research were also developed to address the data gaps identified during the model parameterization. The recommendations include identification of specific study regions, causal pathways, and seasonal effects which need to be further developed to reduce sampling bias and process-related uncertainties in the model. Fish Hg and dietary Hg exposure data was sparce for the Gwitch'in and Inuvialuit groups located in the GBS North region, with few human health risk assessments (Curren *et al.* 2015; Wuttke *et al*. 2013) conducted for Hg exposure since the First Nations Biomonitoring Initiative's 2009-2013 health survey (Wuttke *et al.* 2013), which did not disclose the identity of the fifteen participating First Nations groups. Furthermore, collaborations with university institutions can expand the scope of this project. Research groups involved in the modelling of soil erosion, climate change, aquatic food webs, and mercury-methylation processes would provide invaluable quantitative estimates for the strength of the model's causal relationships. These relationships can be used as one source of evidence for the model and reduce the uncertainty derived from missing data and omitted causal pathways.

The management of Hg in aquatic ecosystems requires a holistic approach that consolidates knowledge across projects and scientific disciplines. Our findings were that the BN-RRM framework is an effective organizational tool for integrating various data sources and knowledge types. These models were parameterized with monitoring data from 21 projects, 2 environmental models, and 24 GIS datasets (Supplemental Tables 1-3). Additionally, the models

can be parameterized by expert judgement such that traditional ecological knowledge (TEK) can be granted equal weight to Western Science experiments. Knowledge gaps were identified by the high uncertainty values associated with variables that were sparsely monitored. A summary of the recent (2005 – 2020) sampling effort across regions and dependent variables (Figure 5) can aid in the development of future monitoring studies.

Acknowledgements:

The ARCRISK project was funded by the Arctic Contaminants Action Program (ACAP) and the Arctic Council Project Support Instrument (PSI) and is co-sponsored by the Norwegian Ministry of Climate and Environment (KLD). The Nordic Environment Finance Corporation (NEFCO) is the fund manager. Jannicke Moe, Cathrine Brecke Gundersen, and Hans Fredrik Vieteberg Braaten from the Norwegian Institute for Water Research (NIVA) were integral to the commencement and operation of the ARCRISK project. Maeve McGovern (NIVA), Wayne Landis and Emma Sharpe (Western Washington University) provided support for the BN model construction. This project would not have been possible without numerous mercury monitoring datasets and environmental model outputs. Environmental models were graciously shared by Camile Sothe (McMaster University and World Wildlife Fund Canada), Kevin Schaeffer (National Snow and Ice Data Center, University of Colorado Boulder) and Ashu Dastoor (Environment Climate Change Canada) through private correspondence. Publicly available mercury monitoring data was obtained from the Mackenzie DataStream (https://mackenziedatastream.ca/), and the following individuals: Mary Gamberg (Northern Contaminants Program funded projects), David Depew (Canadian Fish Mercury Database), Aimee Guile (Wek'èezhìı Renewable Resources Board), Lisa Loseto (University of Manitoba).

Chapter 4: Conclusions and Future Work

This thesis has presented a BN-RRM developed to assess the Hg sources driving Hg concentrations in freshwater and fish in the Mackenzie River region, a spatially grand and remote region in Canada. The project used publicly available data sources to identify local stakeholders, Hg sources and exposure pathways, and monitoring gaps. Following the literature review, the conceptual model (Figure 2) was simplified in accordance with the data available for the study area. Several key pathways and explanatory variables were omitted from the models, including the impact of season and the causal relationship between fish and freshwater Hg. Sampling bias in the monitoring datasets (Figure 5) resulted in greater uncertainty and unfounded sensitivity results.

The GSL model predicted that the probability of tissue-Hg-driven injury to lake whitefish and northern pike is greatest in the GSL Middle region, although this is likely driven by the low sample number (n= 10 and 31, respectively). The highest fish Hg concentrations were observed in the North Arm region which was extensively sampled (n= 202 for lake whitefish, 91 for northern pike) and had the second-highest probability of tissue-Hg-driven injury, while the well-sampled GSL East Arm region had the lowest fish tissue Hg samples (Supplemental Table 5). For the freshwater Hg variable, the highest probability of exceeding the CCME 2003 guideline (26 ng/L- CCME, 2003) was in the GSL East Arm (49.4%, n= 13), followed by the North Arm (38.4%, n= 258), the Middle (38.1%, n= 174), and the Outlet (29.5%, n= 411; Supplemental Table 5). Because freshwater Hg concentrations at the GSL - Mackenzie River outlet were not elevated relative to the other study regions, it is unlikely that Hg from point sources along the lakeshore are a major source of Hg downstream in the Mackenzie River. However, proximity to

mining was an influential Hg source across all effect variables in the GSL North Arm region (Figure 4).

In the GBS model, lake trout were the only fish to be sampled across all study regions and therefore the only biotic effect variable for which the tissue Hg concentrations could be compared. The Canadian guideline for the retail sale of fish (0.5 ppm- Health Canada, 2007) was most likely to be exceeded by lake trout sampled in the GBS West (38.5%, n= 15), followed by the GBS South (36%, n= 30), the North (30.6%, n= 84), and East (16.4%, n= 124). Similarly, the model predicted that the freshwater Hg guideline (CCME, 2003) was most likely to be exceeded in samples from the GBS East (41.1%, n= 38), followed by the West (34.2%, n= 519), the North (24.8%, n= 331), and the South (19.5%, n= 701). Trends for Hg exposure for the biotic and abiotic variables disagree and no single study region was identified as having higher risk probabilities. Discrepancies between the risk probabilities are mostly due to skewed sample sizes and the fact that uncertainty in BN-RRMs is presented as flat distributions with unprecedented large probabilities of high-risk states. Increased lake trout sampling in the GBS West and South, along with freshwater sampling in the GSL East would help reduce the sampling bias and improve the model's predictive capabilities. Sensitivity analysis identified soil erosion as the influential variable for freshwater THg across all study regions, and for lake trout in the GBS East region only (Figure 4).

The fish monitoring datasets represented several limitations to the model development. First, the locations of fish sampling sites were sparce in comparison to the freshwater monitoring (Figure 11) and particularly non-existent (< 1%) in the vicinity of fossil fuel developments. The Imperial Norman Wells Operations (INWO) facility was of interest to this project, as it intersects the Mackenzie River and is one of the larger industrial developments in the study area. Without

fish monitoring data near this facility, it is impossible to predict the impact that fossil fuel exploration is having on tissue Hg concentrations. Local communities and researchers have put pressure on the Imperial facility to include fish contaminant monitoring in the new Norman Wells Aquatic Effects Monitoring Program (Imperial, 2019). If successful, this will be a step towards rectifying this knowledge gap and represents an opportunity for collaborative action as the monitoring study is developed. Second, primary fish monitoring data for food-fish species was difficult to obtain due to the sensitive nature of this data for local Indigenous communities. While this data does exist, the ethical requirements for acquiring it make it inaccessible to the public. Collaborating with Indigenous communities, as well as established local research groups, would be beneficial to this project. Not only would the additional data be a major contribution to improving the model accuracy, but these groups would also be invaluable to the assessment and improvement of the conceptual model. Finally, most fish (60%) and freshwater (84%) monitoring data was collected during the summer sampling period, so seasonal variation in dietary exposure was not accounted for. In addition to increased fish sampling effort during off-summer seasons, the inclusion of season would require knowledge of seasonal impact on freshwater Hg speciation and some quantitative knowledge on the effects of permafrost presence on soil erosion rates. Inclusion of a season variable will account for some of the temporal uncertainty in the model.

Another limitation of the models is the lack of a causal relationship between the inorganic freshwater THg and fish tissue Hg nodes. Bacterial methylation of mercury makes inorganic Hg bio-accessible, allowing it to enter the aquatic food chain and accumulate in fish through a diet of low-trophic level organisms like invertebrates. Therefore, to develop a link between freshwater THg and fish tissue Hg, knowledge is needed on: 1) MeHg concentrations in

freshwater; 2) Hg concentrations in aquatic invertebrates and small fish ; 3) general knowledge of organism trophic levels and local food web structure. The first two gaps can be resolved by the inclusion of freshwater MeHg and invertebrate Hg monitoring into existing monitoring programs (Figure 6). In the study area, Hg concentrations in invertebrates were measured in only two projects (Chetelat *et al.* 2020; Moslemi-Aqdam *et al.* 2022), despite their importance in elucidating Hg transfer throughout the food chain. Structural equation models developed by Moslemi-Aqdam *et al.* (2022) identified invertebrate Hg to be the link between freshwater MeHg and fish tissue Hg. The third knowledge gap can be resolved by the integration of population dynamics and acyclic food web models into the BN-RRM framework (Fahd *et al.* 2021; Uusitalo *et al.* 2018). Models that integrate aquatic population dynamics would be able to predict Hg concentrations at higher trophic levels and more accurately estimate risk or identify influential variables.

Finally, the spatial extent of the models can be expanded to cover the remaining subbasins of the Mackenzie River Basin. Bayesian Network models were not prepared for the Peace, Athabasca, Liard, or Peel subbasins because these regions did not meet the scope of the ARCRISK project. While the Peel subbasin is in the Arctic circle and is a major tributary (8% total flow) to the Mackenzie River, it is also a remote and sparsely monitored region. A lack of publicly available fish monitoring data prevented the development of a Bayesian Network model for the subbasin. This was also the case for the mountainous and uninhabited region of the Liard subbasin. However, it is recommended that additional Hg monitoring programs and BN-RRMs are developed for the Liard subbasin to gain a holistic assessment of the state of Hg in the Mackenzie River. This is because the Liard River is the second largest tributary of the Mackenzie River (26%) and a region of unprecedented climate warming (Connon *et al.* 2014).

Additionally, it is the dominant source of particulate-bound Hg for the Mackenzie River and the location of a large tungsten mine which may see further expansion as the NWT continues to invest in its mining economy (Carrie *et al.* 2012; Silke, 2009). Finally, the Peace and Athabasca subbasins were not included in the model because of their distance from the Arctic Ocean. While the Oil Sand regions of the Athabasca watershed are highly industrialized areas in the MRB, this subbasin was not included in our models since it contributes only a small fraction of the total flow into the Mackenzie River (Erikson, 2020). The industrial point sources in this basin are likely elevating Hg concentrations in the local environment, but there is no evidence in the literature that effluent from these industries will result in a measurable effect in water at distances greater than 50 kilometers from the source. (Kelly *et al.* 2010) Therefore, it is not likely that activities in the Peace and Athabasca subbasins will impact the Hg concentrations in the aquatic ecosystems of Northern Canada and the Beaufort Sea.

Comprehensive BN models will incorporate rightsholder and stakeholder values throughout the ERA process, particularly in the development of the conceptual models. The construction of the conceptual models should be a collaborative effort between the modelers, scientific experts, local industries, and local communities. Due to budget and time constraints, rightsholder and stakeholder outreach was not completed in the time frame of this project. Therefore, the model structure and the subsequent results remain unvalidated and unreliable since they do not necessarily reflect the needs of the end-users. However, these models can still be used to showcase the benefits of BNs as organizational and decision-making tools, and to educate and garner support from rightsholder and stakeholder groups who may be unfamiliar with the probabilistic modelling process. Workshops with rightsholder and stakeholder groups should first encourage the participants to summarize their state of knowledge by devising their

own conceptual model structures without the input of scientists and modelers. The source and endpoints selections by participant groups can be used to inform future model iterations or to validate the model structures presented in this thesis. The development of multiple conceptual diagrams will ensure that the model structure agrees with available knowledge and that the model endpoints illustrate the needs of the end users, creating increased trust in the model output (Kaikkonen *et al.* 2020). Similarly, it is important to engage three industrial stakeholder groups: the Great Slave Lake commercial fishery co-operative, Imperial Norman Wells Operations, and the Canadian federal and NWT provincial government groups leading the Giant Mine Remediation project. These consultations will expand the scope of the models as the conceptual model is adapted and additional data becomes available. Support from all rightsholder and stakeholder groups will be beneficial to the accuracy and relevance of the BN models.

References:

AANDC Water Division (Chris Spence). 2022-04-30. “CIMP 140: Changing hydrology in the Taiga Shield_ Geochemical and resource management implications” (dataset). 2.0.0. *DataStream*. Doi: 10.25976/1ed9-gr10.

Albers S (2017). “tidyhydat: Extract and Tidy Canadian Hydrometric Data.” J. Open-Source Softw. 2(20). Doi:10.21105/joss.00511

AMAP: Arctic Monitoring and Assessment Programme (2011) Mercury and Human Health-Arctic Pollution 2011. P.O. Box8100 Dep., N-0032 Oslo, Norway.

AMAP/ UNEP. (2015) Global Mercury Modelling: Update of modelling results in the Global Mercury Assessment 2013. Arctic Monitoring and Assessment Programme, Oslo, Norway/ UNEP Chemicals Branch, Geneva, Switzerland.

Ayre K. K.; Landis, W. G. (2012) A Bayesian approach to landscape ecological risk assessment applied to the Upper Grande Ronde Watershed, Oregon. *Hum. Ecol. Risk. Assess.* **18** (5) 946–970. Doi: 10.1080/10807039.2012.707925

Ayre, K. K.; Caldwell, C. A.; Stinson, J.; Landis, W. G. (2014) Analysis of regional scale risk of Whirling Disease in populations of Colorado and Rio Grande Cutthroat Trout using a Bayesian Belief Network Model. *Risk. Anal*. **34** (9) 1589- 1605. Doi: 10.1111/risa.12189

Baird, I. G.; Silvano, R. A. M.; Parlee, B.; Poesch, M.; Maclean, B.; Napoleon, A.; Lepine, M.; Hallwass, G. (2021) The downstream impacts of hydroelectric dams and Indigenous and local knowledge: examples from the Peace- Athabasca, Mekong, and Amazon. *Environ. Manage.* **67**, 682-696. Doi: 10.1007/s00267-021-01440-7

Bill C-69, An Act to enact the Impact Assessment Act and the Canadian Energy Regulator Act, to amend the Navigation Protection Act and to make consequential amendments to other Acts, 1st Session, 42nd Parliament, 2019.

Bodaly, R. A.; Reist, J. D.; Rozenberg, D. M.; McCart, P. J.; Hecky, R. E. (1989) Fish and fisheries of the Mackenzie and Churchill river basins, northern Canada. *In* D. P. Dodge: Proceedings of the International Large River Symposium. *Can. Spec. Publ. Fish. Aquat. Sci*. **106**, 128- 144.

Bohning, R. A.; Campbell, D.; Grave, J. (1997) Forests of the Northwest Territories. Forest Management Division, Northwest Territories Department of Resources, Wildlife, and Economic Development.

Borelli, P., Panagos, P; Langhammer, J.; Apostol, B.; Schutt, B. (2016) Assessment of the cover changes and the soil loss potential in European forestland: First approach to derive indicators to capture the ecological impacts on soil-related forest ecosystems. *Ecol. Ind*. **60**, 1208-1220. Doi: 10.1016/j.ecolind.2015.08.053

Bouchard, F.; MacDonald, L.A.; Turner, K.W.; Thienpont, J.R.; Medeiros, A.S.; Biskaborn, B.K.; Korosi, J.; Hall, R.I.; Pienitz, R.; Wolfe, B.B. (2016) Paleolimnology of thermokarst lakes: a window into permafrost landscape evolution. *Arct. Sci*. **3**, 91- 117. Doi: 10.1139/as-2016-0022

Bravo, A. G.; Kothawala, D. N.; Attermeyer, K.; Tessier, E.; Bodmer, P.; Ledesma, J. L. J.; et al. (2018) The interplay between total mercury, methylmercury, and dissolved organic matter in fluvial systems: A latitudinal study across Europe. *Water Res*. **144**, 172- 182. Doi: 10.1016/j.watres.2018.06.064

Bruen, M.; Hallouin, T.; Christie, M.; Matson, R.; Siwicka, E.; Kelly, F.; Bullock, C.; Feeley, H. B.; Hannigan, E.; Kelly-Quinn, M. (2022) A Bayesian modelling framework for integration of ecosystem services into freshwater resource management. *Environ. Manage*. **69**, 781- 800. Doi: 10.1007/s00267-022-01595-x

Brychta, J.; Brychtová, M. (2020) Possibilities of including surface runoff barriers in the slope-length factor calculation in the GIS environment and its integration in the user-friendly LS-RUSLE tool. *Soil Water Res.* **15** (4) 246- 257. Doi: 10.17221/128/2019-SWR

Burn, C.R.; Leqkowicz, A.G. (1990) Canadian landform examples- 17: Regrogressive thaw slumps. *Can. Geogr*

Campeau, A.; Eklöf, K.; Soerensen, A.L.; Åkerblom, S.; Yuan, S.; Hintelmann, H.; Bieroza, M.; Köhler, S.; Zdanowicz, C. (2022) Sources of riverine mercury across the Mackenzie River Basin; inferences from a combined HgC isotopes and optical properties approach. *Sci. Total. Environ.* **806**: 150808. Doi: 10.1016/j.scitotenv.2021.150808.

Canada Gazette (2019) Regulations Repealing the Chlor-Alkali Mercury Release Regulations: SOR/2019-88. Part II, Volume 153, Number 8.

Canada Open Government (2015) Short-duration Rainfall Intensity-Duration-Frequency. Accessed January 22, 2022: https://open.canada.ca/data/en/dataset/15aa455c-9f9f-4405-8eee-4445d02fd35c

Canada Open Government (2016) Soil Texture by Ecodistrict- National Ecological Framework for Canada. Record ID: 0b88062f-ebbe-46c6-ab19-54fd226e9aa7.

Canada Open Government (2012) Modern Treaties. Government of Canada; Indigenous Services Canada; Information Management Branch, Geomatics Services.

CCME Canadian Environmental Quality Guidelines (2003) Canadian Water Quality Guidelines for the Protection of Aquatic Life. Canadian Council of Ministers, 2003.

CCME Canadian Environmental Quality Guidelines (1999). Canadian Sediment Quality Guidelines for the Protection of Aquatic Life. Canadian Council of Ministers, 1999.

Calder, R.S.D.; Schartup, A.T.; Li, M.; Valberg, A.P.; Balcom, P.H.; Sunderland, E.M. (2016) Future impacts of hydroelectric power development on methylmercury exposures of Canadian Indigenous communities. *Environmen. Sci. Technol*. **50**, 13115-13122. Doi: 10.1021/acs.est.6b04447

Carrie, J.; Stern, G. A.; Sanei, H.; Macdonald, R. W.; Wang, F. (2012) Determination of mercury biogeochemical fluxes in the remote Mackenzie River Basin, northwest Canada, using speciation of sulfur and organic carbon. *Appl. Geochemistry*. **27**, 815- 824. Doi: 10.1016/j.apgeochem.2012.01.018

Carriger, J. F.; Thompson, M.; Barron, M. G. (2021) Causal Bayesian networks in assessments of wildfire risk: Opportunities for ecological risk assessment and management. *Integr. Environ. Assess. Manag*. **17** (6), 1168- 1178. Doi: 10.1002/ieam.4443

Carson, M.A. (1987) Mackenzie River, NWT: Sediment-related issues and recommendations. Sediment Survey Section Water Resources Branch Inland Waters Directorate Environment Canada. Ottawa, Ontario, K1A0H3.

Chen, S. H.; Pollino, C. A. (2012) Good practice in Bayesian network modelling. *Environ Model Softw.* 37, 134-145. Doi: 10.1016/j.envsoft.2012.03.012

Chételat, J.; McKinney, M.A.; Amyot, M.; Dastoor, A.; Douglas, T.A.; Heimbürger-Boavida, L.E.; Kirk, J.; Kahilainen, K.K.; Outridge, P.M.; Pelletier, N.; Skov, H.; St. Pierre, K.; Vuorenmaa, J.; Wang, F. (2022) Climate change and mercury in the Arctic: Abiotic interactions. *Sci. Tot. Environ.* **824**: 153715. Doi: 10.1016/j.scitotenv.2022.153715

CIRNAC (2021) Northern Oil and Gas Annual Report 2021. Crown-Indigenous Relations and Northern Affairs Canada. Ottawa, ON, Canada.

Connon, R.F.; Quinton, W.L.; Craig, J.R.; Hayashi, M. (2014) Changing hydrologic connectivity due to permafrost thaw in the lower Liard River valley, NWT, Canada. *Hydrol.* **28**, 4163- 4178. Doi: 10.1002/hyp.10206

Communities of the NWT with support by Environment and Natural Resources, Government of the Northwest Territories. 2023-01-23. "NWT-wide Community-based Monitoring Program" (dataset). 8.1.0. DataStream. Doi: 10.25976/4der-gd31.

Cooke, C. A.; Kirk, J. L.; Muir, D. C. G.; Wiklund, J. A.; Wang, X.; Gleason, A.; Evans, M. S. (2017) Spatial and temporal patterns in trace element deposition to lakes in the Athabasca oil sands region (Alberta, Canada). *Environ. Res. Lett.* **12**: 124001. Doi: 10.1088/1748-9326/aa9505

Cooke, S. J.; Rice, J. C.; Prior, K. A.; Bloom, R.; Jensen, O.; Browne, D. R.; Donaldson, L. A.; Bennett, J. R.; Vermaire, J. C.; Auld, G. (2016) The Canadian context for evidence-based conservation and environmental management. *Environ. Evid.* **5**: 14. Doi: 10.1186/s13750-016-0065-8

Cott, P. A.; Johnston, T. A.; Gunn, J. M. (2011) Food web position of burbot relative to lake trout, northern pike, and lake whitefish in four sub-Arctic boreal lakes. *J. Appl. Ichthyol*. **27**, 49 – 56. Doi: 10.1111/j.1439-0426.2011.01843.x

Cott, P.A.; Zajdlik, B.A.; Palmer, M.J.; McPherson, M.D. (2016) Arsenic and mercury in lake whitefish and burbot near the abandoned Giant Mine of Great Slave Lake. *J. Great Lakes R.* **42**, 223-232. Doi: 10.1016/j.jglr.2015.11.004

Coull, B.A.; Mazzetti, M.; Ryan, L.M. (2003) A Bayesian Hierarchical Model for Risk Assessment of Methylmercury. *J. Agric. Biol. Environ. Stat*. **8**: 253- 270. Doi: 10.1198/1085711032291

Curren, M. S.; Liang, C. L.; Davis, K.; Kandola, K.; Brewster, J.; Potyrala, M.; Chan, H. M. (2015) Assessing determinants of maternal blood concentrations for persistent organic pollutants and metals in the eastern and western Canadian Arctic. *Sci. Tot. Environ*. **527- 528**, 150 – 158. Doi: 10.1016/j.scitotenv.2015.04.079

Dastoor, A. P.; Dunford, D.A. (2014) Arctic Ocean: Is It a Sink or a Source of Atmospheric Mercury? *Environ. Sci. Technol.* **48**, 1707-1717. Doi: 10.1021/es404473e

Dastoor, A.; Ryzhkov, A.; Durnford, D.; Lehnherr, I.; Steffen, A.; Morrison, H. (2015) Atmospheric mercury in the Canadian Arctic. Part II: Insight from modeling. *Sci. Tot. Environ*. **509- 510**, 16-27. Doi: 10.1016/j.scitotenv.2014.10.112

Dastoor, A.; Wilson, S.J.; Travnikov, O.; Ryjkov, A.; Angot, H.; Christensen, J.H.; Steenhuisen, F.; Muntean, M. (2022) Arctic atmospheric mercury: Sources and changes. *Sci. Tot. Environ.* **839**: 156213. Doi: 10.1016/j.scitotenv.2022.156213

DeFries, R.; Nagendra, H. (2017) Ecosystem management as a wicked problem. *Science.* **356** (6335) 265- 270. Doi: 10.1126/science.aal1950

Depew, D. D.; Burgess, N. M.; Anderson, M. R.; *et al.* (2013) An overview of Hg concentrations in freshwater fish species: Anational fish mercury (Hg) dataset for Canada. *Can. J. Fish. Aquat*. **70**, 1- 16. Doi: 10.1139/cjfas-2012-0338

Depountis, N.; Michalopoulou, M.; Kavoura, K.; Nikolakopoulos, K.; Sabatakakis, N. (2020) Estimating soil erosion rate changes in areas affected by wildfires. *ISPRS Int. J. Geo-Inf*. **9**: 562. Doi: 10.3390/ijgi9100562.

Diavik Diamond Mines Ltd. (2009) Diavik Diamond Mine Aquatic Effects Monitoring Program 2008 Annual Report. Unpublished Data. Dataset obtained upon request from the Canadian Fish Mercury Database (Depew *et al.,* 2013).

Dillon, T.; Beckvar, N.; Kern, J. (2010) Residue-based mercury dose-response in fish: An analysis using lethality-equivalent test endpoints. *Environ. Toxicol. Chem*. **29**, 2559-2565. Doi: 10.1002/etc.314

Dittman, J. A.; Shanley, J. B.; Driscoll, C. T.; Aiken, G. R.; Chalmers, A. T.; Towse, J. E.; Selvendiran, P. (2010) Mercury dynamics in relation to dissolved organic carbon concentrations and quality during high flow events in three northeastern U.S. streams. *Water Resour. Res*. **46**: W07522. Doi: 10.1029/2009WR008351

EBA Engineering Consultants Ltd. (2006) Yellowknife Gold Project 2005 Fisheries and Aquatic Resources Report. Prepared for Tyhee Gold Corp. Mackenzie Valley Review Board. Dataset obtained upon request from the Canadian Fish Mercury Database (Depew *et al.,* 2013).

Ecosystem Classification Group (2010) Ecological Regions of the Northwest Territories. Department of Environment and Natural Resources, Government of the Northwest Territories, Yellowknife, NT, Canada.

Ekati Diamond Mine 2018 Aquatic Effects Monitoring Program (2019) Dominion Diamond Mines. ERM Consultants Canada Ltd. 5129 49th Street, Ground Floor. Yellowknife, NT, X1A 1P8, Canada.

Emmerton, C.A.; Graydon, J.A.; Gareis, J.A.L.; St.Louis, V.L., Lesack, L.F.W., Banack, J.K.A.; Hicks, F.; Nafziger, J. (2013) Mercury Export to the Arctic Ocean from the Mackenzie River, Canada. *Environ. Sci. Technol*. **47**, 7644-7656. Doi: 10.1021/es400715r

Environment Canada (2013) HYDAT Database -Canada [https://wateroffice.ec.gc.ca/report/real_time_e.html?stn=10LA002]. Environment Canada, 2013.

Environment and Climate Change Canada (ECCC). (2020) Canadian Environmental Sustainability Indicators. Emissions of harmful substances to air. Accessed December 5, 2022. Available at: www.canada.ca/en/environment-climate-change/services/environmental-indicators/emissionsharmful-substances-air.html

Environment and Climate Change Canada (ECCC), Carleton University. 2022-04-30. "CIMP 177: The influence of forest fires on metal deposition to lakes and peatlands in the North Slave Region, NWT" (dataset). 2.0.0. DataStream. Doi: 10.25976/aw55-bx08

EMAB- Environmental Monitoring Advisory Board for the Diavik Mine. (2020). 2018/19 Annual Report. Accessed on July 6, 2022: https://emab.ca/sites/default/files/147608_emab_annual_report_2018-19.pdf

Erikson, T.J. (2020) Development and Testing of a Hydro-Chemical River Mixing Model to Investigate Sources of Carbon and Mercury in the Mackenzie River Basin, Canada. Uppsala University Department of Earth Sciences.

Evans, M.S.; Lockhart, W.L.; Doetzel, L.; Low, G.; Muir, D.; Kidd, D.; Stephens, G.; Delaronde, J. (2005) Elevated mercury concentrations in fish in lakes in the Mackenzie River Basin: The role of physical, chemical, and biological factors. *Sci. Total Environ*. **351-352**: 479-500. Doi: 10.1016/j.scitotenv.2004.12.086

Fahd, F.; Yang, M.; Khan, F.; Veitch, B. (2021) A food chain-based ecological risk assessment model for oil spills in the Arctic environment. *Mar. Pollut. Bull*. 166, 112164. Doi: 10.1016/j.marpolbul.2021.112164

Feng, D.; Gleason, C. J.; Lin, P.; Yang, X.; Pan, M.; Ishitsuka, Y. (2021) Recent changes to Arctic River discharge. *Nature Commun.* 1**2**: 6917. Doi: 10.5281/zenodo.5604980.

Fenton, N. E.; Neil, M. (2011) The use of Bayes, causal modelling in decision making, uncertainty and risk. Journal of CEPIS (Council of European Professional Informatics Societies). **12** (5), 10-21.

FNIGC- The First Nations Information Governance Centre (2014). Ownership, Control, Access and Possession (OCAP™): The Path to First Nations Information Governance. May 2014. Ottawa: The First Nations Information Governance Centre.

Fisheries Act, Northwest Territories Fishery Regulations, Schedule V (C.R.C., c.847). Last amended 2020-04-01. Retrieved from the Justice Laws website: https://laws-lois.justice.gc.ca/eng/acts/f-14/

Fortune Minerals Limited. (2015) NICO Project Supplemental Baseline Monitoring Plan V1.3. 148 Fullarton Street, Suite 1600 London, Ontario N6A 5P3. Dataset obtained upon request from the Canadian Fish Mercury Database (Depew *et al.,* 2013).

Fraser, A.; Dastoor, A.; Ryjkov, A. (2018) How important is biomass burning in Canada to mercury contamination? *Atmos. Chem. Phys*. **18**, 7263- 7286. Doi: 10.5194/acp-18-7263-2018

French, T. D.; Houben, A. J.; Jean-Pierre, W. D.; Kimpe, L. E.; Kokelj, S. V.; Poulain, A. J.; Smol, J. P.; Wang, X.; Blais, J. M. (2014) Dissolved Organic Carbon Thresholds Affect Mercury Bioaccumulation in Arctic Lakes. *Environ. Sci. Technol*. **48**, 3162- 3168. Doi: 10.1021/es403849d

French, N.H.F., J.A. Graham, L.L. Bourgeau-Chavez, S. Grelick, and E. Whitman. (2020) AboVE: Burn Severity of Soil Organic Matter, Northwest Territories, Canada, 2014-2015. ORNL DAAC, Oak Ridge, Tennessee, USA. Doi: 10.3334/ORNLDAAC/1694

Fuchsman, P.C.; Henning, M.H.; Sorensen, M.T.; Brown, L.E.; Bock, M.J.; Beals, C.D.; Lyndall, J.L.; Magar, V.S. (2016) Critical perspectives on mercury toxicity reference values for protection of fish. *Environ. Toxicol. Chem*. **35**, 529-549. Doi: 10.1002/etc.3267

Gaboriau, D. M.; Asselin, H.; Ali, A. A.; Hély, C.; Girardin, M. P. (2022) Drivers of extreme wildfire years in the 1965- 2019 fire regime of the Tłı̨cho First Nation territory, Canada. *Ećoscience*. **3**, 249- 265. Doi: 10.1080/11956860.2022.2070342

Gamberg, M.; Pratte, I.; Brammer, J.; Cuyler, C.; Elkin, B.; Gurney, K.; Kutz, S.; Larter, N. C.; Muir, D.; Wang, X.; Provencher, J. F. (2020) Renal trace elements in barren-ground caribou subpopulations: Temporal trends and differing effects of sex, age, and season. *Sci. Tot. Environ*. **724**: 138305. Doi: 10.1016/j.scitotenv.2020.138305

Gantner, N.; Gareis, J. (2013) Evaluation of hydro-climatic drivers of contaminant transfer in aquatic food webs in the Husky Lakes Watershed (Inuvialuit Settlement Region, NWT). Aboriginal Affairs and Northern Development- Synopsis of Research.

GOC- Government of Canada (1997) Mackenzie River Basin Transboundary Waters Master Agreement. Signed between the Government of Canada and The Government of the Province of British Columbia and The Government of the Province of Alberta and The Government of the Province of Saskatchewan and The Government of the Northwest Territories and The Government of the Yukon.

GOC Government of Canada (2022) Businesses- Canadian Industry Statistics for the Forestry and Logging Sector. Accessed January 16, 2022:

https://www.ic.gc.ca/app/scr/app/cis/businesses-entreprises/113;jsessionid=0001oKUsrFD43xYfwCZtKtZz5wn:-17I6RQ?wbdisable=true

Gorelick, N.; Hancher, M.; Dixon, M.; Ilyushchenko, S.; Thau, D.; Moore, R. (2017). Google Earth Engine: Planetary-scale geospatial analysis for everyone. Remote Sensing of Environment.

GNWT Centre for Geomatics. Mineral Claims Mineral Tenure Data. Accessed March 28, 2022: https://www.geomatics.gov.nt.ca/en/resources/field_data_category_/economy-112/field_resource_category/data-3

GNWT Centre for Geomatics. Oil and Gas Mineral and Petroleum Resources Data. Accessed March 28, 2022. https://www.iti.gov.nt.ca/en/services/oil-and-gas-rights-management/nwt-oil-and-gas-rights

GNWT Department of Health and Social Services (2016) Fish Consumption Guidance- Site Specific Fish Consumption Advice. Accessed November 12, 2021: https://www.hss.gov.nt.ca/en/services/fish-consumption-guidance/site-specific-fish-consumption-advice

GNWT Department of Transportation (2013) Erosion and Sediment Control Manual. Government of Northwest Territories. Yellowknife, NT, Canada.

GNWT Industry, Tourism, and Investment (2015) Oil and Gas Annual Report 2015. Government of Northwest Territories, Petroleum Resources Division. Inuvik, NT, Canada.

GNWT Industry, Tourism, and Investment (2017) Strategy for Revitalizing the Great Slave Lake Commercial Fishery. Pp 36.

GNWT Health and Social Services (2016) General Fish Consumption Guidelines for the NWT.

GNWT Industry, Tourism, and Investment (2017) Strategy for Revitalizing the Great Slave Lake Commercial Fishery. Pp 36.

GNWT- Government of Northwest Territories (2019) Taltson Hydroelectricity Expansion Project. Department of Infrastructure. Accessed December 20, 2021: https://www.inf.gov.nt.ca/en/Taltson

GNWT Centre for Geomatics. Oil and Gas Mineral and Petroleum Resources Data. Government of the Northwest Territories. Accessed March 28, 2022. https://www.iti.gov.nt.ca/en/services/oil-and-gas-rights-management/nwt-oil-and-gas-rights

GNWT Centre for Geomatics. Mineral Claims Mineral Tenure Data. Government of the Northwest Territories. Accessed March 28, 2022: https://www.geomatics.gov.nt.ca/en/resources/field_data_ category_/economy-112/field_resource_category/data-3

Gundersen, C.B.; Braaten, H.F.V.; Steindal, E.H.; Moe, J.; Yakushev, E.V.; Christensen, F.; Kirk, J.; Hintelmann, H.; Frolova, N.; Terentjev, P.; Roberts, S. (2020) Mercury Risk Evaluation, Management, and Risk Reduction Measures in the Arctic (ARCRISK): Inception Report. Niva Open Access Archive.

Halseth, R. and the NCCAH. (2015) The nutritional health of the First Nations and Métis of the Northwest Territories: A review of current knowledge and gaps. National Collaborating Centre for Aboriginal Health (NCCAH). Prince George, BC, Canada.

Hansen, M.C.; Potapov, P.V.; Moore, R.; Hancher, M.; Turubanova, S.A.; Tyukavina, A.; Thau, D.; Stehman, S. V.; Goetz, S. J.; Loveland, T. R.; Kommareddy, A.; Egorov, A.; Chini, L.; Justice, C. O.; Townshend, J. R. G. (2013) High-resolution global maps of 21st-century forest cover change. *Science*. **342** (6160), 850-853. Doi: 10.1126/science.1244693. Data available online: http://earthenginepartners.appspot.com/science-2013-global-forest

Harris, M.J.; Stinson, J.; Landis, W.G. (2017) A Bayesian Approach to Integrated Ecological and Human Health Risk Assessment for the South River, Virginia, Mercury- Contaminated site. Risk Anal. 37, 1341-1357. Doi: 10.1111/risa.12691

Harrison, R.J. (2016) Review of the Canada Petroleum Resources Act. Minister's Special Representative.

Health Canada (2007) Human Health Risk Assessment of Mercury in fish and health benefits of fish consumption. Bureau of Chemical Safety Food Directorate- Health Products and Food Branch.

Heindel, R. C.; Chipman, J. W.; Virginia, R. A. (2015) The spatial distribution and ecological impacts of aeolian soil erosion in Kangerlussuaq, West Greenland. *Ann. Assoc. Am. Geogr*. **105**, 875- 890. Doi: 10.1080/00045608.2015.1059176

Herring, C. E.; Stinson, J.; Landis, W. G. (2015) Evaluating nonindigenous species management in a Bayesian network derived relative risk framework for Padilla Bay, WA, USA. *Integr. Environ. Assess. And Manag*. **11**, 640- 652. Doi: 10.1002/ieam.1643

Hickey, R. (2000) Slope angle and slope length solutions for GIS. *Cartography*. **29**, 1-8. Doi: 10.1080/00690805.2000.9714334

Hjort, J.l Karjalainen, O.; Aalto, J.; Westermann, S.; Romanovsky, V.E.; Nelson, F.E.; Etzelmüller, B.; Luoto, M. (2018) Degrading permafrost puts Arctic infrastructure at risk by mid-century. *Nat. Commun.* **9**: 5147. Doi: 10.1038/s41467-018-07557-4

Hollebone, B.P.; Yang, C.X. (2007) Mercury in Crude Oil Refined in Canada. Environment Canada, Ottawa, ON.

Hoover, E. (2013) Cultural and health implications of fish advisories in a Native American community. Ecol Process. 2, 20 pages. Doi :10.1186/2192-1709-2-4.

Houben AJ, D'Onofrio R, Kokelj SV, Blais JM (2016) Factors Affecting Elevated Arsenic and Methyl Mercury Concentrations in Small Shield Lakes Surrounding Gold Mines near the Yellowknife, NT, (Canada) Region. PloS ONE 11(4): e0150960. Doi: 10.1371/journal.pone.0150960

Houde, M.; Krümmel, E.M.; Mustonen, T.; *et al.* (2022) Contributions and perspectives of Indigenous Peoples to the study of mercury in the Arctic. *Sci. Tot. Environ*. **841**, 156566. Doi: 10.1016/j.scitotenv.2022.156566

Hrabalíková, M.; Janeček, M. (2015) Comparison of different approaches to LS factor calculations based on a measured soil loss under simulated rainfall. *Soil & Water Res*. **12**, 69-77. Doi: 10.17221/222/2015-SWR

Imperial (2019) Norman Wells Operation Aquatics Effect Monitoring Plan- 2019- Imperial Oil Resources N.W.T. Limited. Bag 5000, 1001 Canol Drive, Norman Wells, Northwest Territories, X0E 0V0, Canada.

INAC- Indian and Northern Affairs Canada (2009) Northern Oil and Gas Annual Report 2009, Catalogue No. R71-47/2009E-PDF. Northern Oil and Gas Branch of Indian and Northern Affairs Canada. Ottawa.

Johns, A. F.; Graham, S. E.; Harris, M. J.; Markiewicz, A. J.; Stinson, J. M.; Landis, W. G. (2016) Using the Bayesian network relative risk model risk assessment process to evaluate management alternatives for the South River and upper Shenandoah River, Virginia. *Integr. Environ. Assess. And Manag*. **13**, 100- 114. Doi: 10.1002/ieam.1765

Jonsson, S.; Mastromonaco, M. N.; Wang, F.; Bravo, A. G.; Cairns, W. R. L.; Chetélat, J.; Douglas, T. A.; Lescord, G.; Ukonmaanaho, L.; Heimburger- Boavida, L. E. (2022) Arctic methylmercury cycling. *Sci. Tot. Environ*. **850**: 157445- 157466. Doi: 10.1016/j.scitotenv.2022.157445

Kaikkonen, L.; Parviainen, T.; Rahikainen, M.; Uusitalo, L.; Lehikoinen, A. (2020) Bayesian Networks in Environmental Risk Assessment: A Review. *Integr. Environ. Assess. Manag*. **17**, 62-78. Doi: 10.1002/ieam.4332

Kelly, E.N.; Schindler, D.W.; Hodson, P.V.; Short, J.W.; Radmanovich, R.; Nielsen, C.C. (2010). Oil sands development contributes elements toxic at low concentrations to the Athabasca River and its tributaries. *PNAS*. **107**, 16178- 16183. Doi: 10.1073/pnas.1008754107

Kirk, J.; Muir, D. C. G.; Gleason, A.; Wang, X.; Frank, R.; Lehnherr, I.; Wrona, F. (2014) Atmospheric deposition of mercury and methylmercury to landscapes and waterbodies of the Athabasca Oil Sands region. *Environ. Sci. Technol.* **48** (13) 7374- 7383. Doi: 10.1021/es500986r

Kirk, J. L.; Lehnherr, I.; Andersson, M.; Braune, B. M.; Chan, L.; Dastoor, A. P.; Durnford, D.; Gleason, A. L.; Loseto, L. L.; Steffen, A.; St. Louis, V. L. (2012) Mercury in Arctic Marine Ecosystems: Sources, pathways, and exposure. *Environ. Res.* **119**, 64-87. Doi: 10.1016/j.envres.2012.08.012

Kokelj, S.V. and GeoNorth Ltd. (2002) Drilling Mud Sumps in the Mackenzie Delta Region: Construction, Abandonment and Past Performance. Submitted to Department of Indian Affairs and Northern Development, NWT Region. Accessed November 23, 2022: https://www.enr.gov.nt.ca/sites/enr/files/drilling_mud_sumps_in_the_mackenzie_delta_region_construction_abandonment_and_past_performance_2002.pdf

Kokelj, S. V.; Tunnicliffe, J.; Lacelle, D.; Lantz, T. C.; Chin, K. S.; Fraser, R. (2015) Increased precipitation drives mega slump development and destabilization of ice-rich permafrost terrain, northwestern Canada. 129, 56- 68. Doi: 10.1016/j.gloplacha.2015.02.008

Kokelj, S.V.; Kokoszka, J.; Van der Sluijs, J.; Rudy, A.C.A.; Tunnicliffe, J.; Shakil, S.; Tank, S.E.; Zolkos, S. (2021) Thaw-driven mass wasting couples slope with downstream systems, and effects propagate through Arctic drainage networks. *Cryosphere.* **15**, 3059- 3081. Doi: 10.5194/tc-15-3059-2021

Kozak, N.; Ostbye, K.; Hayden, B.; Nyberg, K.; Taipale, S. J.; Kahilainen, K. K. (2022) Mercury growth dilution in different fish species along a climate-productivity gradient of subarctic lakes. Available at SSRN: https://ssrn.com/abstract=4254783 or http://dx.doi.org/10.2139/ssrn.4254783

Laird, M. J.; Aristizabal Henao, J. J.; Reyes, E. S.; Stark, K. D.; Low, G.; Swanson, H. K.; Laird, B. D. (2018) Mercury and omega-3 fatty acid profiles in freshwater fish of the Dehcho Region, Northwest Territories: Informing risk benefit assessments. *Sci. Tot. Environ*. **637- 638**, 1508- 1517. Doi: 10.1016/j.scitotenv.2018.04.381

Lamberink, L. (2022) Norman Wells has a waste problem, and Imperial Oil wants to leave more behind. CBC News. Accessed November 10, 2022: https://www.cbc.ca/news/104anada/north/norman-wells-waste-imperial-oil-1.6546278

Lamoureux, S. (2000) Five centuries of interannual sediment yield and rainfall-induced erosion in the Canadian High Arctic recorded in lacustrine varves. *Water Resour. Res*. **36**, 309- 318. Doi: 10.1029/1999WR900271

Landis W. G.; Wiegers, J. K. (2005) Chapter 2: Introduction to the regional risk assessment using the relative risk model. In: Landis WG, editor. Regional scale ecological risk assessment using the relative risk model. Boca Raton (FL): CRC. P 11–36.

Landis, W. G. (2020) The origin, development, application, lessons learned, and future regarding the Bayesian Network Relative Risk Model for Ecological Risk Assessment. *Integr. Environ. Asess. Manag*. **17**, 79- 94. Doi: 10.1002/ieam.4351

Lantz, T. C.; Kokelj, S. V. (2008) Increasing rates of retrogressive thaw slump activity in the Mackenzie Delta region, NWT, Canada. *Geophys. Res. Lett.* **35**: L06502. Doi: 10.1029/2007GL032433

Lavoie, R. A.; Amyot, M.; Lapierre, J. F. (2019) Global meta-analysis on the relationship between mercury and dissolved organic carbon in freshwater environments. J. *Geophys. Res. Biogeosci*. **124,** 1508- 1523. Doi: 10.1029/2018JG004896

Leitch, D.R.; Carrie, J.; Lean, D.; Macdonald, R.W.; Stern, G.A.; Wang, F. (2007) The delivery of mercury to the Beaufort Sea of the Arctic Ocean by the Mackenzie River. *Sci. Total. Environ*. **373**, 178-195. Doi: 10.1016/j.scitotenv.2006.10.041

Legrand, M.; Feeley, M.; Tikhonov, C.; Schoen, D.; Li-Muller, A. (2010) Methylmercury Blood Guidance Values for Canada. *Can. J. Public Health*. **101**, 28 – 31. Doi: 10.1007/BF03405557.

Lescord, G. L.; Kidd, K. A.; Kirk, J. L.; O'Driscoll, N. J.; Wang, X.; Muir, D. C. G. (2015) Factors affecting biotic mercury concentrations and biomagnification through lake food webs in the Canadian high Arctic. *Sci. Tot. Environ*. **509- 510**, 195- 205. Doi: 10.1016/j.scitotenv.2014.04.133

Li, R.; Wu, H.; Ding, J.; Fu, W.; Gan, L.; Li, Y. (2017) Mercury pollution in vegetables, grains and soils from areas surrounding coal-fired power plants. *Sci Rep* **7**, 46545. Doi: 10.1038/srep46545

Littlefair, C.A.; Tank, S.E.; Kokelj, S.V. (2017) Retrogressive thaw slumps temper dissolved organic carbon delivery to streams of the Peel Plateau, NWT, Canada. *Biogeosciences*. **14**, 5487- 5505. Doi: 10.5194/bg-14-5487-2017

Lumb, A.; Halliwell, D.; Sharma, T. (2006) Application of CCME Water Quality Index to monitor water quality: A case study of the Mackenzie River Basin, Canada. *Environ. Monit. Assess*. **113**, 411- 429. Doi: 10.1007/s10661-005-9092-6

Lockhart, W.L.; Stern, G.A.; Low, G.; Hendzel, M.; Boila, G.; Roach, P.; Evans, M.S.; et al. (2005) A history of total mercury in edible muscle of fish from lakes in northern Canada. *Sci. Total Environ*. **351-352,** 427-463. Doi: 10.1016/j.scitotenv.2004.11.027

Lu, Y.; Zheng, Q.; Quinn, D. (2022) Introducing causal inference using Bayesian Networks and *do*- calculus. *J. Stat. Educ*. 00 (0) 1- 15. Doi: 10.1080/26939169.2022.2128118

Mackenzie Valley Review Board (2010) EA0709- 007: Dezé Energy Corporation Ltd. Taltson Hydroelectic Expansion Project. Report of Environmental Assessment and Reasons for Decision.

Maavara, T.; Lauerwald, R.; Regnier, P.; Van Cappellen, P. (2017) Global perturbation of organic carbon cycling by river damming. *Nature Commun.* **8**: 15347. Doi: 10.1038/ncomms15347

Marcot, B.; Steventon, J. D.; Sutherland, G.; Mccann, R. (2006) Guidelines for developing and updating Bayesian Belief Networks applied to ecological modeling and conservation. *Can. J. For. Res*. 36 (12) 3063- 3074. Doi: 10.1139/x06-135

McCann, R.; Marcot, B.; Ellis, R. (2006) Bayesian belief networks: Applications in ecology and natural resource management. *Can. J. For. Res*. **36**, 3053- 3062. Doi: 10.1139/x06-238

McCool, D. K.; Foster, G. R.; Mutchler, C. K.; Meyer, L. D. (1989) Revised slope length factor for the Universal Soil Loss Equation. *Transactions of the ASAE.* **32**, 1571 – 1576. Doi: 10.13031/2013.31192

Mitasova, H.; Hofierka, J.; Zlocha, M.; Iverson, L. R. (1996) Modelling topographic potential for erosion and deposition using GIS. *Int. J. Geogr. Inf*. **10**, 629 – 641. Doi: 10.1080/02693799608902101

Moore, I. D.; Burch, G. J. (1986) Physical basis of the length-slope factor in the Universal Soil Loss Equation. *Soil Sci. Soc. Am. J*. **50**, 1294 – 1298. Doi: 10.2136/sssaj1986.03615995005000050042x

Moore, I. D.; Wilson, J. P. (1992) Length-slope factors for the Revised Universal Soil Loss Equation: Simplified method of estimation. *J. Soil Water Conserv.* **47**, 423 – 428.

Morris, A. D.; Wilson, S. J.; Fryer, R. J.; Thomas, P. J.; Hudelson, K.; et al. (2022) Temporal trends of mercury in Arctic biota: 10 more years of progress in Arctic monitoring. *Sci. Tot. Environ*. **839**: 155803. Doi: 10.1016/j.scitotenv.2022.155803

Moslemi- Aqdam, M.; Baker, L. F.; Baltzer, J. L.; Branfireun, B. A.; Evans, M. S.; Laird, B. D.; Low, G.; Low, M.; Swanson, H. K. (2022) Understanding among-lake variability of mercury concentrations in Northern Pike (Esox Lucius): A whole-ecosystem study in subarctic lakes. *Sci. Tot. Environ*. **822**: 153430. Doi: 10.1016/j.scitotenv.2022.153430

MRBB- Mackenzie River Basin Board (2003) 2003 State of the Aquatic Ecosystem Report; Whole Basin Overview.

MRBB- Mackenzie River Basin Board (2021). 2021 State of the Aquatic Ecosystem Online Web-based Report. Accessed December 13, 2022: https://soaer.ca/

Mu, C.; Schuster, P. F.; Abbott, B. W.; Kang, S.; Guo, J.; Sun, S.; Wu, Q.; Zhang, T. (2020) Permafrost degradation enhances the risk of mercury release on Oinghai- Tibetan Plateau. *Sci. Tot. Environ.* **708**: 135127. Doi: 10.1016/j.scitotenv.2019.135127

NASA Earth Observatory (2000) Measuring Vegetation (NDVI and EVI). Accessed November 15, 2022: https://earthobservatory.nasa.gov/features/MeasuringVegetation/measuring_vegetation_2.php#:~:text=NDVI%20is%20calculated%20from%20the,and%20less%20near%2Dinfrared%20light.

National Forestry Database (2020) Forest area harvested on private and crown lands in Canada. Accessed January 16, 2022: http://nfdp.ccfm.org/en/data/harvest.php

Natural Resources Canada (2013) Canadian Digital Elevation Model Edition 1.1. Accessed March 25, 2022: https://open.canada.ca/data/en/dataset/7f245e4d-76c2-4caa-951a-45d1d2051333

Natural Resources Canada.: National Hydro Network – NHN – GeoBase Series [dataset], Ottawa, ON, Canada, Natural Resources Canada. Accessed February 20, 2022: https://open.canada.ca/data/en/dataset/a4b190fe-e090-4e6d-881e-b87956c07977

NCP. (2017) Canadian Arctic Contaminants Assessment Report: Human Health Assessment 2017. Northern Contaminants Program.

Nielsen, D. M.; Pieper, P.; Barkhordarian, A.; Overduin, P. Ilyina, T.; Brovkin, V.; Baehr, J.; Dobrynin, M. (2022) Increase in Arctic coastal erosion and its sensitivity to warming in the twenty-first century. *Nat. Clim. Chang*. **12**, 263- 270. Doi: 10.1038/s41558-022-01281-0

NORSYS (2005) Netica. www.norsys.com

NORSYS (2009) Netica-J Manual Version 3.25+. Norsys Software Corp, Vancouver, Canada.

Northwest Territories Power Corporation (2009) Power Generation in Your Community. Published 2009, archived.

NRC National Research Council. (2000) Toxicological Effects of Methylmercury. Washington, DC: The National Academies Press. Doi: 10.17226/9899.

Obrist, D.; Agnan, Y.; Jiskra, M.; Olson, C.L.; Colegrove, D.P.; Hueber, J.; Moore, C.W.; Sonke, J.E.; Helmig, D. (2017) Tundra uptake of atmospheric elemental mercury drives Arctic mercury pollution. *Nature*. **547**, 201- 204. Doi: 10.1038/nature22997

Okulitch, A. V., and Irwin, D. (2017) Geological Compilation of the Western Mainland and Arctic Islands of the Northwest Territories; Northwest Territories Geological Survey, NWT Open File 2016-09.

Oliveira, J.A.; Dominguez, J.M.L.; Nearing, M.A.; Oliveira, P.T.S. (2015) A GIS-based procedure for automatically calculating soil loss from the Universal Soil Loss Equation: GISus-M. *Appl. Eng. Agric.* **31**, 907- 917. Doi: 10.13031/aea.31.11093

Palmer, M.; Higgins, J.; Gah, E. (2008) A Freshwater Classification of the Mackenzie River Basin. Northwest Territories Protected Areas Strategy. Accessed October 5, 2021: https://www.roundriver.org/wp-content/uploads/pubs/northwest-territories/reports/Freshwater_Tech_Report_Draft_NCC_28jan10.pdf?fbclid=IwAR18sa3bPVrUc1VJ0B5DXdTDTtwLdxyuh_QEH_2WHAZEnNNsKiBFHoJrUrw

Parlee, B.; Maloney, E. (2016) Tracking Change: Local and Traditional Knowledge in Watershed Governance. Report of the 2016 Community-Based Research projects in the Mackenzie River Basin.

Parlee, B.; Maloney, E.; Howlett, T.; D'Souza, A. (2019) Tracking Change: Local and Traditional Knowledge in Watershed Governance. Report of the 2018-2019 Community-Based Research projects in the Mackenzie River Basin.

Pearl, J.; Mackenzie, D. (2018). The book of why: The new science of cause and effect. Basic Books, Kindle version.

Peeters, L. J. M.; Holland, K. L.; Huddlestone-Holmes, C.; Boulton, A. J. (2022) A spatial causal network approach for multi-stressor risk analysis and mapping for environmental impact assessments. *Sci. Tot. Environ.* **802**: 149845. Doi: 10.1016/j.scitotenv.2021.149845

Peterson, B. J.; Holmes, R. M.; McClelland, J. W.; Vörösmarty, C. J.; Lammers, R. B.; Shiklomanov, A. I.; Shiklomanov, I. A.; Rahmstorf, S. (2002) Increasing river discharge to the Arctic Ocean. *Science*. **298** (5601) 2171- 2173. Doi: 10.1126/science.1077445

Pierre, K. A.; Zolkos, S.; Shakil, S.; Tank, S. E.; St. Louis, V. L.; Kokelj, S. V. (2018) Unprecedented increases in total and methyl mercury concentrations downstream of retrogressive thaw slumps in the western Canadian Arctic. *Environ. Sci. Technol*. **52** (24) 14099-14109. Doi: 10.1021/acs.est.8b05348

Pollino, C.A.; Hart, B.T. (2008) Developing Bayesian network models within a Risk Assessment framework. International Congress on Environmental Modeling and Software (iEMSs 2008), ed.

Conference Program Committee, International Environmental Modelling and Software Society, Barcelona Spain. **55**, 1-8.

Pollino, C. A.; Woodverry, O.; Nicholson, A.; Korb, K.; Hart, B. T. (2007) Parameterisation and evaluation of a Bayesian network for use in an ecological risk assessment. *Environ. Model. Softw*. **22** (8) 1140- 1152. Doi: 10.1016/j.envsoft.2006.03.006

Rachold, V.; Grigoriev, M.N.; Are, F.E.; Solomon, S.; Reimnitz, E.; Kassens, H.; Antonow, M. (2000) Coastal erosion vs riverine sediment discharge in the Arctic Shelf seas. *Int. J. Earth Sciences*. **89**: 450-460. Doi: 10.1007/s005310000113

Ratelle, M.; Skinner, K.; Bfrandow, D.; Packull-McCormick, S.; Laird, B. (2019) Results report: Contaminant biomonitoring in the Northwest Territories Mackenzie Valley: Investigating the links between contaminant exposure, nutritional status, and country food use. University of Waterloo, Waterloo (ON).

Ratelle, M. Packull- McCormick, S.; Bouchard, M.; Majowicz, S.; Laird, B. (2020a) Human biomonitoring of metals in sub-Arctic Dene communities of the Northwest Territories, Canada. *Environ. Res*. **190**: 110008. Doi: 10.1016/j.envres.2020.110008

Ratelle, M.; Skinner, K.; Packull- McCormick, S.; Laird, B. (2020b) Food frequency questionnaire assessing traditional food consumption in Dene/ Métis communities, Northwest Territories, Canada. *Int. J. Circumpolar Health*. **79**: 1760071. Doi: 10.1080/22423982.2020.1760071.

Regan, H. M.; Colyvan, M.; Burgman, M. A. (2002) A taxonomy and treatment of uncertainty for ecology and conservation biology. *Ecol Appl*. **12** (2) 618- 628. Doi: 10.1890/1051-0761(2002)012[0618:ATATOU]2.0.CO;2

Rescan Environmental Services Ltd. (2009) Ekati Diamond Mine: A study of fish in cell E of the long lake containment facility, 2008. Prepared for BHP Billiton Diamonds Inc. Northwest Territories EA repository. Dataset obtained upon request from the Canadian Fish Mercury Database (Depew *et al.,* 2013).

Richardson, S., Tracz, B., Vecsei, P., Goose, E., Dion, N., Judas, R. and Schnurr, M. (2017) Tlicho Aquatic Ecosystem Monitoring Program (TAEMP) – Behchoko 2015. Waterloo, Canada: Canadian Cryospheric Information Network (CCIN). Unpublished Data.

Rigét, F.; Braune, B.; Bignert, A.; Wilson, S.; Aars, J.; Born, E.; et al. (2011) Temporal trends of Hg in Arctic biota, an update. *Sci. Tot. Environ.* **409**, 3520-3526. Doi: 10.1016/j.scitotenv.2011.05.002

Ritz C, Baty F, Streibig JC, Gerhard D (2015). Dose-Response Analysis Using R. *PLOS ONE*. 10(e0146021). Doi: 10.1371/journal.pone.0146021

Rohonczy, J.; Cott, P. A.; Benwell, A.; Forbes, M. R.; Robinson, S. A.; Rosabal, M.; Amyot, M.; Chételat, J. (2020) Trophic structure and mercury transfer in the subarctic fish community of Great Slave Lake, Northwest Territories, Canada. *J. Great Lakes Res*. **46** (2) 402- 413. Doi: 10.1016/j.jglr.2019.12.009

Rood, S. B.; Kaluthota, S.; Philipsen, L. J.; Rood, N. J.; Zanewich, K. P. (2016) Increasing discharge from the Mackenzie River system to the Arctic Ocean. *Hydrol*. **31**, 150- 160. Doi: 10.1002/hyp.10986

Roux, M. J.; Sparling, P.; Felix, J.; Harwood, L. A. (2014) Ecological assessment of Husky Lakes and Sitidgi Lake, Northwest Territories, 2000 – 2004. Canadian Technical Report of Fisheries and Aquatic Sciences 3071. Central and Arctic Region Fisheries and Oceans Canada. 501 University Crescent, Winnipeg, MB R3T 2N6, Canada.

Segal, R.A., Kokelj, S.V., Lantz, T.C., Durkee, K., Gervais, S., Mahon, E., Snijders, M., Buysse, J., and Schwarz, S., 2016. Broad-scale mapping of terrain impacted by retrogressive thaw slumping in Northwestern Canada; Northwest Territories Geological Survey, NWT Open Report 2016-008, 17 pages. Doi: org/10.46887/2016-008

Schaefer, K.; Elshorbany, Y.; Jafarov, E.; Schuster, P.F.; Striegl, R.G.; Wickland, K.P.; Sunderland, E.M. (2020) Potential Impacts of Mercury Released from Thawing Permafrost. *Nat Commun*. **11**: 4650. Doi: 10.1038/s41467-020-18398-5

Schmidt, S.; Tresch, S.; Meusburger, K. (2019) Modification of the RUSLE slope length and steepness factor (LS-factor) based on rainfall experiments at steep alpine grasslands. *MethodsX*. **6**, 219-229. Doi: 10.1016/j.mex.2019.01.004

Scholten, R.C.; Veraverbeke, S.; Jandt, R.; Miller, E. A.; Rogers, B. M. (2021) AboVE: Ignitions, Burned Area, and Emissions of Fires in AK, YT, and NWT, 2001-2018. ORNL DAAC, Oak Ridge, Tennessee, USA. Doi: 10.3334/ORNLDAAC/1812

Schuster, R. C.; Wein, E. E.; Dickson, C.; Chan, H. M. (2011) Importance of traditional foods for the food security of two First Nations communities in the Yukon, Canada. *Int. J. Circumpolar Health*. **70**, 286- 300. Doi: 10.3402/ijch.v70i3.17833

Schuster, P.F.; Schaefer, K.M.; Aiken, G.R.; Antweiler, *et al.* (2018) Permafrost stores a globally significant amount of mercury. *Geophys. Res. Lett.* **45**, 1463- 1471. Doi: 10.1002/2017GL075571

Sheehan, M.C.; Burke, T.A.; Navas-Acien, A.; Breysse, P.N.; McGready, J.; Fox, M.A. (2014) Global methylmercury exposure from seafood consumption and risk of developmental neurotoxicity: a systematic review. *Sys. Rev*. **92**, 254- 269. Doi: 10.2471/BLT.12.116152

Silke, R. (2009). The Operational History of Mines in the Northwest Territories, Canada. Yellowknife, NWT. Funded by NWT Geoscience Office (NTGO).

Soerensen, A.L.; Jacob, D.J.; Schartup, A.T.; Fisher, J.A.; Lehnherr, I.; St. Louis, V.L.; Heimbürger, L.E.; Sonke, J.E.; Krabbenhoft, D.P.; Sunderland, E.M. (2016) A mass budget for mercury and methylmercury in the Arctic Ocean. *Glob. Biogeochem. Cycles.* **30**, 560 – 575. Doi: 10.1002/2015GB005280

Sothe, C.; Gonsamo, A.; Arabian, J.; Snider, J. (2022) Large scale mapping of soil organic carbon concentration with 3D machine learning and satellite observations. *Geoderma*. **45**, 115402- 115416. Doi: 10.1016/j.geoderma.2021.11540

Statistics Canada (2022) Table 10-10-0005-01 Canadian Classification of Functions of Government (CC0FOG) by consolidated government component (x 1,000,000). Doi: 10.25318/1010000501-eng

Statistics Canada (2017) Northwest Territories, Canada (table). Census Profile. 2016 Census. Statistics Canada Catalogue no. 98-316-X2016001. Ottawa. Released November 29, 2017.

Stephenson, S. A. (2004) Harvest studies in the Inivialuit Settlement Region. Department of Fisheries and Oceans, Northwest Territories, Canada.

Stubley, M.P. and Irwin, D. (2019) Bedrock Geology of the Slave Craton, Northwest Territories and Nunavut; Northwest Territories Geological Survey, NWT Open File 2019-01. Accessed May 15, 2022: https://www.nwtgeoscience.ca/news/new-bedrock-geology-map-slave-craton

Teather, K.; Parrott, J. (2006) Assessing the chemical sensitivity of freshwater fish commonly used in toxicological studies. Water Qual. Res. J. Canada. **41** (1) 100- 105. Doi: 10.2166/wqrj.2006.011

Tendler, B.; Ohiozebau, E.; Codling, G.; Giesy, J. P.; Jones, P. D. (2020) Concentrations of metals from the Athabasca and Slave Rivers of Northern Canada. *Environ. Toxicol. Chem*. **39** (11) 2180- 2195. Doi: 10.1002/etc.4852

Thienpont, J.R.; Korosi, J.B.; Hargan, K.E.; Williams, T.; Eivkmeyer, D.C.; Kimpe, L.E.; Palmer, M.J.; Smol, J.P.; Blais, J.M. (2016) Multi-trophic level response to extreme metal contamination from gold mining in a subarctic lake. *Proc. R. Soc. B*. **283**: 20161125. Doi: 10.1098/rspb.2016.1125.

Thompson, P.C. (1981) The Economic performance of the commercial skiff fishery in Western Canada. Canadian Technical Report of Fisheries and Aquatic Sciences 1037.

Tłı̨chǫ Aquatic Ecosystem Monitoring Program (TAEMP). Reports for 2010- 2018 rom Wekweètì, Gamètì, Whatì, and Behchokǫ̀. Waterloo, Canada: Canadian Cryospheric Information Network (CCIN). PolarData CCIN Catalogue Reference No. 12013, 12012, 11906, 12161, 12663, 12793, 12922, and 13028. Link to summary reports: https://www.wrrb.ca/projects/tlicho-aquatic-ecosystem-monitoring-program

UNEP. (2002) Global Mercury Assessment. UNEP Chemicals Branch: Geneva, Switzerland, 2002.

UNEP. (2019) Minamata Convention on Mercury: Text and Annexes.

UNEP. (2021) Progress Report 2020: Overview of the Minamata Convention on Mercury activities

UNEP (2022) “Mercury from Oil and Gas”. UNEP Global Mercury Partnership Study Report Draft.

University of Alberta. 2022-04-30. “CIMP 199: Water quality of peatland ponds and streams on a latitudinal transect” (dataset). 4.0.0. DataStream. Doi: org/10.25976/rzkg-7n02.

University of Waterloo. 2022-04-30. “Dehcho Region Water Quality Data” (dataset). 2.0.0. DataStream. Doi: org/10.25976/j1fz-z275.

University of Waterloo; Dehcho AAROM. 2022-03-31. “CIMP154 Understanding fish mercury concentrations in Dehcho lakes- Big Island Lake, Cli Lake, Fish Lake, and Little Doctor Lake”. NWT Discovery Portal.

U.S. EPA. (2000) Reference Dose for Methylmercury. External Review Draft, 2000. U.S. Environmental Protection Agency, Washington, D.C., NCEA-S-0930.

Uusitalo, L. (2007) Advantages and challenges of Bayesian networks in environmental modelling. *Ecol. Modell*. **203**, 312- 318. Doi: 10.1016/j.ecolmodel.2006.11.033

Uusitalo, L.; Tomczak, M. T.; Müller- Karulis, B.; Putnis, I.; Trifonova, N.; Tucker, A. (2018) Hidden variables in a dynamic Bayesian Network identify ecosystem level change. *Ecol. Inform*. **45**, 9-15. Doi: 10.1016/j.ecoinf.2018.03.003

Vonk, J. E.; Tank, S. E.; Bowden, W. B.; Laurion, I.; Vincent, W. F.; Alekseychik, P.; et al. (2015) Reviews and syntheses: Effects of permafrost thaw on Arctic aquatic ecosystems, *Biogeosciences*. **12**, 7129–7167. Doi: 10.5194/bg-12-7129-2015, 2015.

Wall,G.J.; Coote, D.R.; Pringle, E.A.; Shelton, I.J. (2002) RUSLEFAC — Revised Universal Soil Loss Equation for Application in Canada: A Handbook for Estimating Soil Loss from Water Erosion in Canada. Research Branch, Agriculture and Agri-Food Canada. Ottawa. Contribution No. AAFC/AAC2244E. 117 pp.

Wasiuta, V.; Kirk, J. L.; Chambers, P. A.; Alexander, A. C.; Wyatt, F. R.; Rooney, R. C.; Cooke, C. A. (2019) Accumulating mercury and methylmercury burdens in watersheds impacted by Oil Sands pollution. *Environ. Sci. Technol.* **53** (21) 12856- 13864. Doi: 10.1021/acs.est.9b02373

Wein, E.E.; Sabry, J.H.; Evers, F.T. (1991) Food consumption patterns and use of country foods by Native Canadians near Wood Buffalo National Park, Canada. *Arctic.* **44**, 196-205. Doi: 10.14430/arctic1539

WRRB- Weekezzhii Renewable Resources Board (2014) Common fish in the Tłı̨chǫ Region. Powerpoint Presentation accessed February, 2022: https://wrrb.ca/sites/default/files/Tlicho%20Fish%20Guide%205%20Jul%202012-2_0.pdf

WHO (1990) International Programme on Chemical Safety (IPCS) Methylmercury (Environmental Health Criteria 101): World Health Organization Report. Geneva, Switzerland.

Wuttke, S.; LaCorte, E.; Garcia, D.; Ooi, M. (2013) First Nations Biomonitoring Initiative: National Results (2011). Assembly of First Nations. Print.

Xu, J.; Liem-Nguyen, V.; Buck, M.; Bertilsson, S.; Björn, E.; Bravo, A.G. (2021) Mercury methylating microbial community structure in boreal wetlands explained by local physiochemical conditions. *Front. Environ. Sci*. **8**: Article 518662. Doi: 10.3389/fenvs.2020.518662

Yoshimura, A.; Suemasu, K.; Veiga, M.M. (2021) Estimation of mercury losses and gold production by artisanal and small-scale gold mining (ASGM). *J. Sustain. Metall*. **7**, 1- 15. Doi: 10.1007/s40831-021-00394-8

Zanden, M. J. V.; Rasmussen, J. B. (1996) A trophic position model of pelagic food webs: Impact on contaminant bioaccumulation in Lake trout. *Ecol. Monogr*. **66**, 451- 477. Doi: 10.2307/2963490

Zanden, M. J. V.; Cabana, G.; Rasmussen, J. B. (1997) Comparing trophic position of freshwater fish calculated using stable nitrogen isotope ratios (δ15N) and literature dietary data. *Can. J. Fish. Aquat. Sci*. **54**, 1142- 1158. Doi: 10.1139/f97-016

Zhang, H.; Yang, Q.; Li, R.; Liu, Q.; Moore, D.; He, P.; Ritsema, C. J.; Geissen, V. (2013) Extension of a GIS procedure for calculating the RUSLE equation LS factor. *Comput. Geosci*. 52, 177- 188. Doi: 10.1016/j.cageo.2012.09.027

APPENDEX A: SUPPLEMENTAL FIGURES

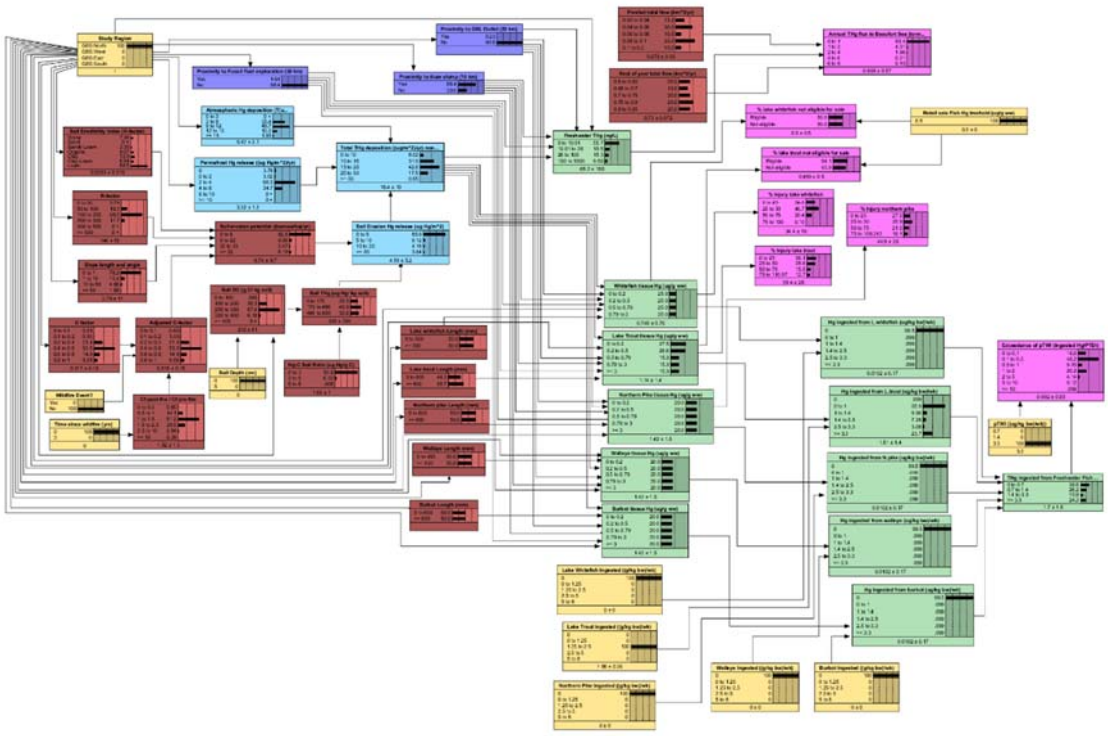

Supplemental Figure 1. The parameterized GBS model for the GBS North (SR1) study region. The Scenario nodes (yellow) are interactive; in this model configuration, the endpoint risk probabilities represent an adult male (pTWI = 3.3) consuming a single serving (2.5 g tissue $kgbw^{-1}wk^{-1}$) of lake trout per week, in a region of the GBS SR1 which has not experienced recent wildfires (Wildfire Event? = No). Probability distributions (black bars) are uniform for variables where no monitoring data was available; this includes lake whitefish, northern pike, walleye, and burbot.

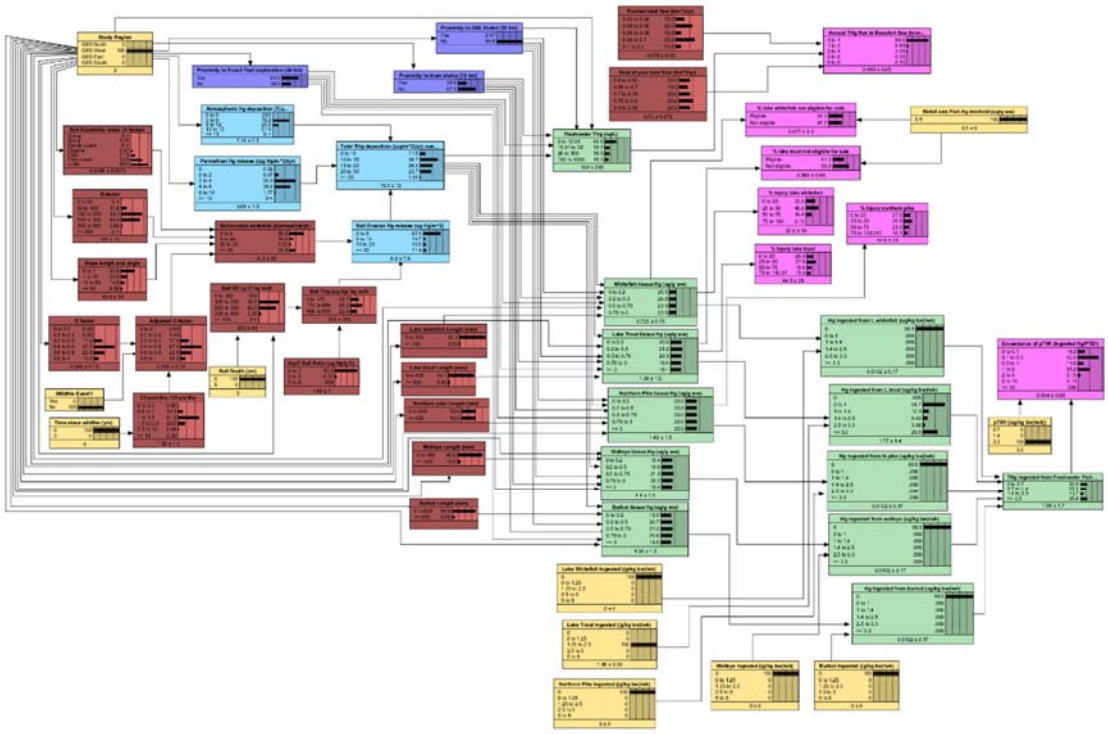

Supplemental Figure 2. The parameterized GBS model for the GBS West (SR2) study region. The Scenario nodes (yellow) are interactive; in this model configuration, the endpoint risk probabilities represent an adult male (pTWI = 3.3) consuming one serving (2.5 g tissue $kgbw^{-1}wk^{-1}$) of lake whitefish and half a serving (1.25 g tissue $kgbw^{-1}wk^{-1}$) of lake trout per week, in a region of the GBS SR1 which has not experienced recent wildfires (Wildfire Event? = No). Probability distributions (black bars) are uniform for the northern pike variable, for which no monitoring data was available.

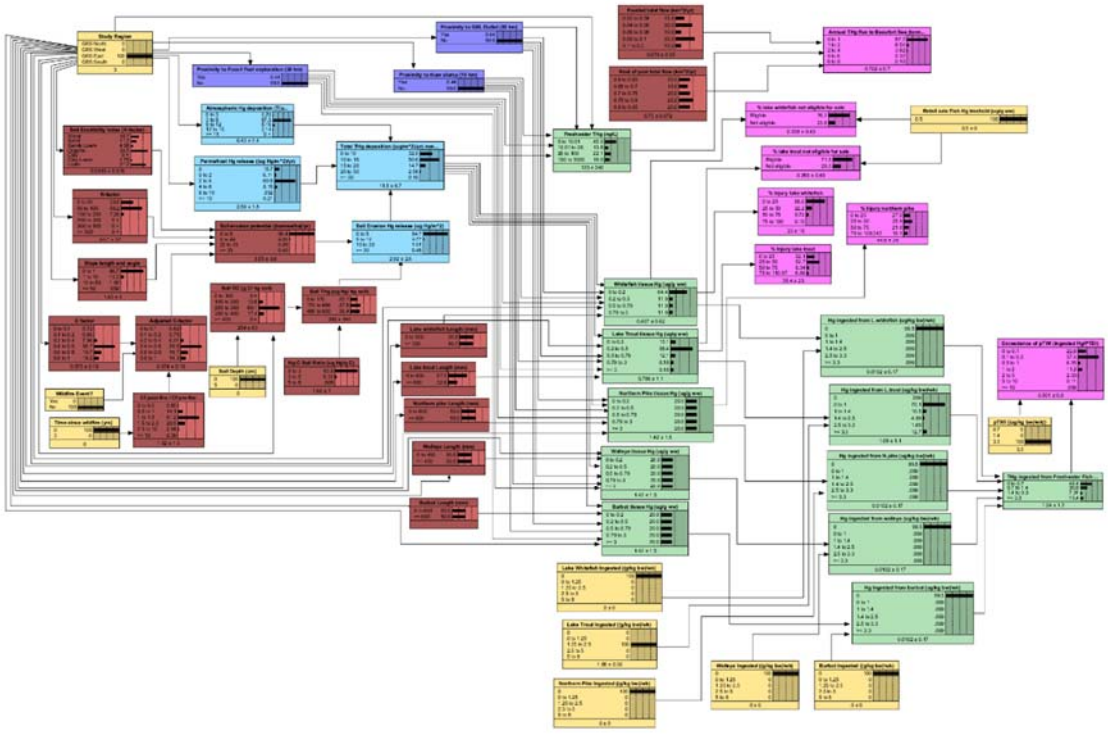

Supplemental Figure 3. The parameterized GBS model for the GBS East (SR3) study region. The Scenario nodes (yellow) are interactive; in this model configuration, the endpoint risk probabilities represent an adult male (pTWI = 3.3) consuming one serving (2.5 g tissue $kgbw^{-1}wk^{-1}$) of lake whitefish and half a serving (1.25 g tissue $kgbw^{-1}wk^{-1}$) of lake trout per week, in a region of the GBS SR3 which has not experienced recent wildfires (Wildfire Event? = No). Probability distributions (black bars) are uniform when no monitoring data was available, including for the northern pike, walleye, and burbot tissue Hg variables.

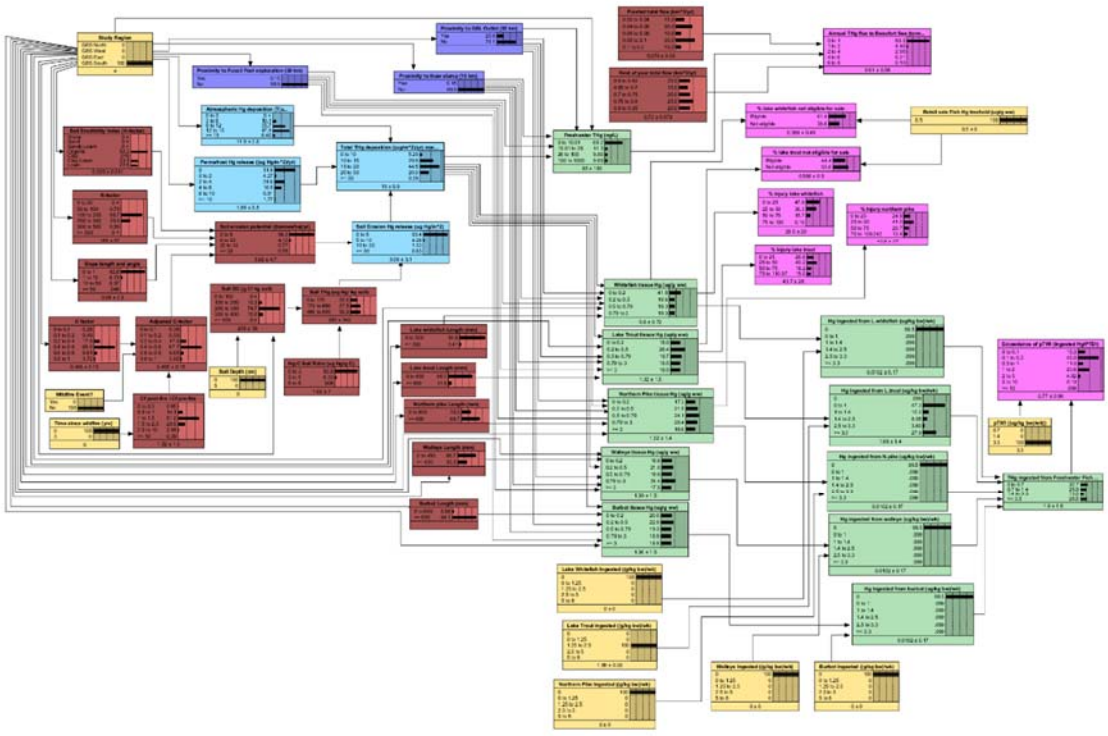

Supplemental Figure 4. The parameterized GBS model for the GBS South (SR4) study region. The Scenario nodes (yellow) are interactive; in this model configuration, the endpoint risk probabilities represent an adult male (pTWI = 3.3) consuming one serving (2.5 g tissue $kgbw^{-1}wk^{-1}$) of lake whitefish and half a serving (1.25 g tissue $kgbw^{-1}wk^{-1}$) of lake trout per week, in a region of the GBS SR1 which has not experienced recent wildfires (Wildfire Event? = No). Probability distributions (black bars) are uniform for the northern pike variable, for which no monitoring data was available.

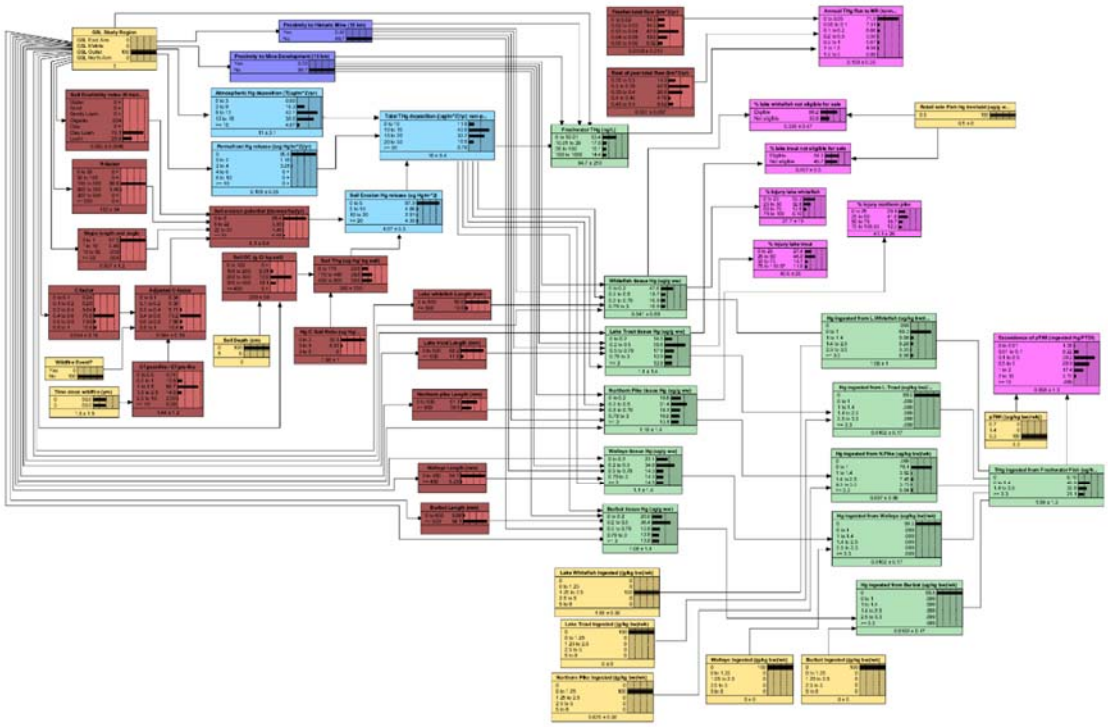

Supplemental Figure 5. The parameterized GSL model for the GSL Outlet study region. The Scenario nodes (yellow) are interactive; in this model configuration, the endpoint risk probabilities represent an adult male (pTWI = 3.3) consuming one serving (2.5 g tissue $kgbw^{-1}wk^{-1}$) of lake whitefish and half a serving (1.25 g tissue $kgbw^{-1}wk^{-1}$) of northern pike per week, in a region of the GSL Outlet which has not experienced recent wildfires (Wildfire Event? = No). Mercury data was available for all effect variables.

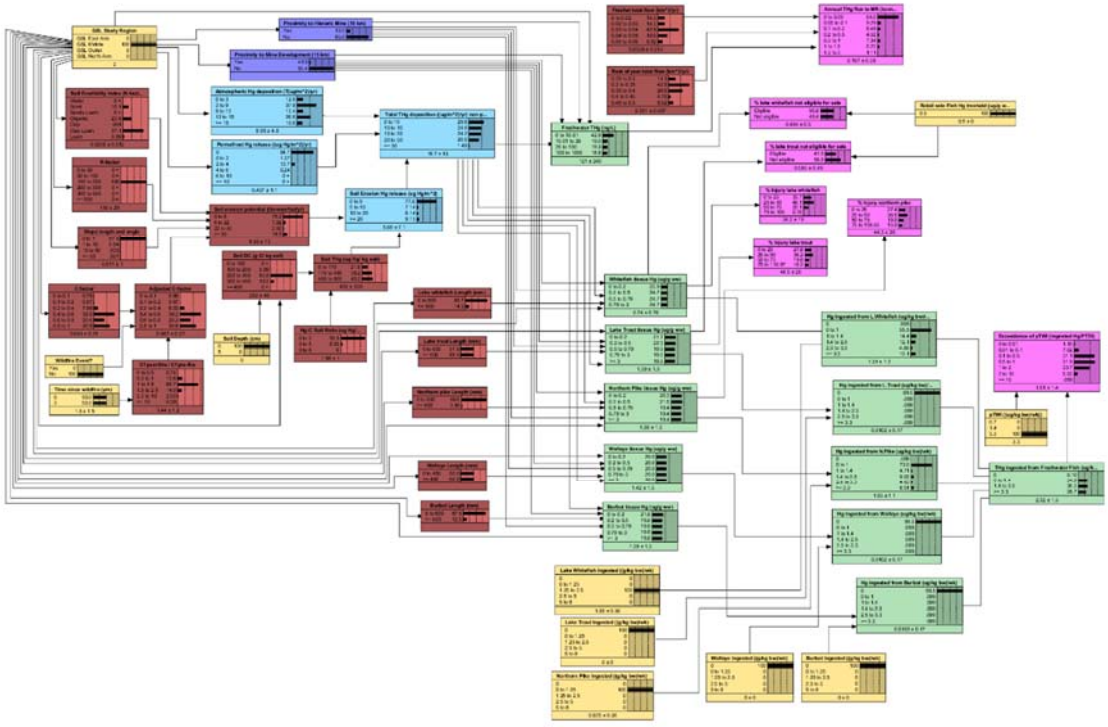

Supplemental Figure 6. The parameterized GSL model for the GSL Middle study region. The Scenario nodes (yellow) are interactive; in this model configuration, the endpoint risk probabilities represent an adult male (pTWI = 3.3) consuming one serving (2.5 g tissue $kgbw^{-1}wk^{-1}$) of lake whitefish and half a serving (1.25 g tissue $kgbw^{-1}wk^{-1}$) of northern pike per week, in a region of the GSL Middle which has not experienced recent wildfires (Wildfire Event? = No). There was no mercury data available for the walleye effect variable.

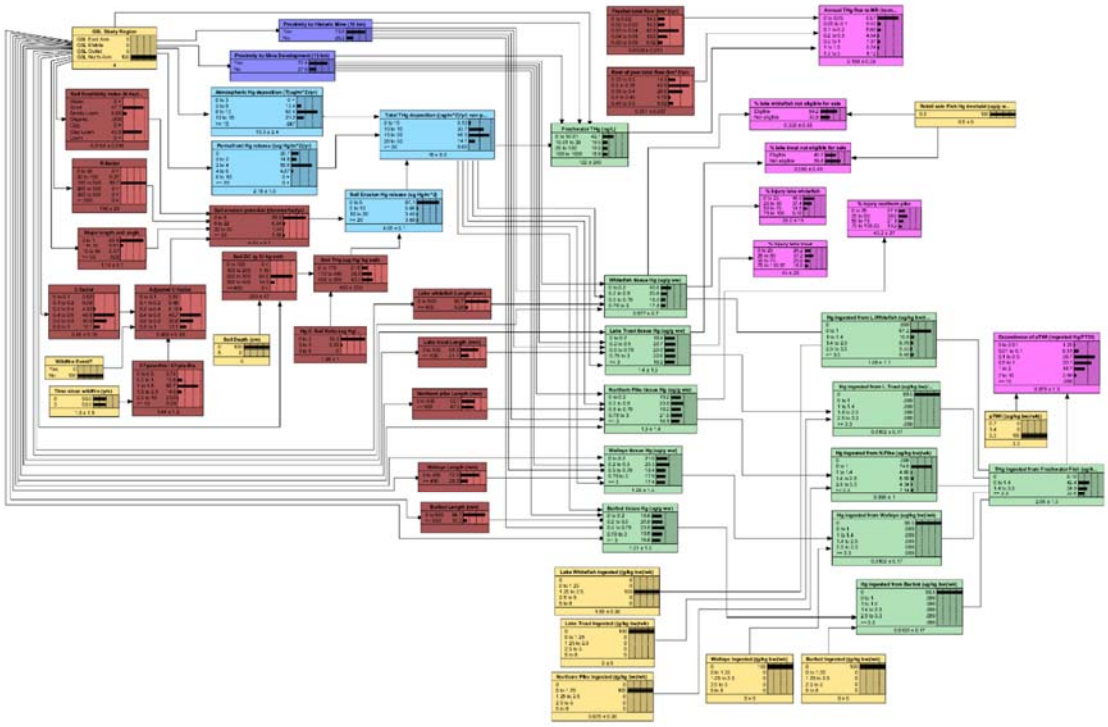

Supplemental Figure 7. The parameterized GSL model for the GSL North Arm study region. The Scenario nodes (yellow) are interactive; in this model configuration, the endpoint risk probabilities represent an adult male (pTWI = 3.3) consuming one serving (2.5 g tissue $kgbw^{-1}wk^{-1}$) of lake whitefish and half a serving (1.25 g tissue $kgbw^{-1}wk^{-1}$) of northern pike per week, in a region of the GSL North Arm which has not experienced recent wildfires (Wildfire Event? = No). Mercury data was available for all effect variables.

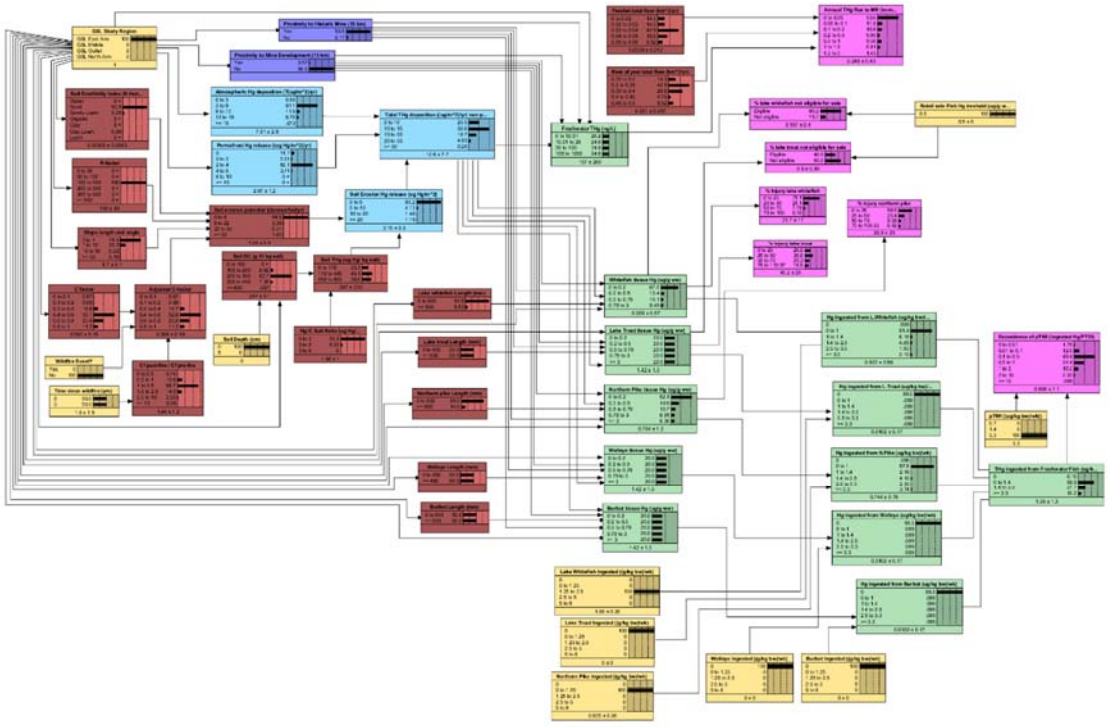

Supplemental Figure 8. The parameterized GSL model for the GSL East Arm study region. The Scenario nodes (yellow) are interactive; in this model configuration, the endpoint risk probabilities represent an adult male (pTWI = 3.3) consuming one serving (2.5 g tissue $kgbw^{-1}wk^{-1}$) of lake whitefish and half a serving (1.25 g tissue $kgbw^{-1}wk^{-1}$) of northern pike per week, in a region of the GSL East Arm which has not experienced recent wildfires (Wildfire Event? = No). Probability distributions (black bars) are uniform for the burbot, walleye, and lake trout variables.

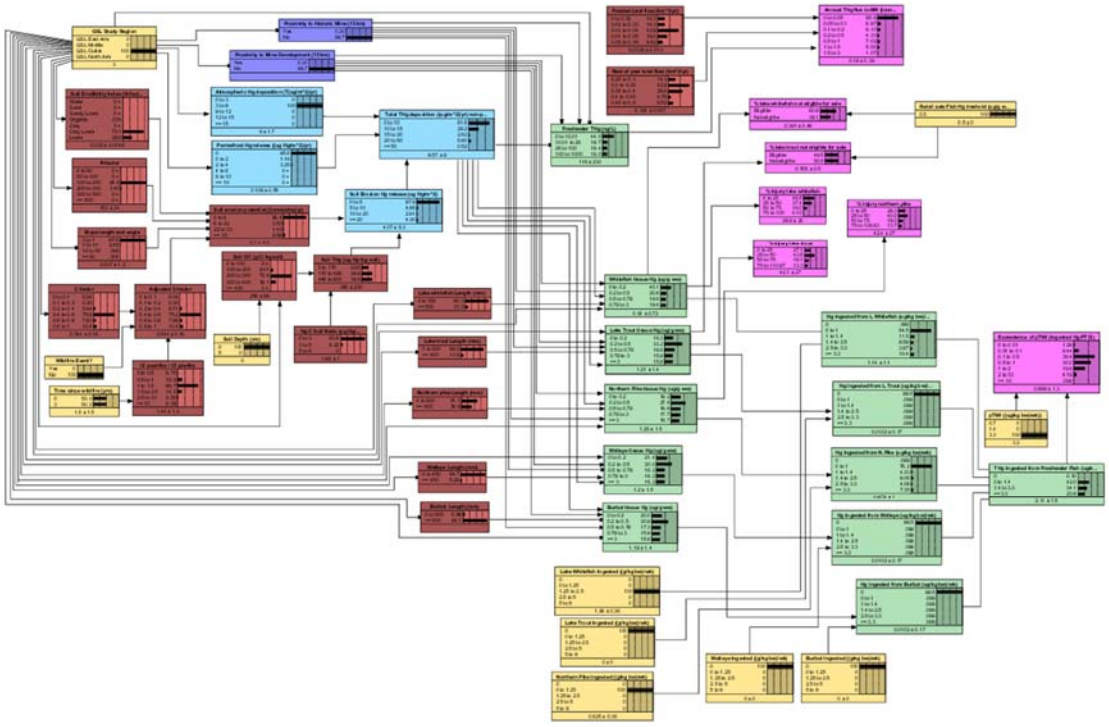

Supplemental Figure 9. Results of the Minamata counterfactual quarry for the GSL Outlet study region, where a lower value (3 – 9 ug Hg/m^2/ yr) was selected for the atmospheric Hg deposition variable. Comparing to Supplemental Figure 5, the probability distributions of the Minamata counterfactual model indicate a higher probability of risk to effect variables, contrary to causal expectations.

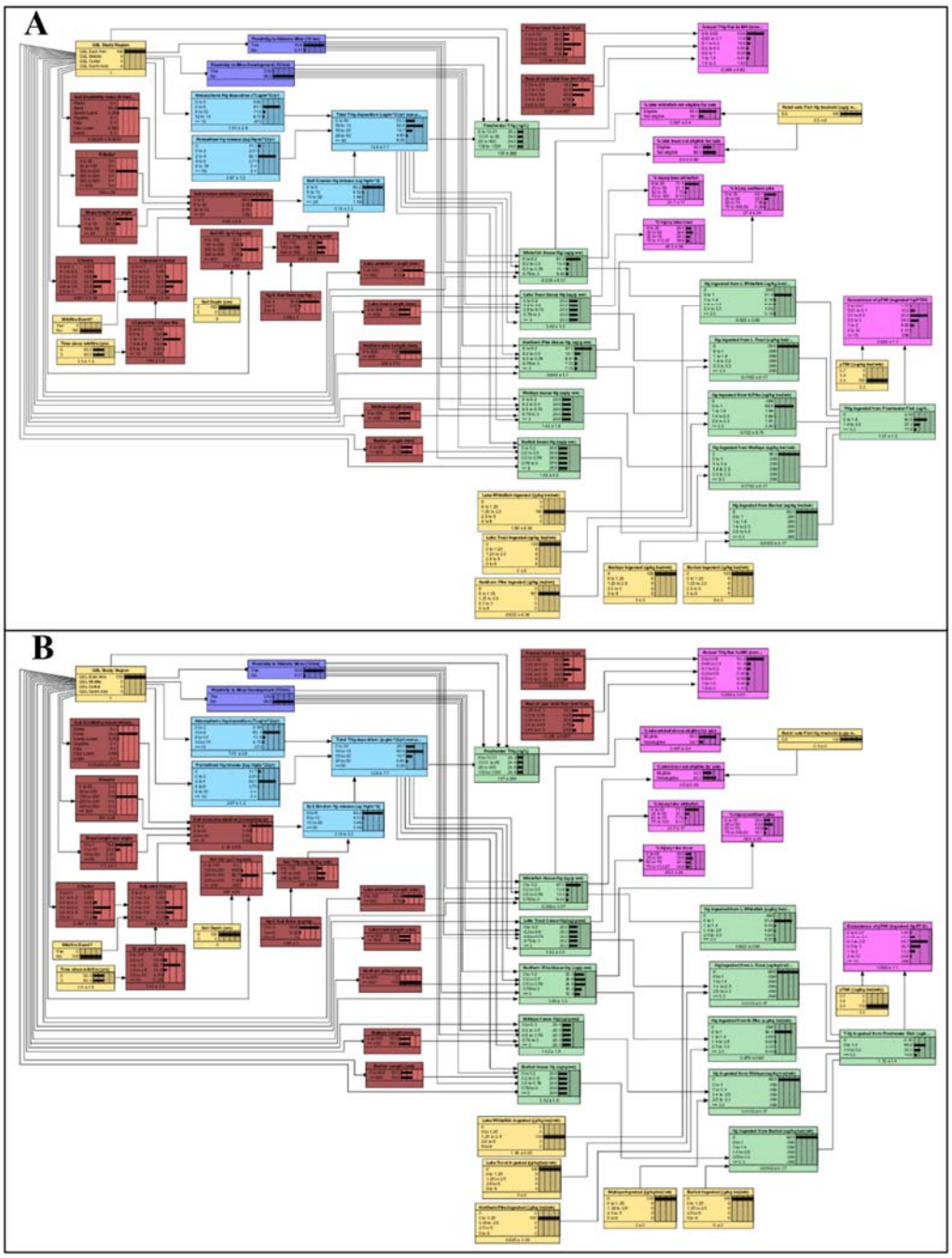

Supplemental Figure 10. Results of the northern pike consumption advisory counterfactual quarry for the GSL East Arm study region. The top figure (A) shows the impact of consuming only small sized (< 600 mm) pike on the risk probabilities for the "Exceedance of pTWI" endpoint, while the bottom figure (B) shows the impact of consuming only large sized (> 600 mm) pike. There is a slightly greater risk of exceeding the weekly mercury consumption regulatory threshold when consuming larger northern pike, which agrees with our causal understanding of Hg bioaccumulation.

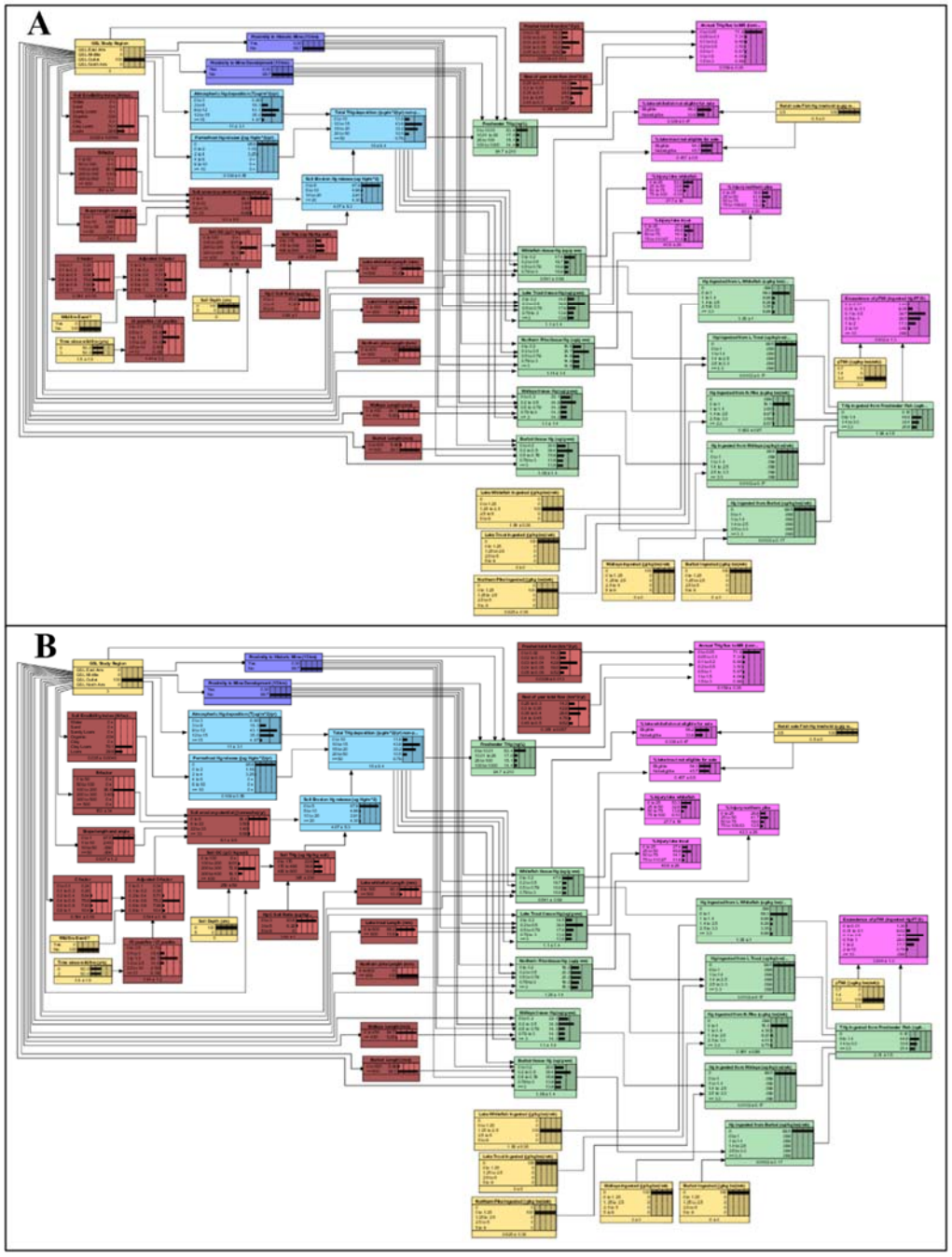

Supplemental Figure 11. Results of the northern pike consumption advisory counterfactual quarry for the GSL Outlet study region. The top figure (A) shows the impact of consuming only small sized (< 600 mm) pike on the risk probabilities for the "Exceedance of pTWI" endpoint, while the bottom figure (B) shows the impact of consuming only large sized (> 600 mm) pike. There is a slightly greater risk of exceeding the weekly mercury consumption regulatory threshold when consuming larger northern pike, which agrees with our causal understanding of Hg bioaccumulation in fish.

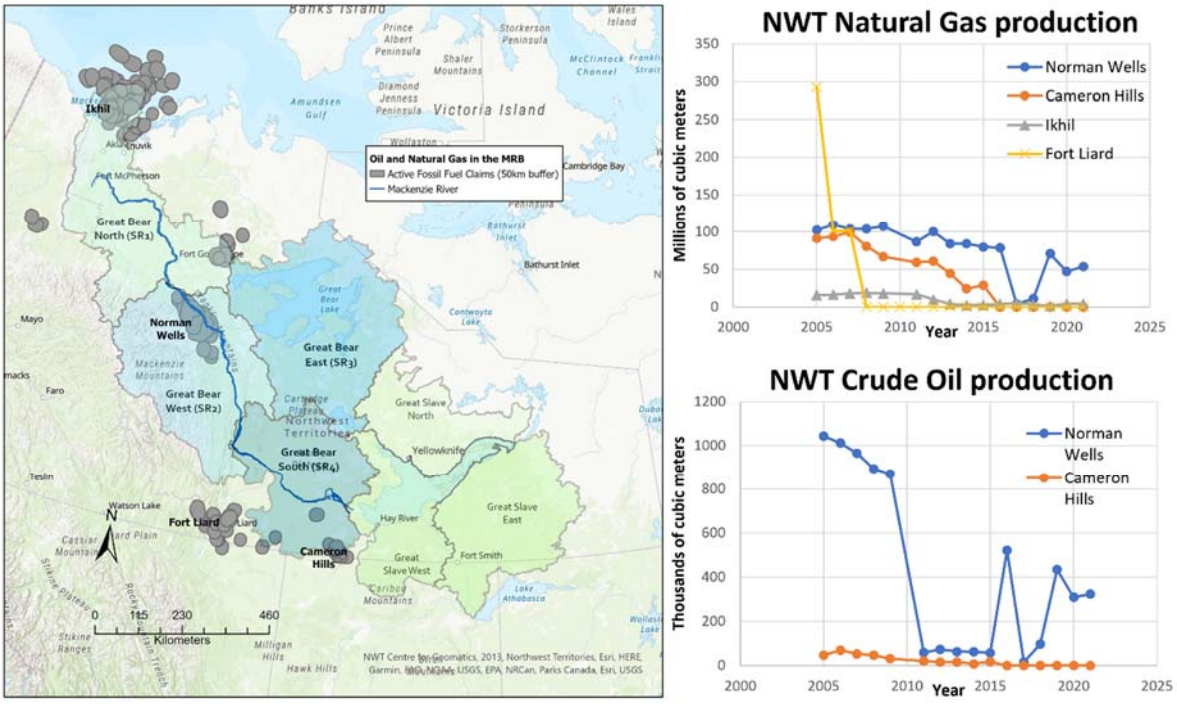

Supplemental Figure 12. Location and activity of oil and natural gas exploration or extraction facilities in the Mackenzie River Basin. (12a) A map of the four fossil fuel development regions in proximity to the Mackenzie River: Cameron Hills (south), Fort Liard (southwest), Norman Wells (west), and Ikhil (North). The facilities are represented by a grey polygon layer signifying a 250 km buffer around an active fossil fuel claim (GNWT Geomatics: Oil and Gas). (12b) Annual crude oil and natural gas production at the four fossil fuel development regions over the 2005- 2020 study period. Norman Wells, a town situated on the Mackenzie River, is the largest producer of both crude oil and natural gas in the NWT.

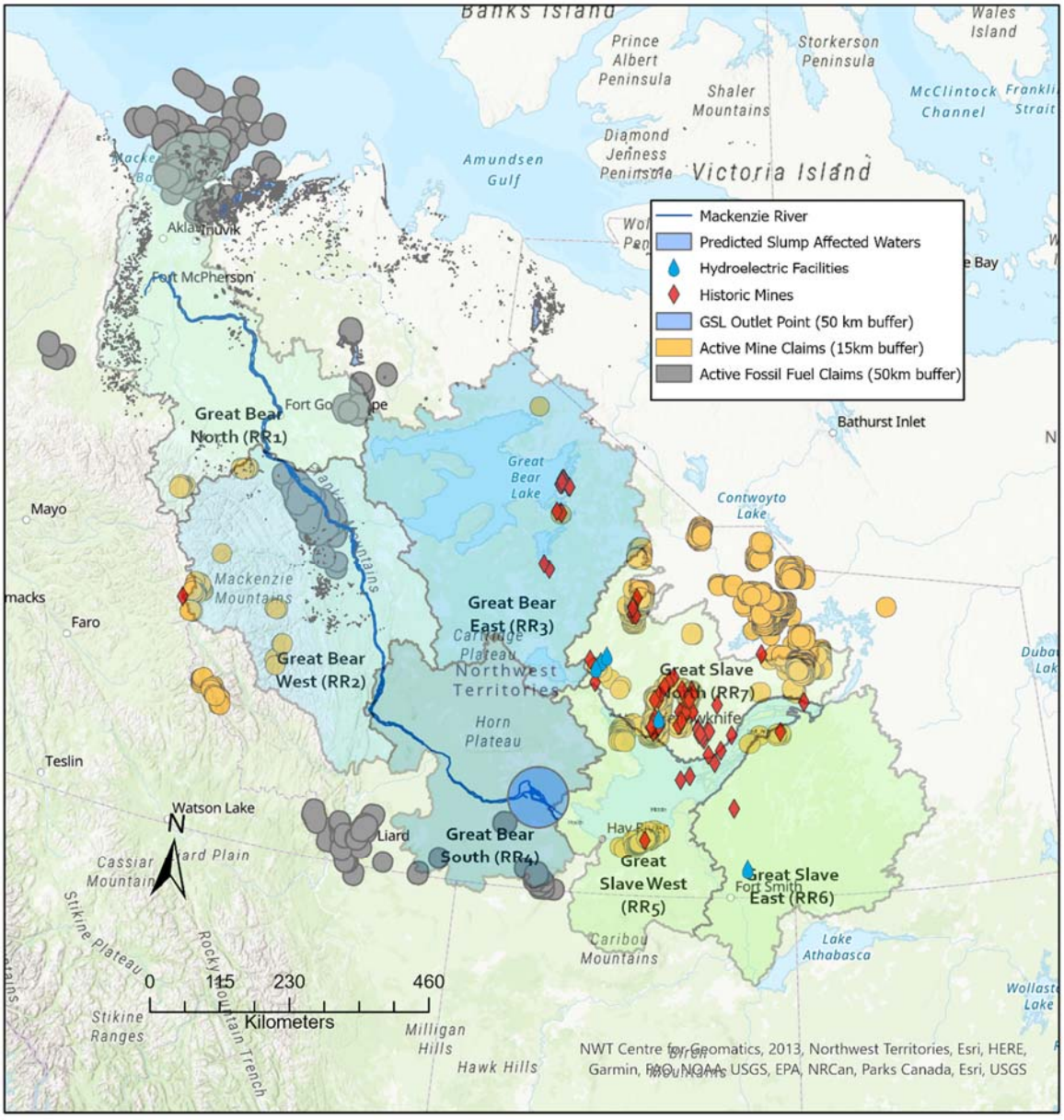

Supplemental Figure 13. The location of point sources considered in the GSL and GBS model frameworks. The polygon layers for the mining (orange circle) and fossil fuel developments (grey circles) represent a buffer layer around the facilities of 15 km and 50 km, respectively. Additional point sources for the GBS model include the polygons for the GSL outlet (50 km buffer) and the waterbodies impacted by retrogressive permafrost thaw slumps (10 km buffer). An additional source for the GSL model is the historic mines (red diamonds), displayed as a point-layer.

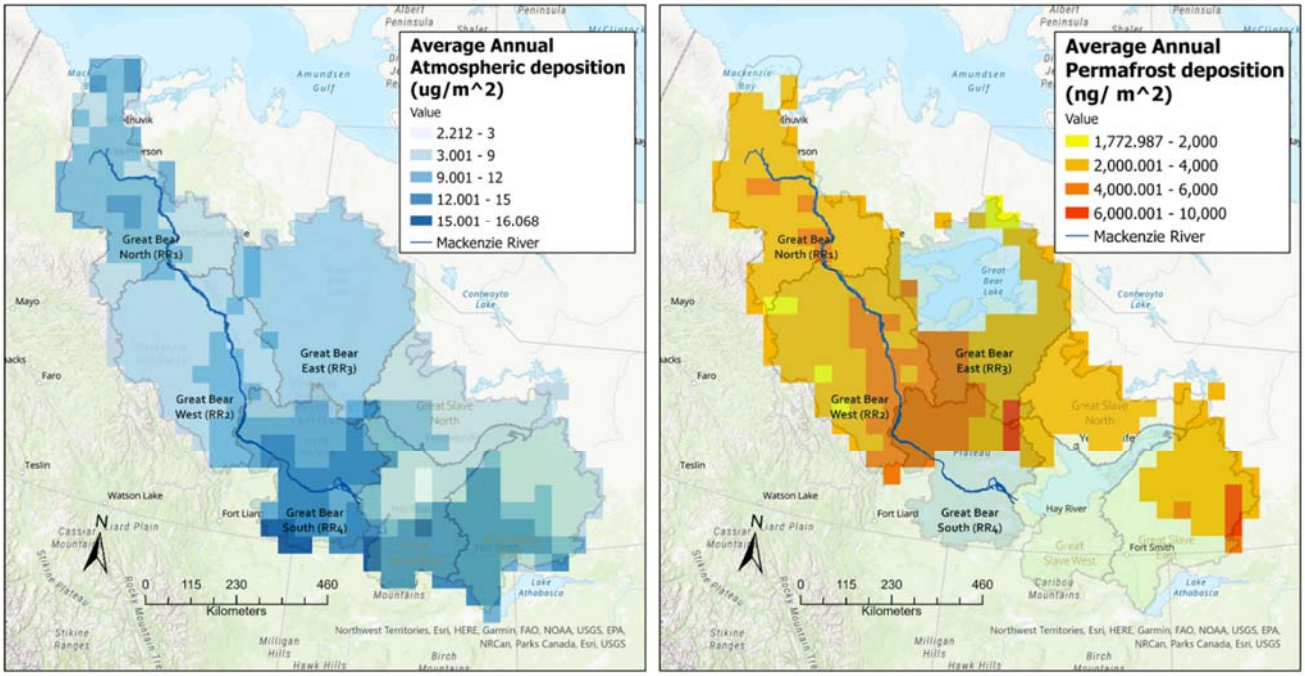

Supplemental Figure 14. The average annual atmospheric Hg deposition and Hg release from permafrost thaw for the 2005 – 2020 period. Raster map layers were obtained from predictive model outputs, with raster resolutions of approximately 1874 km^2. The left figure shows the GEM-MACH-Hg model output for THg deposition from anthropogenic sources and wildfires (Fraser et al. 2018; Dastoor et al. 2015), while right figure is the SiBCASA- Hg biogeochemical model output predicting the DHg release from permafrost thaw into the aquatic ecosystem (Schaefer et al. 2020).

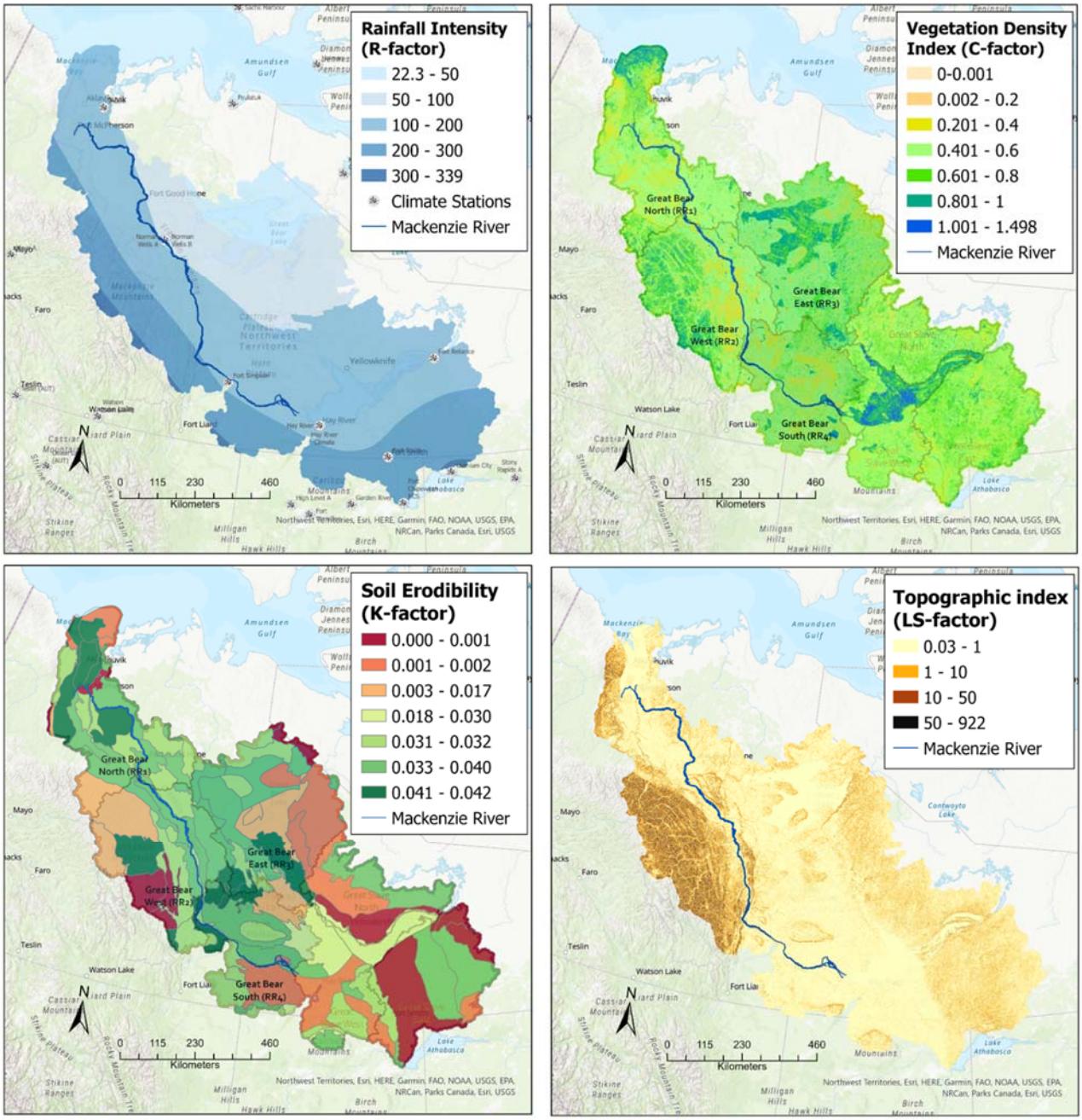

Supplemental 15. Maps of the four abiotic factors used to calculate soil erosion potential. The top-left figure shows the results of an Empirical Bayesian-Kriging interpolated surface map of the R-factor (MJ mm ha^{-1} yr^{-1}) over the 2005-2017 period. The climate stations with calculated R-factor data are shown as snowflake points; see Supplemental Figure 20 all 46 climate station locations. The top-right and bottom-left figures show the C-factor (unitless; calculated from a Landsat image map of NDVI from September 2020) and the K-factor (tonnes hr MJ^{-1} mm^{-1}) which was approximated from a map of soil texture classes (Canada Open Government, 2016). The bottom-right figure displays the LS-factor (unitless), which represents a combination of the slope length and angle estimates. The layer was calculated using the ArcGIS Pro Hydrology toolkit and a Digital Elevation Model (DEM) file with a resolution of 16 meters (Supplemental Table 4).

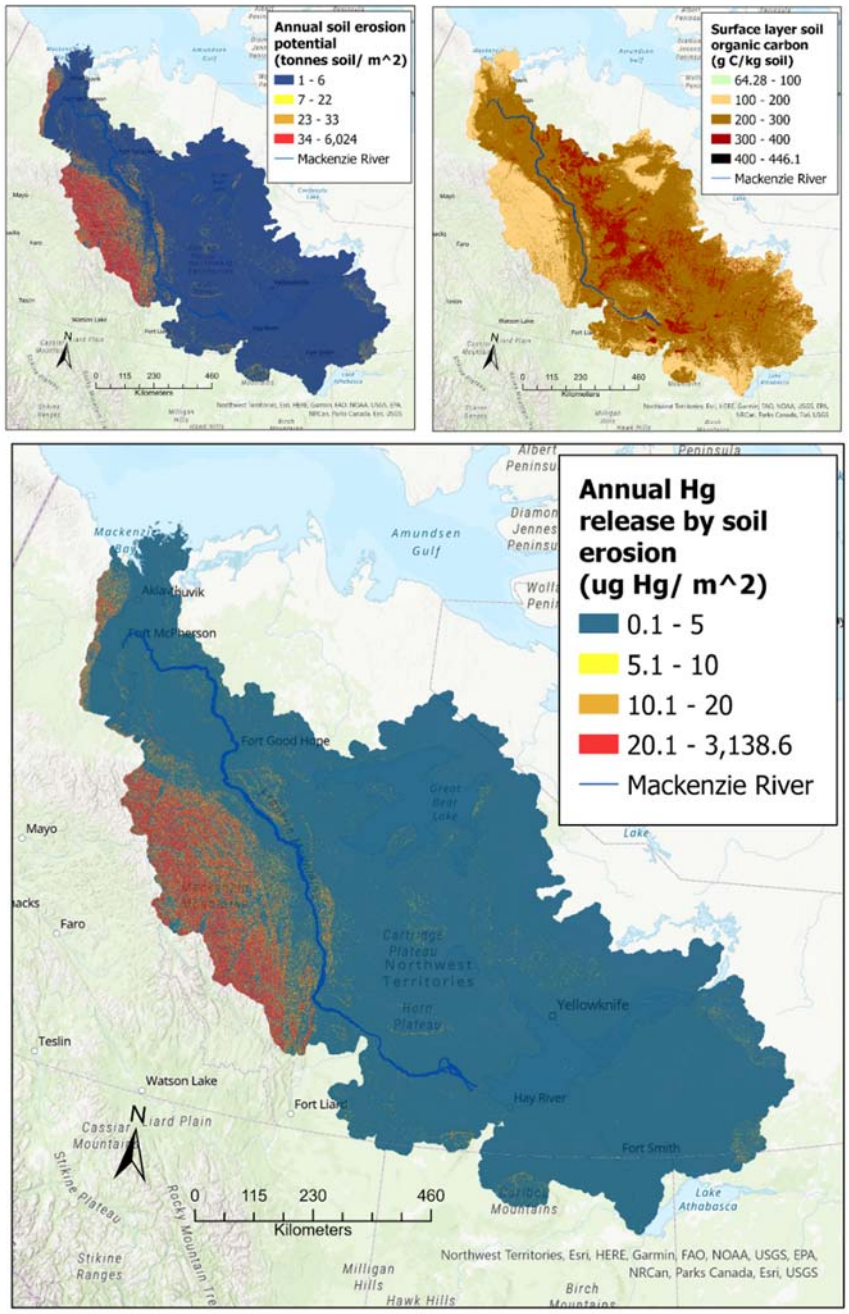

Supplemental 16. The calculation of Hg release due to rainfall-induced soil erosion of the surface soil layer. On the left are the results of the RUSLE calculation of rainfall-induced soil erosion (tonnes ha^{-1} yr^{-1}). Soil erosion input was calculated by creating a polygon layer around a sample site waterbody and the soil erosion values within the polygon were summed and divided by the polygon area. The right figure represents the model output (Sothe *et al.* 2022) for soil organic carbon (SOC) concentrations at the surface soil layer (depth = 0 cm) which was used to estimate soil mercury concentrations assuming a generalized mercury: carbon ratio of 1.6 ug Hg/kg C (Schuster, 2018). These two layers were used to approximate the Hg release via rainfall-induced soil erosion shown in the bottom figure. This calculation assumes that 1.5% of the released mercury will reach a waterbody (Supplemental Table 4).

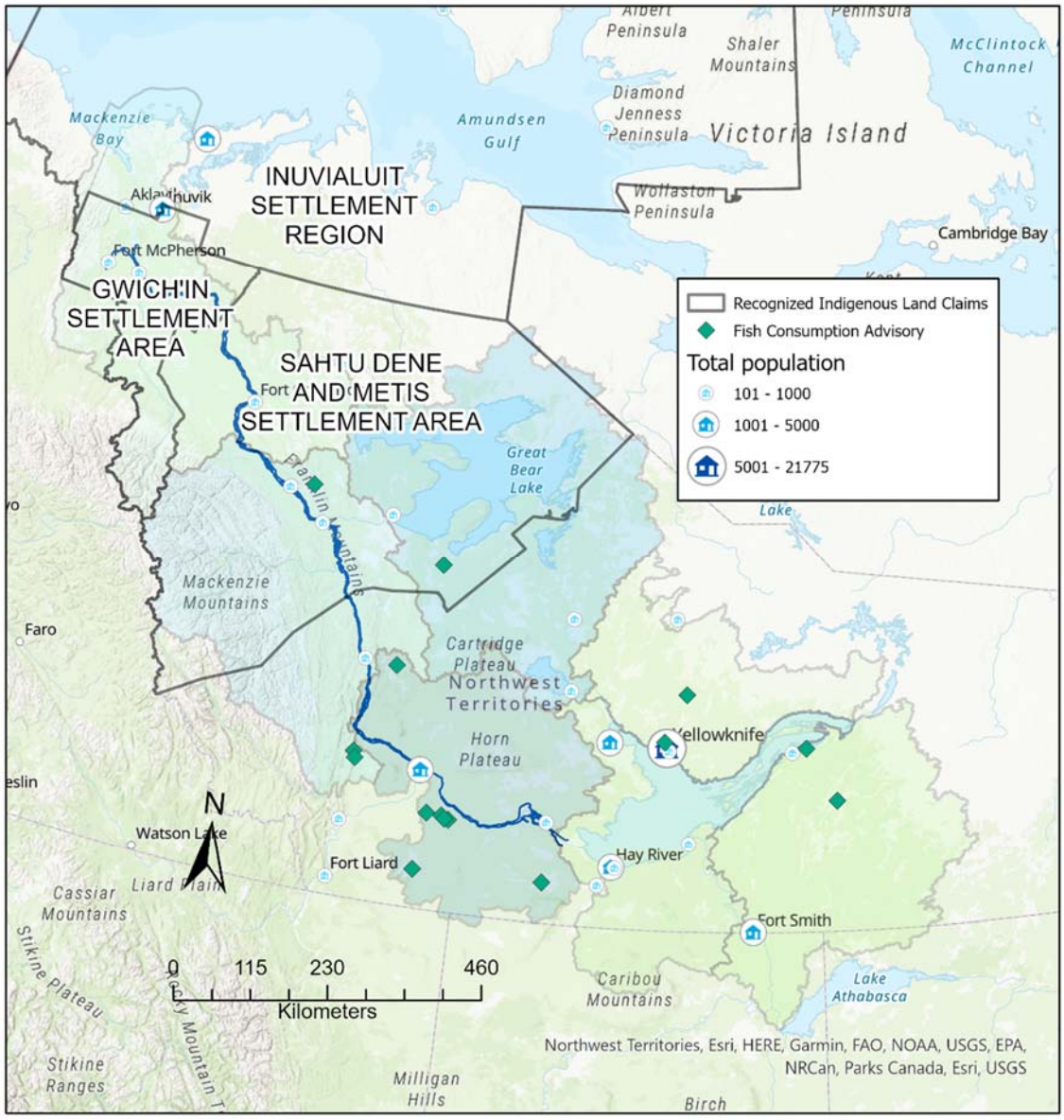

Supplemental 17. Human settlements and land regions included in modern treaties between the Canadian federal government and Indigenous communities. Only three Indigenous groups have been recognized in modern treaties: The Inivialuit, Gwch'in, and Sahtu Dene. The Dehcho Dene, Chipaweyan and Tlicho First Nations do not have treaty agreements. The largest communities are in the southern study area, with half the population residing in Yellowknife. Also shown on the map are the locations of lakes with fish consumption advisories from the GNWT (GNWT Department of Health and Social Services, 2021), to indicate which locations are likely to contain a greater risk of mercury exposure in humans.

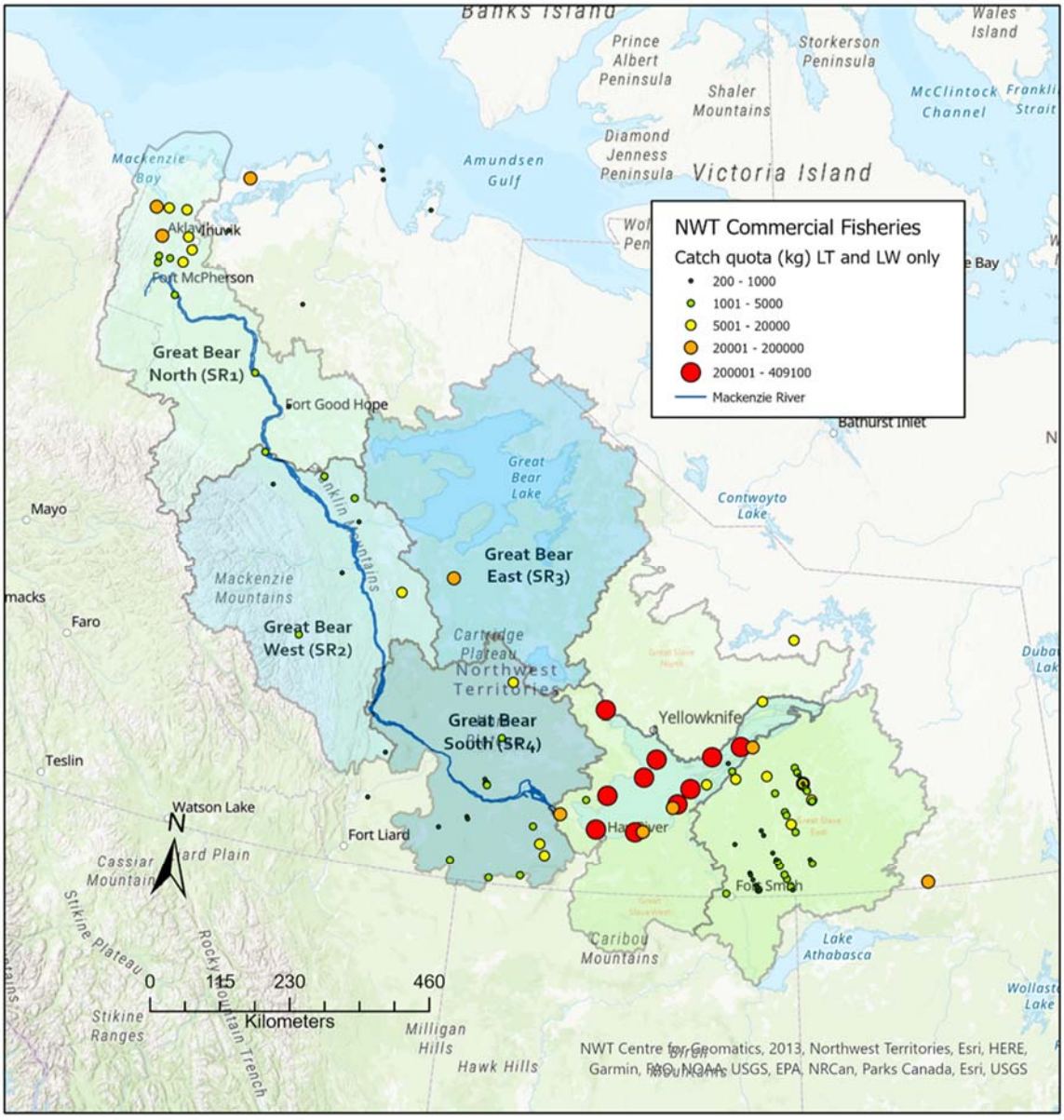

Supplemental 18. The location of NWT lakes which allow commercial fishing, visualized by the fish catch quotas indicative of the size of the commercial fishing operations that can be supported. The largest commercial fishing operations are in Great Slave Lake. The endpoint variable "% Fish not eligible for sale" is therefore most relevant for the GSL BN-RRM, and not the GBS model. In the GBS model, the largest commercial fisheries are in the Mackenzie Delta region of the GBS North study region.

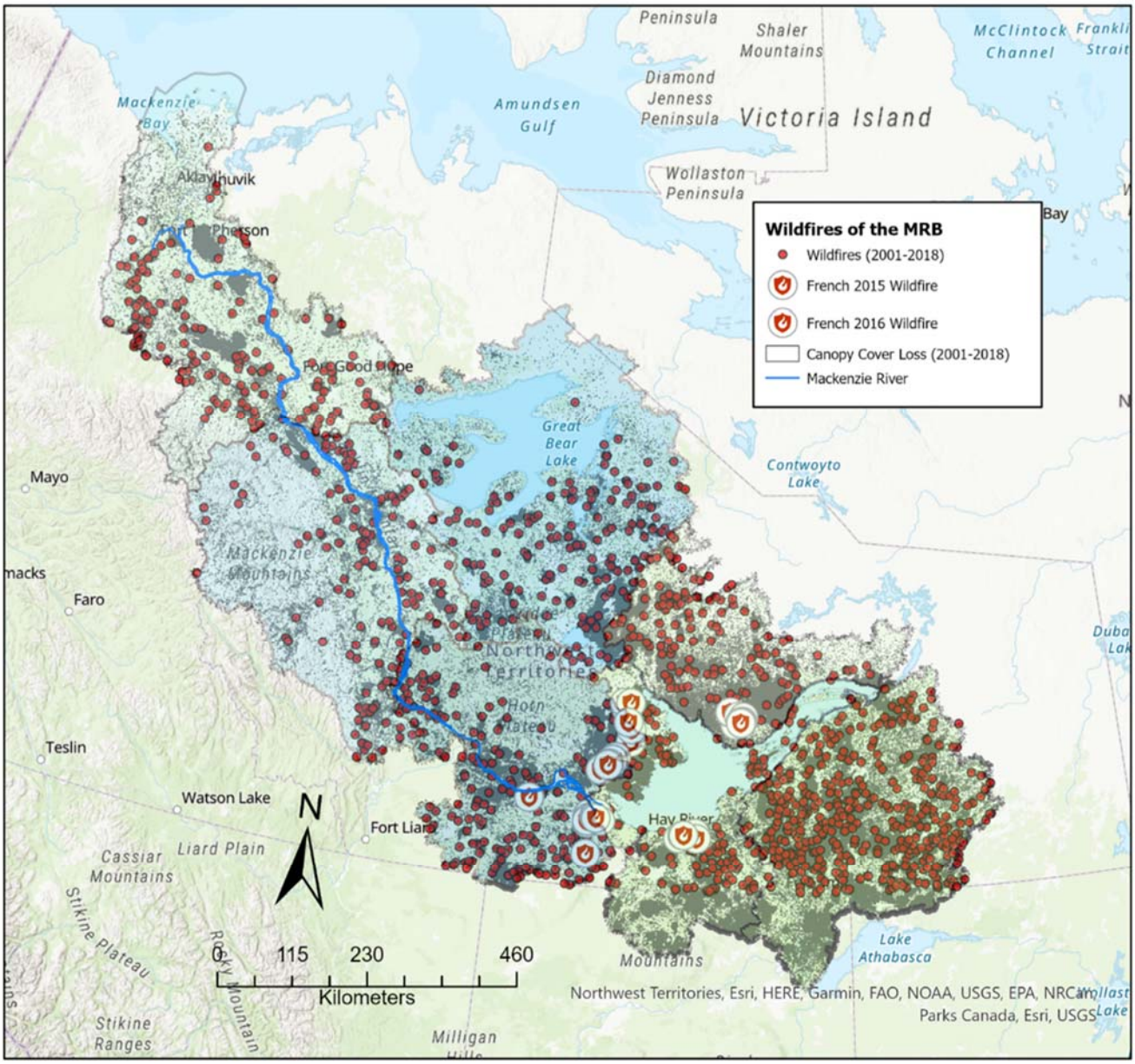

Supplemental 19. Wildfire events in the Northwest Territories. Canopy cover loss over the 2001-2018 period (Hansen *et al.* 2013) overlaid onto a map of wildfires (2001-2018; Scholten *et al.* 2021). The location of wildfires was obtained from two datasets: a general dataset with only wildfire locations and wildfire year (Scholten *et al.* 2021), and a detailed dataset with information on burn intensity (French *et al.* 2020).

Supplemental Figure 20. Location of the 46 climate stations used to interpolate the rainfall intensity (R-factor) RUSLE layer. Climate stations were spread across six provinces and territories: British Columbia (3), Alberta (8), Saskatchewan (6), Yukon (10), Northwest Territories (9), and Nunavut (10). All climate stations reported R-factor values from the 2005- 2018 period and were used in the Empirical Bayesian-Kriging interpolation (Supplemental Table 4).

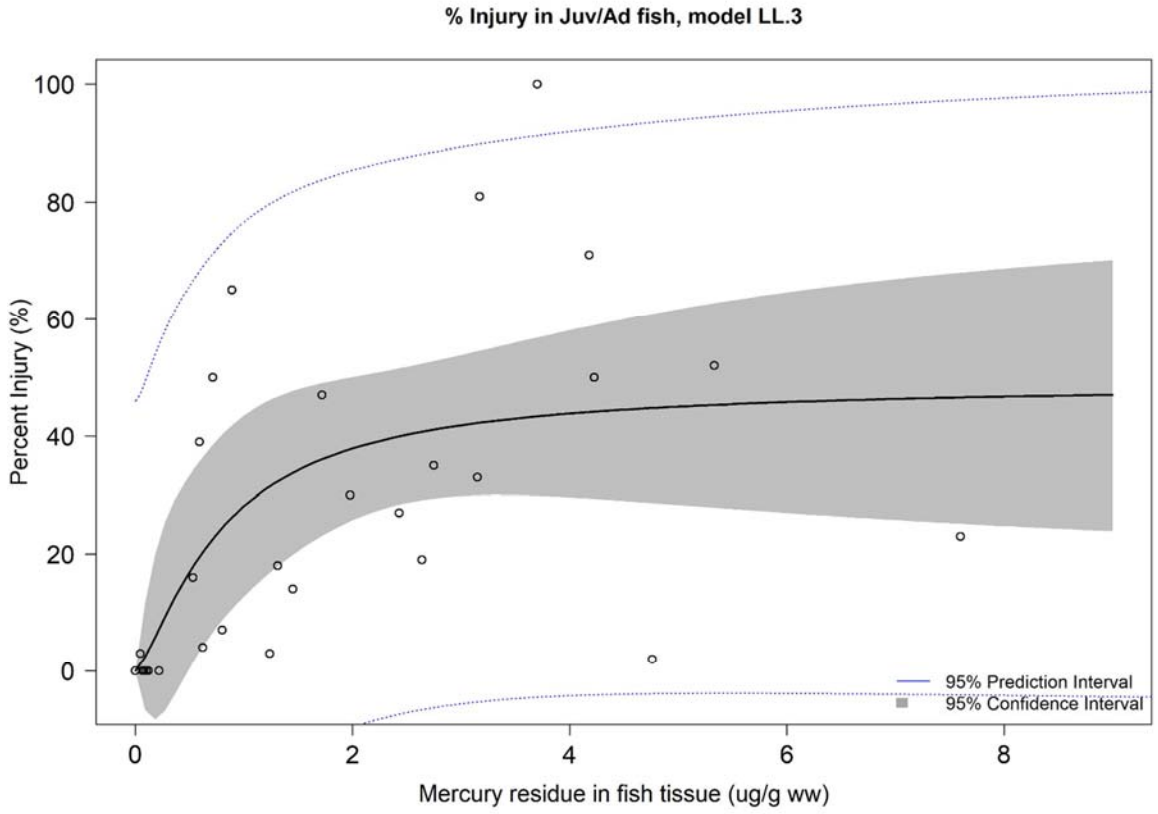
% Injury in Juv/Ad fish, model LL.3
Percent Injury (%)
Mercury residue in fish tissue (ug/g ww)
95% Prediction Interval
95% Confidence Interval

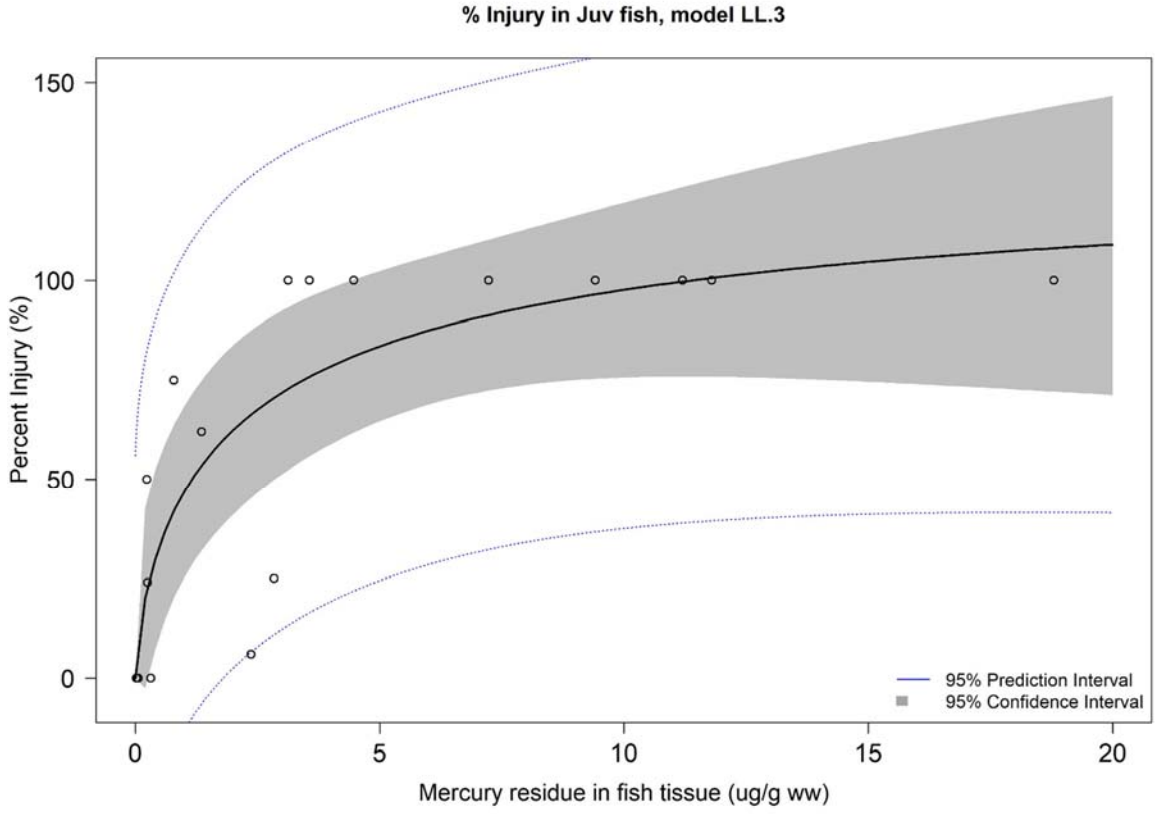
% Injury in Juv fish, model LL.3
Percent Injury (%)
Mercury residue in fish tissue (ug/g ww)
95% Prediction Interval
95% Confidence Interval

Supplemental 21. The dose-response curve used to develop the relationship between fish tissue mercury concentrations and likelihood of injury, which represents the combined impact of mortality, developmental abnormalities, and spawning success endpoints (Dillon et al. 2010). The data for the top curve represents results from toxicology experiments on juvenile and adult fathead minnow, which were exposed to mercury through both aqueous and dietary routes (Dillon et al. 2010), while the bottom dose-response curve was generated using data from only juvenile life stage fathead minnows. The top curve converged to a %injury value of 50% and when input into Netica it resulted in the faulty prediction that even extreme tissue Hg concentrations (>3 ug/g ww) would cause only a 50% probability of injury in fish. Therefore the equation generated by the bottom "Juvenile" dataset graph was used to predict the %injury endpoint in the BN-RRM. Both dose-response curves were generated using the LL.3() function from the Rstudio *drc* package (Ritz, 2015), and the equation was used to calculate the CPTs for the "%Injury to Fish" endpoint.

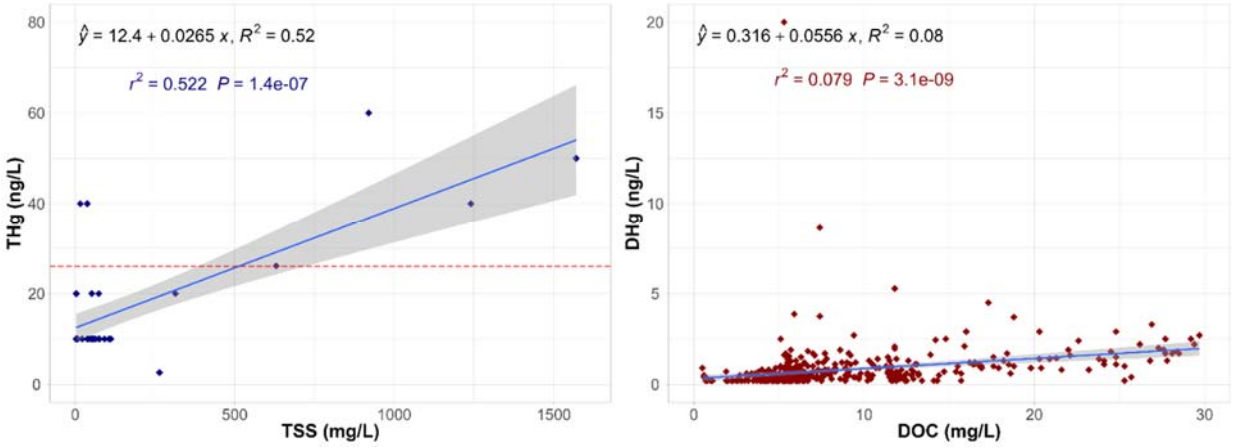

Supplemental 22. Exploratory data analysis between freshwater organic carbon and mercury concentrations collected in lakes and rivers in the study area. Two significant relationship ($p < 0.05$) were found. On the left, the linear relationship between total suspended solids (a measure of particulate matter) and total mercury based on 41 datapoints. The dotted line represents the Canadian regulatory inorganic mercury guideline (26 ng THg/L) for the protection of aquatic life (CCME, 2003). On the right, the linear relationship between dissolved organic carbon and dissolved mercury (432 datapoints).

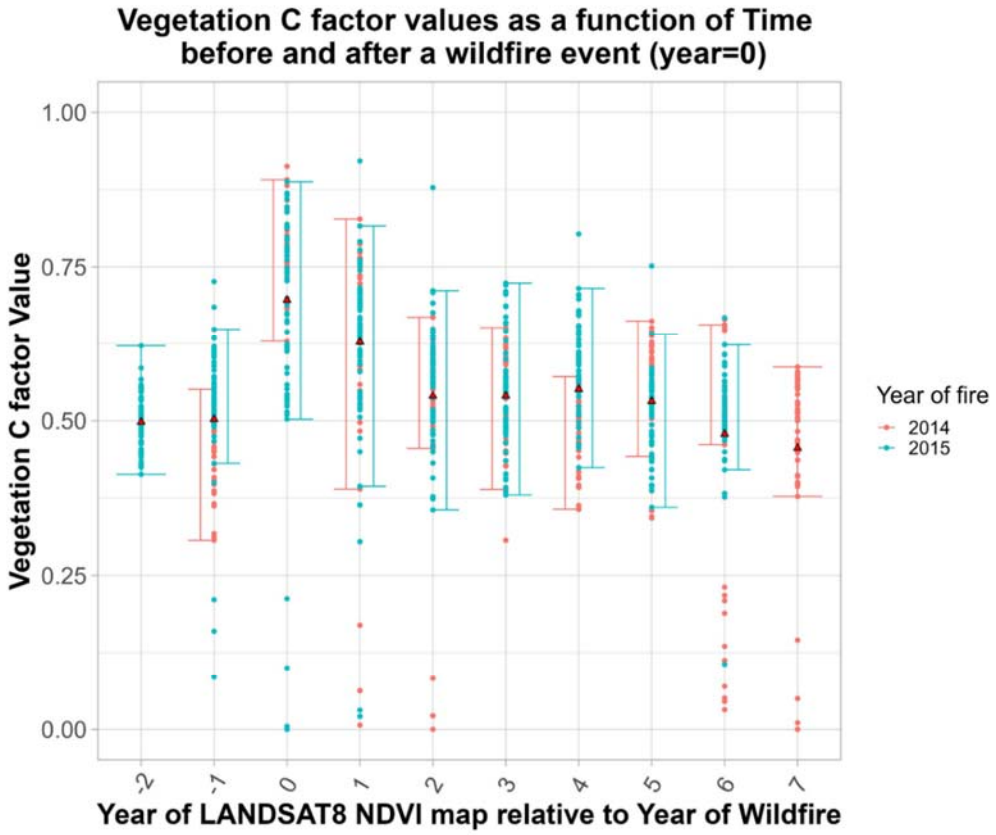
Vegetation C factor values as a function of Time
before and after a wildfire event (year=0)
Vegetation C factor Value
1.00
0.75
0.50
0.25
0.00
-2
-1
0
1
2
3
4
5
6
7
Year of LANDSAT8 NDVI map relative to Year of Wildfire
Year of fire
2014
2015

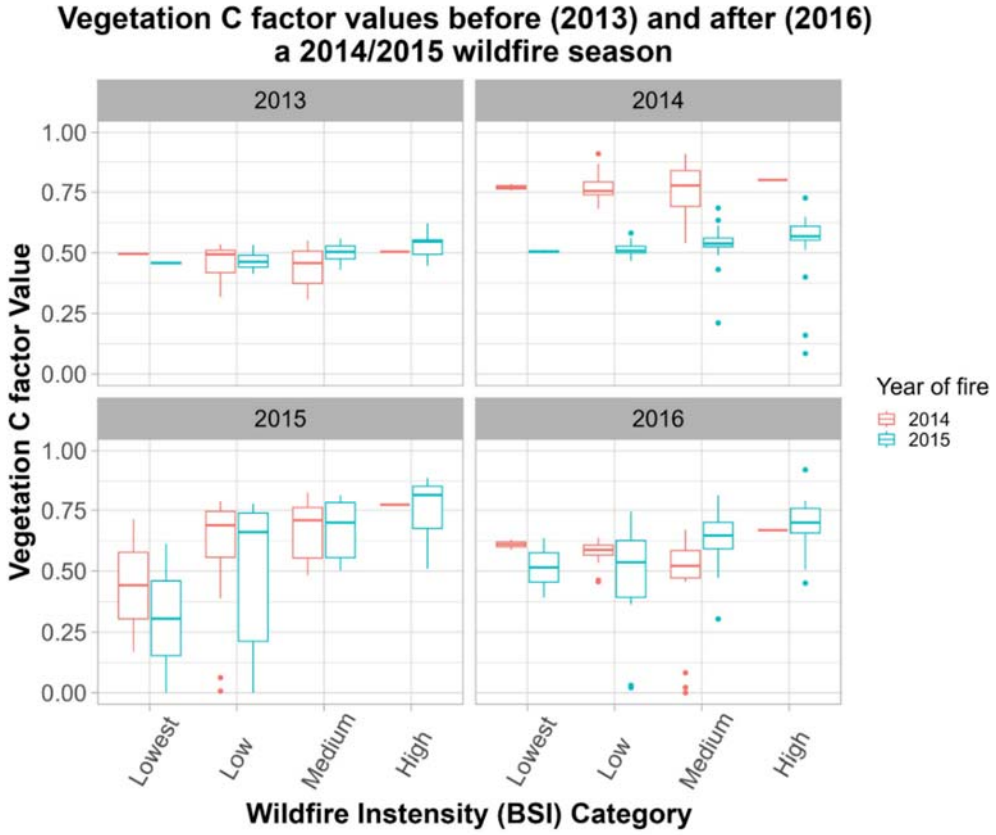
Vegetation C factor values before (2013) and after (2016)
a 2014/2015 wildfire season
2013
2014
2015
2016
Vegetation C factor Value
1.00
0.75
0.50
0.25
0.00
Lowest
Low
Medium
High
Wildfire Instensity (BSI) Category
Year of fire
2014
2015

Supplemental Figure 23. Changes in vegetation density (C-factor) following a wildfire event in the Great Slave Lake region. A detailed wildfire dataset (French *et al.* 2020) included a characterization of wildfire intensity based on percentage of moss vegetation burnt. The top figure shows the change in C-factor relative to the wildfire event year, and the bottom figure considers the effect of wildfire intensity on the C-factor shift. In the top figure, negative x-axis values represent years prior to the wildfire event and positive values are the years after the wildfire. The C-factor does significantly increase the year of a wildfire event ($F(1, 128) = 67.86$, $p = 1.77e^{-13}$). However, the effect of wildfire intensity was statistically identical except between the "lowest" and the "high" categories. Wildfire intensity was not included in the final iteration of the BN-RRM because the study-area-wide dataset (Scholten *et al.* 2021) did not include information on fire intensity.

APPENDEX B: SUPPLEMENTAL TABLES

Supplemental Table 1. Summary of the freshwater mercury monitoring efforts in the NWT MRB. A total of 2147 datapoints were used to populate the water THg node.

Reference	Sampling Years	(n) THg measurements	Chemical detected	Detection limit (ng/L)	Location
AANDC Water Division: CIMP 140 (2022)	2004-2013	30	THg, DHg	10	7; West Arm
ECCC, Carleton University: CIMP 177 (2022)	2016	14	THg	0.2	4, 5, 7 West Arm
University of Alberta: CIMP 199 (2022)	2019	72	Hg	0.2? USEPA Method 1631	1, 2, 4, outside (37)
University of Waterloo: Dehcho Region Water Quality Data (2022)	2013-2019	101	DHg, THg	0.2 USEPA TM0811	4, Mouth
K'ágee Tú First Nation: Community Based Monitoring (2022)	2011-2016	30	DHg, THg	10 ng/L – Taiga labs	4
GNWT: NWT-wide community-based monitoring program (2023)	2012-2021	1697	THg, DHg	10 ng/L- USEPA 200.8	1, 2, 4-7; East Arm, Middle, Mouth, West Arm, outside (59)
TAEMP: Tłı̨chǫ Aquatic Ecosystem Monitoring Program (2010-2018)	2011-2018	51	THg	10 ng/L- USEPA 200.8	3, 7, West Arm, outside (12)
Norman Wells Aquatic Monitoring Program (2019)	2017 - 2020	143	THg, DHg	0.2 ng/L	2
Ekati Diamond Mine Aquatic Effects Monitoring Program (2019)	2017	9	THg	0.2 EPA 245.7	3
Campeau et al, 2022	2018-2020	0	TSS, PHg, DHg, MeHg (No THg measured, did not include)	0.2 – EPA method 1631E Cold-Vapor Atomic Fluorescence Spectroscopy	3, 7, West Arm

Supplemental Table 2. Summary of the fish tissue mercury monitoring efforts in the NWT MRB. A total of 1150 datapoints were used to populate the five freshwater fish nodes: lake whitefish, lake trout, northern pike (Jackfish), walleye (Pickerel), and burbot (Lota lota).

Reference	Sampling Years	Season/ Month?	Fish Species (n)	(n) Tissue measurements	Size information?	Age information?	Location
Fortune Minerals Limited (2015): NICO Project	2005, 2006, 2008, 2009	No	Lake whitefish, northern pike, lake trout	86	Yes	No	7, West Arm, Outside (10)
Cox et al. 2010	2008 - 2010	No	Lake whitefish, northern pike	213	Yes	No	5, 7, East Arm
Tendler et al. 2020	2011	No	Burbot, lake whitefish, northern pike, walleye	20			5, Middle
Rohonczy et al. 2020.	2013- 2015	Yes	Burbot, northern pike, lake whitefish, lake trout, walleye	111	Yes!	Yes!	5, West Am
University of Waterloo & Dehcho AAROM (2022)	2012	Yes! Winter too!	Burbot, lake trout, lake whitefish, northern pike	167	Yes	No	2, 4, Mouth
Gantner and Gareis, 2013 Roux et al. 2014	2002	No	Lake trout	84	Yes	No	1
Lockhart et al. 2005	2001- 2005	Yes	Northern pike, walleye, lake trout, burbot, lake whitefish	90	Yes	No	4, 5, Mouth, Middle
TAEMP: Tłı̨chǫ Aquatic Ecosystem Monitoring Program (2010-2018)	2011, 2014, 2015, 2018	Yes	Lake trout, lake whitefish, walleye, northern pike	328	Often	Often	3, 7, West Arm
Diavik Diamond Mine Ltd. 2009	2008	No	Lake trout	40	Yes	No	Outside
Rescan Environmental Services Ltd. 2009	2008	No	Lake trout	23	Yes	No	Outside
EBA Engineering Consultants Ltd. 2006	2005	No	Lake whitefish, lake trout	40	Yes	No	Outside

Supplemental Table 3. Summary of the GIS datasets and environmental model raster layers utilized in the construction and parametrization of the BN-RRMs.

Reference	Measured or modelled?	GIS file type?	Raster resolution	Description	Variable?
GNWT Mineral Claims Mineral Tenure Data	Obtained from extent of claim	Polygon	N/A	Active (2022) mineral claims	Proximity to Mining
GNWT Oil and Gas Mineral and Petroleum Resources Data	Extent of claim	Polygon	N/A	Active (2022) oil and gas licenses	Proximity to Oil and Gas developments
Canada Open Government 2015	Calculated	Point	N/A	Rainfall intensity calculations at 52 monitoring sites in the NWT and Northern Canada. 2000 – 2018	R-factor rainfall intensity map created with Empirical-Bayesian Kriging transformation in ArcGIS Pro.
Hansen et al. 2013	Satellite data	Raster	30 m	Global tree cover extent, loss, and gain, from 2000 to 2019	Wildfire
Sothe et al. 2022	Modelled	Raster	250 m	Canadian model of national carbon concentrations in soil at different depths. Only 0 cm was used; depths up to 30 cm are available.	Soil Organic Carbon (SOC). Necessary factor for the soil erosion Hg release calculation.
Silke, 2009	GPS Coordinates	Point	NA	History of mining in the Northwest Territories; includes mine name, GPS coordinates, ore extraction, dates of operation, mineral mined (1920-2008)	Historic Gold Mines. Proximity to Historic Mining.
Canada Open Government 2016	Estimated	Polygon	NA	Fairly low-resolution database of national soil texture.	K-factor soil texture. Necessary factor for soil erosion.
Gorelick et al. 2017	Satellite data	Raster	21 m	NDVI was downloaded for the study area. The timeframe selected was Aug – Oct, 2013 – 2021, < 10% cloud cover	C-factor vegetation density. Necessary factor for soil erosion.
Natural Resources Canada, 2013	Satellite elevation data	Raster	16 m	The DEM was used to calculate Flow Accumulation ArcGIS, an essential input for the LS factor calculation.	LS factor slope length and angle. Necessary factor for soil erosion.
Natural Resources Canada.: National Hydro Network (NHN)	Modelled	Polygon	NA	National dataset of watershed boundaries. Used to set the study area extent	Scenario / Study Regions
Segal et al, 2016	Satellite data (10 m resolution)	Polygon	NA	Location of active thaw slumps in the Peel and Willow River regions of the Northern MRB study area	Proximity to thaw slumps
Kokelj et al. 2021	Satellite data (10 m resolution)	Polygon	NA	Model results: Lakes/ streams/ coastal areas that are predicted to be affected by thaw slumps This layer was used for the proximity to thaw slump (10 km) node.	Proximity to thaw slumps
Okulitch and Irwin, 2017	Approximation from survey maps	Polygon	NA	Spatial ESRI dataset of bedrock geology for the northern Mackenzie River	Bedrock geology (ultimately not used in model)
Stubley and Irwin, 2019	Approximation from survey maps	Polygon	NA	Spatial ESRI dataset of bedrock geology for the Great Slave Lake region	Bedrock geology (ultimately not used in model)
Open Canada: Modern Treaties. Government of Canada and Indigenous Services Canada.	Treaty Boundary	Polygon	NA	Post-1975 treaty boundary dataset	NA
Albers, 2017	R package to access the Canadian National Hydrology dataset	Point – location of sampling	NA	Hydrology data was used to estimate flux from Mackenzie River into Arctic Ocean	Riverine Hg input into Arctic Ocean from MR
Statistics Canada, 2017	Human population census results (2016)	Point	NA	Downloaded the Community Population Estimates by detailed ethnicity. Accessed July 1, 2021.	NA
Fisheries Act-Schedule V (CRC c.847)	Commercial fishing lakes	Point	NA	Location of lakes where commercial fishing is allowed. Includes fish species and catch quotas.	NA

Northwest Territories Power Corporation (2009)	Location of hydroelectric facilities	Point	NA	Location of NWT hydroelectric facilities and their generator capacity	Did not use in the model since all future hydroelectric projects are run-of-the-river
GNWT Department of Health and Social Services, 2021	Location of lakes with consumption advisories	Point	NA	Lakes where the GNWT has issued a fish consumption advisory that is still in place. Includes species and # portions allowed.	NA
French et al. 2020	Detailed dataset of 2014 – 2015 wildfires around Great Slave Lake	Point	NA	Dataset with fire location and intensity. Used to determine that wildfire intensity does not have significant effect on C-factor recovery.	Wildfire effect
Scholten et al. 2021	Basic dataset that shows only the year and location of wildfire events.	Point	NA	This dataset was considered since it covered the entire study area. However, decided to use the detailed French dataset instead for observing C-factor shift.	Wildfire effect
Schaefer et al. 2020	Model	Raster	43291 m	NCD files from the SiBCASA model were shared by Kevin Schaeffer.	Permafrost thaw release of Hg into aquatic ecosystems
Fraser, A.; Dastoor, A.; and Ryjkov, A., 2018	Model	Raster	43291 m	NCD files from GEM-MACH_Hg model were shared by Andre Ryjkov	Atmospheric Hg deposition

Supplemental Table 4. A detailed description of the discretization, assumptions, and equations used to calculate nodes across all BN-RRM categories, which are represented by colour (Scenario/ interactive nodes = yellow; Sources = blue; Stressors = orange; Effect = green; Impact = pink).

Node	Category	Discretization	Comments and Assumptions	Equations	Reference
Great Bear Subbasin (GBS) Model study regions	SR1	Great Bear North	1) The study area was split into regions to reduce epistemic uncertainty 2) See Table 1 for differences between study regions	NA	NA
	SR2	Great Bear West			
	SR3	Great Bear East			
	SR4	Great Bear South			
Great Slave Lake (GSL) Model study regions	North Arm	GSL North Arm	1) The study area was split into regions to reduce epistemic uncertainty 2) See Table 1 for differences between study regions	NA	NA
	East Arm	GSL East Arm			
	Middle Basin	GSL Middle Basin			
	Outlet	GSL Outlet to Mackenzie			
Freshwater fish species	Lake whitefish	NA	1) These 5 freshwater fish species were selected because they are important food fish species for Indigenous communities in the MRB, and are commonly sampled for mercury 2) Preferences and diet vary amongst Indigenous communities.	NA	Ratelle et al. 2019
	Burbot				
	Walleye				
	Lake trout				
	Northern pike				
Proximity to mine (15 km)	Yes	0 – 15 km	1) Mining is only a potential mercury source for the Great Slave Lake (GSL) models. 2) Mining will have no significant impacts on lakes which are over 15 km distant from the mining source.	Count data	Thienpont et al. 2016
	No	> 15 km			
Oil development distance (km)	Yes	0 – 50 km	1) Oil and Gas exploration is a potential mercury source for the Great Bear Subbasin (GBS) models only. 2) After 50 km from fossil fuel sources, there will be no significant impacts on aquatic ecosystems.	Count data	Kelly, et al. 2010
	No	≥ 50 km			
Proximity to historic mine	Yes	0 – 15 km	1) Historic mining is only a potential mercury source for the Great Slave Lake (GSL) models. 2) Mining will have no significant impacts on lakes which are over 15 km distant from the mining source.	Count data	Thienpont et al. 2016 Kokelj, 2002
	No	> 15 km			
Proximity to retrogressive permafrost thaw slump (RPTS)	Yes	0 – 10 km	1) Lakes impacted by RPTS have elevated THg and MeHg concentrations (St. Pierre, 2018) 2) RPTS will have an impact on waterbodies within a 10 km radius of a thaw slump impacted lake	Count data	St. Pierre et al. 2018 Lantz et al. 2008
	No	> 10 km			
Proximity to GSL Outlet	Yes	0 – 50 km	1) Proximity to Great Slave Lake is only a potential source in the GBS models. 2) If freshwater quality of Great Slave Lake is impacted by mining, it may be acting as an Hg source for the MR.	Count data	Cott et al. 2016 Thienpont et al. 2016
	No	> 50 km			
Permafrost Hg release (ug DHg m^{-2} yr^{-1})	None	0	1) Model outputs (Schaeffer et al. 2020) were provided as monthly estimates of permafrost DHg release into aquatic ecosystems for the 2005- 2020 study period 2) Seasonal effect was not considered	Model outputs (monthly) were summed to produce annual estimates, and then averaged over the study period	Schaeffer et al. 2018
	Very low	0 – 2			
	Low	2 – 4			
	Medium	4 – 6			
	High	6 – 10			
	Very high	> 10			
Soil erosion Hg release (ug THg m^{-2} yr^{-1})	Low	0 – 5	1) Assuming that 1.5% of mercury released by soil erosion will enter the freshwater ecosystem (Schaeffer, 2020) 2) This equation was theorized for this project and does not reflect information found in a literature search	[Hg]water = [Hg]soil * Erosion Potential * 0.015 * Time (1 year)	Schaeffer et al. 2020
	Medium	5 – 10			
	High	10 – 20			
	Very High	> 20			
Atmospheric Hg deposition (ug THg m^{-2} yr^{-1})	Very low	0 – 3	1) Model outputs (Dastoor et al. 2015) were provided as annual estimates of THg deposition for the 2005 – 2020 period Maps of annual atmospheric THg deposition values are from the GEM-MACH-Hg model output. These were summed for the duration of the study period (2005 – 2020)	Model output (annual estimates of emission) were averaged over the study period	Dastoor et al. 2015
	Low	3 – 9			
	Medium	9 – 12			
	High	12 – 15			
	Very high	> 15			
Total Hg deposition	Low	0 – 10	1) The total Hg deposition is likely underestimated because the Permafrost SiBCASA model output is for dissolved Hg (DHg). Other models are estimating total Hg	Sum of permafrost thaw Hg release, atmospheric Hg deposition, and	NA
	Moderate	10 – 15			
		15 – 20			
	High	20 – 50			

	Very high	> 50	(THg). Since the major form of mercury in the MR is particulate (PHg), the results of the permafrost model are underestimated compared to the other two.	RUSLE soil erosion Hg release	
Time since wildfire (yrs)	Short – recent fire	0 years	Immediately following a wildfire event, the C-factor will increase. With time the vegetation recovers, and the C-factor will continue to decrease. This variable allows you to visualize the impact on the C-factor at two points in the recovery process.	NA	Scholten et al. 2021
	Following moderate recovery period	3 years			
Wildfire event	Yes	Select to see effect of fire on C-factor	If the default "No" is selected, the soil erosion calculation does not account for expected change in C-factor following a wildfire.	NA	Scholten et al. 2021
	No	Default selection			
Ratio of C-factor post-fire/ C-factor pre-fire	NA	0 – 0.5	1) The C-factor values were calculated from an NDVI layer (Fall 2013 – 2021). 2) Wildfire locations (~3300 final) were obtained from the Scholten (2021) dataset which was filtered to select fires post-2014 and in the GBS risk regions 1- 4. 3) Distributions of the C-factor ratio were used to populate the CPTs for either 1-year or 3-years post-fire.	Data was discretized and the counts were input into Netica. Did not use any equations or assume a normal distribution	Scholten et al. 2021
		0.5 – 1			
		1 – 1.5			
		1.5 – 2.5			
		2.5 – 10			
		≥ 10			
Adjusted C-factor	Dense forest	0 – 0.1	1) The distribution is bound by the limits of 0 (min) and 1 (max).	If Wildfire event is "Yes" : Adjusted C-factor = Ratio of C-factor * C-factor If Wildfire event is "No" Adjusted C-factor = C-factor	Borelli et al. 2016
	Dense vegetation	0.1 – 0.2			
	Moderate vegetation	0.2 – 0.4			
	Little vegetation	0.4 – 0.6			
	Sparce vegetation	0.6 – 0.8			
	Very sparce vegetation or Water (1.0)	0.8 – 1			
Rainfall Intensity Index (R-factor) (MJ mm ha^{-1} hr^{-1} yr^{-1})	Zero	0 – 50	1) Data from 52 climate stations with calculated R-factors were used to interpolate rainfall intensity throughout the study area 2) Only data from the 2005- 2018 period was considered. R-factor values were not available post-2018. 3) The interpolated rainfall-intensity factors were averaged for the 2005- 2018 period prior to the calculation of soil erosion potential	Interpolated for the study area using ArcGIS Pro - Bayesian Empirical Kriging geoprocessing tool	Canada Open Government, 2015 Wall et al. 2002
	Very low	50 – 100			
	Low	100 – 200			
	Low- medium	200 – 300			
	Medium	300 – 400			
	Medium-high	400 – 500			
	High	> 500			
Crop/ Vegetation and management factor (C-factor) (unitless)	Dense forest	0 – 0.1	1) Landsat images of the NDVI were selected for the fall post-fire season (August 31- Oct 1) with<10% cloud cover. Cloud cover was present but mostly limited to the two great lakes. 2) C-factor values were obtained for the 2013- 2021 period only 3) For the year 2021, images were obtained from Spring and Summer seasons, and the values were found to be comparable to the 2021 Fall C-factors. 4) The C-factor calculation from NDVI was developed for European soils and may not be accurate for the Arctic tundra regions.	C-factor = exp((-2*NDVI)/((1-NDVI)))	Gorelick et al. 2017
	Dense vegetation	0.1 – 0.2			
	Moderate vegetation	0.2 – 0.4			
	Little vegetation	0.4 – 0.6			
	Sparce vegetation	0.6 – 0.8			
	Very sparce vegetation or Water (1.0)	0.8 – 1.0			
Soil Erodibility Index (K-factor) (tonnes hr MJ-1 mm-1)	Water	0	1) K-factor can be calculated if soil maps of %silt, %clay, and %organic carbon are available. If they are not, it can be estimated from a map of soil texture class. The latter method was used in this project. 2) K-factor values for all texture classes except for "Organic" were obtained from the GNWT Erosion manual. 3) The eco-district soil texture map (Canada Open Government, 2013) is a polygon file of limited resolution. 4) The RUSLE Equation was not developed for soils with high Carbon content (> 4%) since organic matter can have a stabilizing	K-factor values were obtained from GNWT Transportation (2013), no calculations necessary.	GNWT Transportation, 2013 Canada Open Government, 2013
	Sand	0.02			
	Organic	0.015			
	Sandy Loam	0.017			
	Clay	0.03			
	Clay Loam	0.032			
	Loam	0.042			

			effect. A value of 0.015 was assigned for the purpose of this project		
Slope length and angle factor (LS-factor) (Unitless)	Very low	0 – 1	1) The LS-factor was calculated remotely using a 16m- resolution DEM layer and the ArcGIS Hydrology tools to calculate the Flow Accumulation (As) factor.	Calculated using the McCool equation: LS= ((As/22.13)^m)*S Where S is conditional on the slope angle, and m is conditional on the slope length (approximated by As)	Hrabalíková, M. and Janeček, M., 2015
	Low	1 – 10			
	Medium	10 – 50			
	High	> 50			
Soil erosion Hg release	Low	0 – 5	1) Calculation of soil erosion uses RUSLE method, developed for European agricultural soils not Arctic regions underlain by permafrost 2) Soil erosion calculation is the average over the 2013- 2018 period (see precipitation intensity and vegetation density definitions) 3) Erosion into waterbody was calculated by summing all erosion values within 500 meters of the waterbody shore and then dividing by the polygon area.	Soil erosion = Precipitation intensity * Soil erodibility factor * Slope-angle factor * Vegetation density	Wall et al. 2002
	Medium	5 – 10			
	High	10 – 20			
	Very High	> 20			
Soil organic carbon (OC) (g C/ kg soil)	Inorganic soil	0 - 100	1) Soil OC is for depths of 0cm and 5cm, based on terrestrial model output (Sothe et al. 2022) 2) Making assumption that the Hg/ C ratio for the NWT is 1.6 ug Hg/ g C (Schuster et al. 2018), the average in North American soils 2) Interim sediment quality guideline for Hg is 170 ug Hg/ kg sediment, corresponding to ~ 100 g C/ kg sediment 3) Probable Effects Level (PEL) for mercury (486 ug/ kg sediment) corresponds to ~ 300 g C/ kg sediment	Count data	Sothe et al, 2022 Schuster et al. 2018 Canadian Environmental Quality Guidelines, 1999
	Moderate organic	100 – 200			
		200 – 300			
	Highly organic soil	300 – 400			
		> 400			
Soil Depth (cm)	Surface layer	0 cm	1) Interactive node controlling the probability distribution of the Soil OC node 2) The recommended selection is 0cm since this is the top layer of soil and will be the first to erode during a rainfall event.	Count data	Sothe et al. 2022
	Near-surface	5 cm			
Hg: C soil ratio	Low	0 – 3	1) This node was populated by assuming that the distribution reported by Schuster et al. (2018) for North American soils is normally distributed and accurate for Arctic soils	Assume that Hg:C ratio follows a normal distribution: 1.6 ± 0.9 ug Hg/ g C	Schuster et al. 2018
	Medium	3 – 5			
	High	5 -8			
Soil THg (ug Hg/ kg soil)	Low	0 – 170	1) CCME ISQG guideline is 170 ug Hg/kg soil 2) CCME PEL guideline is 486 ug Hg/kg soil	Soil THg = Soil OC * Hg:C soil ratio	Canadian Environmental Quality Guidelines, 1999
	Medium	170 – 486			
	High	>= 486			
Freshet total flow (km^3/yr)	Q1	0 – 0.2	1) GBS Model: Flow data obtained from Arctic Red River station (HYDAT, ID: 10LA002) 2) GSL Model: Flow data obtained from Fort Simpson station at Strong Point (HYDAT, ID: 10FB006) 3) In the GBS model, this node is only relevant for the GBS North (SR1) study region; in GSL model, only for the North Arm study region	The freshet season began when the discharge rate was 1.5-fold greater than the average 30-day discharge, until 10-days after the peak flow (Leitch, 2007).	Environment Canada, 2013 Leitch et al. (2007).
	Q2	0.2 – 0.4			
	Q3	0.4 – 0.6			
	Q4	0.6 – 0.8			
	> Q4	0.8 – 1.0			
Rest of year total flow (km^3/yr)	Q1	0 – 2. 6	See “Freshet total flow” node for details	The sum of flow for all days outside of the freshet season	Environment Canada, 2013 Leitch et al. 2007
	Q2	2.6 – 3.0			
	Q3	3.0 – 3.4			
	Q4	3.4 – 3.6			
Fish length (cm)	Small	<600 mm for burbot, N.pike, and L.trout; <500 mm for L.whitefish ; <45cm for walleye	1) Sizes were selected based on size-restrictions to the consumption advisories posted by GNWT (2016) 2) No consumption advisories exist for lake whitefish since this is a lower trophic level fish species with lower Hg concentrations. Older individuals can reach sizes up to 70cm.	Count data	GNWT Health and Social Services 2016
	Large	>600 mm for burbot, N.pike, and L.trout; >500 mm for L.			

		whitefish ; >450 mm for walleye			
Weekly Fish consumption (g kgbw^{-1} wk^{-1})	None	0	1) This is an interactive node for a user-specified diet 2) Five of these variables total, one for each fish species 3) A child portion size is 75g, and 150g for an adult (Health Canada, 2007). Note that the NWT consumption advisories assume that a portion size is 75 g (GNWT, 2016)	NA	Health Canada, 2007 GNWT Health and Social Services 2016
	½ serving (75 g)	0 – 1.25			
	1 serving (150 g)	1.25 – 2.5			
	2 servings (300 g)	2.5 – 5.0			
	3.2 servings (480 g)	5.0 – 8.0			
pTWI (ug Hg kgbw^{-1} wk^{-1})	US EPA reference dose	0.7	1) This is an interactive node that allows the user to select a threshold that is most relevant for their age and lifestyle. 2) The US EPA reference dose is the strictest and should be applied for younger, rapidly developing individuals 3) The Health Canada dose is most relevant for adult males or menopausal (> 49 years) women	NA	Health Canada, 2007 WHO, 1990 U.S.EPA, 2002
	WHO, 1990 threshold for women and children	1.4			
	Health Canada	3.3			
Freshwater THg (ng/L)	Low (below DL)	0 – 10	1) The highest acceptable detection limit in the THg monitoring datasets was 10 ng/ L 2) The CCME 2003 guidelines for the protection of aquatic life from inorganic Hg is 26 ng/L. 3) CCME guideline is based on most sensitive LOAEL for juvenile fathead minnows, which was not a species included in this study.	Count data	Canadian Environmental Quality Guidelines, 2003
	Medium	10 - 26			
	High	>26			
Freshwater fish tissue Hg (ug/g ww)	Low	0-0.2	1) Subsistence threshold is 0.2 ug Hg/g tissue (Lockhart et al. 2005). Canada guideline for retail sale of fish is 0.5 ug Hg/ g tissue (Health Canada, 2007). The EC20 and EC50 values are based on the dose-response model developed for adult and juvenile fathead minnows (Dillon et al. 2010; Fuchsman et al. 2016) 2) Used the Dillon et al. (2010) dose-response curve for discretizing this node, but a different curve equation for the "%Injury to Fish" endpoint. 3) Only data from fish muscle tissue was included in the dataset	Count data	Lockhart et al. 2005 Health Canada, 2007 Dillon et al. 2010 Fucshman et al. 2016
	Subsistence	0.2-0.5			
	EC20	0.5-0.77			
	EC50	0.77-3			
	Above EC50	>3			
MeHg ingested from Freshwater Fish consumption (ug Hg kgbw^{-1} wk^{-1})	None	0	1) Discretization based on pTWI guidelines 2) Total of 6 "Weekly MeHg ingestion" nodes: 1 for each freshwater fish species (5) and another for the total ingestion (1) 3) Total ingestion was the sum of all species-specific ingestion nodes	Weekly MeHg ingestion was calculated as: Weekly fish consumption * Freshwater fish tissue Hg	Health Canada, 2007 WHO, 1990 U.S.EPA, 2002
	Low mercury consumption	0 – 1			
	Moderate mercury consumption	1 – 1.4			
		1.4 – 2.5			
		2.5 – 3.3			
	High mercury consumption	>= 3.3			
% Injury to fish	Low risk	0-25	1) The %Injury calculation is based on the LL.3 dose-response model prepared with the Dillon et al. (2010) dataset. 2) The study organism in the Dillon et al. (2010) dataset were juvenile fathead Minnow, a species not included in this project 3) The EC20 and EC50 values predicted by this model were lower than those reported in the original publication, because the dose-response equations were different (Supplemental Figure 21). Additionally the dose-response curve in the Dillon et al. (2010) publication was from both juvenile and adult fish, while the dose-response curve used in this project is from juvenile fish. 4) This node was not prepared for the burbot and walleye nodes because the monitoring data was more limited for these 2 species	% Injury = 133.99106/(1+ exp(-0.69873*(log(FishHg)-log(2.43453))))	Dillon et al. 2010
	Moderate risk	25 – 50			
	High risk	50 – 75			
	Very high risk of injury	75 - 100			

% Fish not eligible for sale	Eligible	Tissue Hg < 0.5 ug Hg/g tissue	1) This node is a proxy for the risk probability of commercial fish catch exceeding Canadian guidelines for sale. If commercial fisheries or distribution centers are required to monitor Hg, fish with elevated Hg concentrations (> 0.5 ug Hg/g) would represent catch-losses to the commercial fisheries, assuming that there are no control or mitigation strategies employed.	Netica equation: %FishNotEligible = if(Fish_Hg >= Fish_sale_threshold, 1, 0) Where Fish_sale_threshold is 0.5 ug Hg/g tissue	Health Canada, 2007
	Not eligible	Tissue Hg > 0.5 ug Hg/g tissue			
Exceedance of pTWI (ingested Hg/ pTWI)	Expected weekly MeHg intake is lower than the selected threshold	0 – 0.01	1) The results of this node are dependent on the user-selected "Weekly Fish Consumption" node and the "pTWI" node 2) Values below 1 indicate no/ low risk, values above 1 indicate a risk of exceedance	The risk quotient was calculated as: MeHg ingested / pTWI	Health Canada, 2007 WHO, 1990 U.S.EPA, 2002
		0.01 – 0.1			
		0.1 – 0.5			
		0.5 - 1			
	Weekly MeHg intake is higher than the threshold	1 - 2			
		2 – 10			
		>= 10			
Annual THg flux to Beaufort Sea (tonnes)	These values fall within the range reported in Leitch et al. 2007	0 - 1	1) Discharge was calculated as km^3/yr, but converted to tonnes when calculating the annual flux 2) A correction of 0.81 was applied based on the findings of Emmerton et al. (2013) that ~19% of the THg is deposited in the Mackenzie Delta prior to reaching the Beaufort Sea	Flux = ($[Hg]_{freshet}$* Freshet discharge + $[Hg]_{rest\text{-}of\text{-}year}$ *Non-freshet discharge) * 0.81	Emmerton et al. 2013 Leitch et al. 2007
		1 – 2			
		2 - 4			
	These values are above the range	4 - 6			
		6 - 8			
		8 - 10			
		>= 10			

Supplemental Table 5. A comparison of the probability distributions from the raw data ("Observed data: probability" column) and the BN-RRM outputs ("Model probability prediction" column). The effect variables include freshwater THg, lake whitefish Hg, lake trout Hg, and northern pike Hg; however, they do vary between the study regions based on data availability. Node states which are highly probable in the raw dataset are being underestimated by the model (negative discrepancy values). Unlikely node states, which are coincidentally the states that coincide with higher Hg exposure, are being overestimated by the model (positive discrepancy values). Discrepancy values are highest when the number of observations is low and when all observations are of a single node state.

Location	Effect variable	Total observations (n)	Node state	Observed data: Counts	Observed data: probability	Model probability prediction	Discrepancy
GBS North (SR1)	Freshwater THg (ng THg/L)	331	0 to 10	230	69.5	55.7	-13.8
			10 to 26	58	17.5	19.5	2.0
			26 to 100	36	10.9	15.3	4.4
			>100	7	2.1	9.5	7.4
	Lake trout Hg (ug Hg/g tissue)	84	0 to 0.2	49	58.3	27.5	-30.8
			0.2 to 0.5	35	41.7	26.5	-15.2
			0.5 to 0.79	0	0.0	15.3	15.3
			0.79 to 3	0	0.0	15.3	15.3
			> 3	0	0.0	15.3	15.3
GBS West (SR2)	Freshwater THg (ng THg/L)	519	0 to 10	405	78.0	46.6	-31.4
			10 to 26	60	11.6	19.2	7.6
			26 to 100	48	9.2	18.9	9.7
			>100	6	1.2	15.3	14.1
	Lake whitefish Hg (ug Hg/g tissue)	20	0 to 0.2	9	45.0	25.5	-19.5
			0.2 to 0.5	11	55.0	26.8	-28.2
			0.5 to 0.79	0	0.0	23.9	23.9
			0.79 to 3	0	0.0	23.9	23.9
	Lake trout Hg (ug Hg/g tissue)	15	0 to 0.2	3	20.0	20.0	0.0
			0.2 to 0.5	7	46.7	21.2	-25.5
			0.5 to 0.79	4	26.7	20.3	-6.4
			0.79 to 3	1	6.7	19.4	12.7
			> 3	0	0.0	19.1	19.1
GBS East (SR3)	Freshwater THg (ng THg/L)	38	0 to 10	32	84.2	45.0	-39.2
			10 to 26	1	2.6	13.8	11.2
			26 to 100	3	7.9	22.1	14.2
			>100	2	5.3	19.0	13.7
	Lake whitefish Hg (ug Hg/g tissue)	126	0 to 0.2	125	99.2	64.4	-34.8
			0.2 to 0.5	1	0.8	11.9	11.1
			0.5 to 0.79	0	0.0	11.9	11.9
			0.79 to 3	0	0.0	11.9	11.9
	Lake trout Hg (ug Hg/g tissue)	124	0 to 0.2	10	8.1	13.1	5.0
			0.2 to 0.5	99	79.8	58.4	-21.4
			0.5 to 0.79	13	10.5	12.1	1.6
			0.79 to 3	2	1.6	8.2	6.6
			> 3	0	0.0	8.2	8.2
GBS South (SR4)	Freshwater THg (ng THg/L)	701	0 to 10	678	96.7	69.2	-27.5
			10 to 26	12	1.7	11.3	9.6
			26 to 100	8	1.1	9.8	8.7
			>100	3	0.4	9.7	9.3
	Lake whitefish Hg (ug Hg/g tissue)	53	0 to 0.2	51	96.2	41.8	-54.4
			0.2 to 0.5	2	3.8	19.6	15.8

			0.5 to 0.79	0	0.0	19.3	19.3
			0.79 to 3	0	0.0	19.3	19.3
	Lake trout Hg (ug Hg/g tissue)	30	0 to 0.2	0	0.0	18.0	18.0
			0.2 to 0.5	24	80.0	26.4	-53.6
			0.5 to 0.79	6	20.0	19.7	-0.3
			0.79 to 3	0	0.0	18.0	18.0
			> 3	0	0.0	18.0	18.0
	Northern pike Hg (ug Hg/g tissue)	50	0 to 0.2	4	8.0	17.3	9.3
			0.2 to 0.5	26	52.0	21.5	-30.5
			0.5 to 0.79	13	26.0	24.1	-1.9
			0.79 to 3	7	14.0	20.4	6.4
			> 3	0	0.0	16.6	16.6
GSL North Arm	**Freshwater THg (ng THg/L)**	258	0 to 10	243	94.2	42.1	-52.1
			10 to 26	7	2.7	19.5	16.8
			26 to 100	7	2.7	19.5	16.8
			>100	1	0.4	18.9	18.5
	Lake whitefish Hg (ug Hg/g tissue)	202	0 to 0.2	169	83.7	40.6	-43.1
			0.2 to 0.5	32	15.8	23.6	7.8
			0.5 to 0.79	1	0.5	18.0	17.5
			0.79 to 3	0	0.0	17.8	17.8
	Lake trout Hg (ug Hg/g tissue)	87	0 to 0.2	10	11.5	19.4	7.9
			0.2 to 0.5	68	78.2	20.7	-57.5
			0.5 to 0.79	7	8.0	20.0	12.0
			0.79 to 3	2	2.3	20.6	18.3
			> 3	0	0.0	19.2	19.2
	Northern pike Hg (ug Hg/g tissue)	91	0 to 0.2	14	15.4	19.2	3.8
			0.2 to 0.5	30	33.0	23.9	-9.1
			0.5 to 0.79	18	19.8	19.2	-0.6
			0.79 to 3	28	30.8	21.5	-9.3
			> 3	1	1.1	16.1	15.0
GSL East Arm	**Freshwater THg (ng THg/L)**	13	0 to 10	13	100.0	26.2	-73.8
			10 to 26	0	0.0	24.6	24.6
			26 to 100	0	0.0	24.6	24.6
			>100	0	0.0	24.6	24.6
	Lake whitefish Hg (ug Hg/g tissue)	121	0 to 0.2	111	91.7	67.0	-24.7
			0.2 to 0.5	9	7.4	13.4	6.0
			0.5 to 0.79	1	0.8	10.1	9.3
			0.79 to 3	0	0.0	9.5	9.5
	Northern pike Hg (ug Hg/g tissue)	91	0 to 0.2	66	72.5	52.1	-20.4
			0.2 to 0.5	19	20.9	19.9	-1.0
			0.5 to 0.79	5	5.5	10.7	5.2
			0.79 to 3	1	1.1	8.9	7.8
			> 3	0	0.0	8.4	8.4
GSL Middle	**Freshwater THg (ng THg/L)**	174	0 to 10	157	90.2	42.9	-47.3
			10 to 26	8	4.6	19.0	14.4
			26 to 100	7	4.0	19.3	15.3
			>100	2	1.1	18.8	17.7
	Lake whitefish Hg (ug Hg/g tissue)	10	0 to 0.2	10	100.0	25.9	-74.1
			0.2 to 0.5	0	0.0	24.7	24.7
			0.5 to 0.79	0	0.0	24.7	24.7
			0.79 to 3	0	0.0	24.7	24.7
	Lake trout Hg (ug Hg/g tissue)	29	0 to 0.2	22	75.9	21.2	-54.7
			0.2 to 0.5	7	24.1	20.3	-3.8
			0.5 to 0.79	0	0.0	19.5	19.5
			0.79 to 3	0	0.0	19.5	19.5
			> 3	0	0.0	19.5	19.5
		32	0 to 0.2	10	31.3	20.3	-11.0

	Northern pike Hg (ug Hg/g tissue)		0.2 to 0.5	20	62.5	21.5	-41.0
			0.5 to 0.79	0	0.0	19.4	19.4
			0.79 to 3	2	6.3	19.4	13.2
			> 3	0	0.0	19.4	19.4
GSL Outlet	Freshwater THg (ng THg/L)	411	0 to 10	395	96.1	53.4	-42.7
			10 to 26	12	2.9	17.0	14.1
			26 to 100	3	0.7	15.1	14.4
			>100	1	0.2	14.4	14.2
	Lake whitefish Hg (ug Hg/g tissue)	36	0 to 0.2	34	94.4	47.6	-46.8
			0.2 to 0.5	2	5.6	18.7	13.1
			0.5 to 0.79	0	0.0	16.9	16.9
			0.79 to 3	0	0.0	16.9	16.9
	Lake trout Hg (ug Hg/g tissue)	30	0 to 0.2	0	0.0	14.5	14.5
			0.2 to 0.5	24	80.0	39.8	-40.2
			0.5 to 0.79	6	20.0	17.9	-2.1
			0.79 to 3	0	0.0	13.9	13.9
			> 3	0	0.0	13.9	13.9
	Northern pike Hg (ug Hg/g tissue)	32	0 to 0.2	4	12.5	18.8	6.3
			0.2 to 0.5	22	68.8	31.4	-37.4
			0.5 to 0.79	4	12.5	18.1	5.6
			0.79 to 3	2	6.3	16.6	10.4
			> 3	0	0.0	15.1	15.1

Supplemental Table 6. The three dose-response models developed for the %Injury to fish endpoint using the R-studio *drc* package. The toxicological endpoints were compared between these models and to the Dillon et al. (2010) model results, which used the same primary data for the dose-response curve plots.

Model Name	Model used	ED10	ED20	ED50	Datapoints (n)
Using all data	LL.3(fixed=c(NA, 100, NA))	0.133	0.386	2.410	76
Juvenile data	LL.3(fixed=c(NA, 100, NA))	0.105	0.335	2.435	18
Juvenile adult data	LL.3(fixed=c(NA, 100, NA))	0.229	0.627	5.472	30
Dillon et al. (2010)	See equation 3 in publication	~ 0.406	~ 0.77	~ 3.013	~ 49